REFERENCE ONLY

UNIVERSITY OF LONDON THESIS

Degree PhD Year 2007 Name of Author BORROWDALE, David

Epicardium Development In *Xenopus*

David Borrowdale

Division of Developmental Biology
MRC National Institute for Medical Research
Mill Hill, London

University College London

Presented in 2007 for the degree of Doctor of Philosophy

ProQuest LLC
789 East Eisenhower Parkway
P.O. Box 1346
Ann Arbor, MI 48106-1346

Statement Of Declaration

I, David Borrowdale, declare that the work presented in this thesis was conducted in the laboratory of Doctor Timothy J. Mohun in the Division of Developmental Biology, MRC National Institute for Medical Research, Mill Hill, London. I confirm that the work included in this thesis is my own. Where information or reagents have been derived from other sources, this has been stated within the thesis.

Signed: Date: 24/10/07

Abstract

The epicardium is the outermost layer of the mature vertebrate heart. In birds and mice the epicardium originates from an extracardiac primordium - the proepicardium - and envelops the developing heart of the embryo.

The epicardium of birds and mice has two main functions in normal heart development: 1) a subset of epicardial cells undergo an epithelial to mesenchymal transition, generating the pluripotent progenitors of the coronary vascular system; 2) the epicardium secretes signals required for the proliferation and survival of cardiac myocytes.

Whilst the first role has been the subject of considerable study, much less is understood about the role of the epicardium in maintenance and development of the heart myocardium. The heart of the amphibian, *Xenopus laevis*, differs from that of mammals in a number of ways. The frog myocardium has a spongy, less compact structure and completely lacks coronary vasculature. As a result, studying the epicardium in *Xenopus* could provide a useful model for investigating the role of this tissue in the structure and development of heart muscle.

The structure of the epicardium in adult *Xenopus laevis* was analysed using histological methods and is shown to comprise a single cell-layered simple squamous epithelium. The embryonic origin and developmental progression of the epicardium was analysed histologically, by scanning electron microscopy, and by episcopic fluorescence image capturing. The epicardium is shown to be derived from the proepicardium, a clump of cells approximately 161μm wide by 133μm high, located caudally to the heart on the septum transversum. The proepicardium is shown to be located asymmetrically to the right of the sagittal plane. Cell lineage analyses confirm the unilateral, right-sided origin of the epicardium. At around stage 42 in development the proepicardium can be seen to be in direct contact with the ventricular myocardium, and proepicardial cells can be observed migrating over this 'proepicardial bridge.' Once proepicardial cells contact the ventricular myocardium, they proceed to envelop the heart beginning with the atrioventricular and conoventricular canals. Epicardial cells in *Xenopus laevis* were identified using the

expression patterns of three genes - Tbx18, epicardin and Wilms tumour 1 - that have been shown to demarcate the avian or mammalian epicardium. Morpholino knock-downs of these candidate genes were performed in order to investigate the roles of these genes in epicardium development, and therefore the wider roles of the epicardium in heart development. However, epicardium formation was found to be occurring too late in development to be accessible to morpholino knockdown analysis.

Acknowledgements

I would like to thank my supervisor, Tim Mohun, and the rest of the lab (Mike Bennett, Ross Breckenridge, Laurent Dupays, Lynne Fairclough, Surendra Kotecha, Rob Orford, Mike Sargent, Catherine Shang, and Norma Towers) for providing a supportive and knowledgeable environment in which to complete my PhD. Thanks to Anita Abu-Daya, Mike Reilly, and Lyle Zimmerman for their help with the little frogs, and to Aquatics for taking care of the big frogs. I am very grateful for histological assistance from Wendy Hatton, and Liz Hirst's SEM expertise. I must say a special thank you to Stuart Smith for showing a particular interest in my work.

I would like to thank my friends and family, especially my parents, Dorothy and Richard, and sister Jayne, for their unconditional love and support.

My biggest thanks I save for Katy for her encouragement, understanding and patience when it was most needed.

Contents

List Of Figures

List Of Tables

Abbreviations

a	Atrium/Atria
AV	Atrioventricular
avc	Atrioventricular Canal
avs	Atrioventricular Septum
bHLH	Basic Helix Loop Helix
BMP	Bone Morphogenetic Protein
CV	Conoventricular
cvc	Conoventricular Canal
E	Embryonic Day
ECE1	Endothelin Converting Enzyme 1
EFIC	Episcopic Fluorescence Image Capturing
EGF	Epidermal Growth Factor
EMT	Epithelial to Mesenchymal Transition
en	Endocardium
ep	Epicardium
EPDCs	Epicardium-Derived Cells
EST	Expressed Sequence Tag
ET-1	Endothelin-1
Ets1/2	v-ets Erythroblastosis Virus E26 Oncogene Homolog 1/2
FGF	Fibroblast Growth Factor
FOG-2	Friend of GATA2
gDNA	Genomic DNA
GFP	Green Fluorescent Protein
hCG	Human Chorionic Gonadotropin
HH	Hamburger and Hamilton Stage
HIF1α	Hypoxia-Inducible Factor 1 Alpha
HRP	Horseradish Peroxidase
Itga4	Integrin Alpha-4
la	Left Atrium
m	Myocardium
MEMFA	MOPS/EGTA/Magnesium Sulfate/Formaldehyde Buffer

mes	(Subepicardial) Mesenchyme
MET	Mesenchymal to Epithelial Transition
MMR	Modified Marc's Ringers
MO	Antisense Morpholino Oligonucleotide
MS222	3-Aminobenzoate Methanesulfonate
NAM	Normal Amphibian Medium
NCAM	Neural Cell Adhesion Molecule
OFT	Outflow Tract
p	Pericardium
PDGF-BB	Platelet-Derived Growth Factor BB
PDGFRβ	Platelet-Derived Growth Factor Receptor β
pe	Proepicardium
ra	Right Atrium
RALDH2	Retinaldehyde Dehydrogenase
se	Subepicardial Space
SEM	Scanning Electron Microscopy
snv	Sinus Venosus
st	Septum Transversum
sv	Spiral Valve
t	Trabeculae
TTw	TBS/0.1% Tween 20
v	Ventricle
VCAM-1	Vascular Cell Adhesion Molecule
VEGF	Vascular Endothelial Growth Factor
VEGFR2	Vascular Endothelial Growth Factor Receptor 2
WAGR	Wilms tumor, Aniridia, Genitourinary anomalies, mental Retardation syndrome
WT1	Wilms tumour 1
Xl	*Xenopus laevis*
Xt	*Xenopus tropicalis*

1 Introduction

1.1 Origins Of Cardiac Tissue

The vertebrate heart is formed from mesodermal precursors that arise as bilaterally symmetric patches at the prospective dorsal region of the gastrulating embryo (Mohun and Sparrow, 1997). Due to convergent extension movements, these patches move ventrally and fuse at the ventral midline to form the primary heart field. During subsequent development, the heart field will form a simple contractile linear tube. This then undergoes a series of complex morphological changes in order to give rise to the mature heart.

1.2 Extracardiac Contributions To The Developing Heart

Until recently it was thought the entire heart was derived from the primary heart field. However, a number of migratory cell populations, originating from outside the primary heart field, have now been shown to play essential roles in normal heart development. These include a population of myocardial precursor cells, the 'anterior' or 'secondary' heart field, found in pharyngeal mesoderm which give rise to the majority of the arterial pole of the heart (Kelly et al., 2001; Mjaatvedt et al., 2001; Waldo et al., 2001).

The cardiac neural crest has also been shown to make a significant contribution to the developing heart. These are migrating cells that originate from the neural tube and migrate through the posterior branchial arches to the outflow tract (OFT) and the proximal great vessels (Kirby and Waldo, 1990; Kirby and Waldo, 1995). The fate of cardiac neural crest cells has been traced using a quail chick chimera system (Kirby et al., 1983). Once they reach the OFT the cardiac neural crest cells specifically contribute to the aorticopulmonary septation complex - two opposing spirals which will later merge together and dissect the single OFT into two vessels, the aorta and the pulmonary artery.

Another example of an extracardiac tissue essential for heart development is the outer layer of the heart - the epicardium. This tissue is of great importance for correct

development of the heart, and yet it has received a disproportionately small amount of scientific study. The importance of the epicardium was first demonstrated by blocking its development in the chick (Manner, 1993). Failure to form the epicardium caused lethal cardiac phenotypes.

1.3 Origins Of The Epicardium

The epicardium is the final layer of the heart to develop. It is the only layer of the heart to originate exclusively from outside the primitive heart field. It originates from the proepicardium - a cluster of cells located ventrally at the limit between the liver and sinus venosus, but its structure differs depending on the species. The proepicardium can be bilateral (in the mouse), or unilateral, located to the right of the sagittal plane (in the chick). The structure of the proepicardium has been described for a representative of all vertebrate groups.

The dogfish (*Scyliorhinus canicula*) is the most primitive species to have its proepicardium structure described (Munoz-Chapuli et al., 1997). Here two large clusters of mesothelial cells develop on the ventral anterior portion of the epithelium covering the primitive liver at its limit with the sinus venosus. Later the septum transversum will develop in this limit, displacing the proepicardial cells towards the pericardial surface of the cardiac septum.

No comparable structure has yet been examined in a teleost species. However, the epicardium of the plaice (*Pleuronectes platessa*) has been described as coming from an extracardiac source although its characteristics are unclear (Santer and Cobb, 1972). Similarly the development of the epicardium of a reptile, the turtle (*Chelydra serpentina*), has been described as being similar to the chick though without further elaboration (Hiruma and Hirakow, 1989).

Amongst amphibians, the proepicardium has only been described for urodeles. The proepicardium of the axolotl (*Ambistoma mexicanum*), has been analysed using Scanning Electron Microscopy (SEM) to analyse the surface structure of the heart (Fransen and Lemanski, 1989; Fransen and Lemanski, 1990). In this species the

epicardium originates from spherical mesothelial cells located on the anterior aspect of the septum transversum. No comparable study has been made of anuran amphibians.

The structural organisation of the chick (*Gallus gallus*) proepicardium has been extensively described. Outgrowth of the proepicardium can first be observed at Hamburger and Hamilton stage (HH) 14 (Ho and Shimada, 1978). This is seen as rapid proliferation of the mesothelium that covers the horns of the sinus venosus at the limit of the primitive liver. Soon after it begins, proliferation of the left side stops, whilst proliferation of the right side continues until it is greatly increased in size by HH17. By this stage of development the proepicardium consists of multiple protrusions and as such has been described as having a 'cauliflower-like' appearance (Manner, 1992) . These protrusions are covered by mesothelium and contain large numbers of mesenchymal cells in an extracellular matrix.

Unlike the unilateral, right-sided proepicardium of the chick, the equivalent structure in the mammal is bilateral. Development of the mouse proepicardium begins at E9.5 from the pericardial surface of the septum transversum adjacent to the sinus venosus (Viragh and Challice, 1981). Here the protrusions first consist of rounded cells. It is not until later that the protrusions are covered by mesothelium and contain mesenchymal cells and extracellular matrix. At this stage the mouse proepicardium is structurally similar to the avian equivalent.

1.4 Transfer Of Proepicardial Cells To The Myocardium

Since the proepicardium originates and proliferates outside of the primary heart region, cells must migrate from the proepicardium to the heart in order to constitute the epicardial layer. The method of transfer is another source of variation between species. Two main mechanisms of transfer have been described. The first involves individual cells, or groups of cells, being shed from the proepicardium into the pericardial cavity (Komiyama et al., 1987). These cells then attach to specific areas of the naked myocardium. The main areas of attachment are the atrioventricular (AV) and conoventricular (CV) canals. Once the proepicardial cells have adhered to these

areas, they flatten and fuse to form an epithelium that will progressively develop over the surface of the heart. This is the only method of transfer thought to be present in the dogfish (Munoz-Chapuli et al., 1997). It is also thought to coexist in both mammals (Komiyama et al., 1987) and urodele amphibians (Fransen and Lemanski, 1989; Fransen and Lemanski, 1990) together with the second method.

The second method of proepicardial transfer involves direct adhesion of the proepicardial protrusions to the cardiac surface (Nahirney et al., 2003). Due to the physical proximity of the proepicardium, the area of attachment is usually the posterior dorsal region of the ventricles and the AV canal. This method of transfer is thought to be the primary one used by the chick (Manner, 1992; Nahirney et al., 2003), although free floating cells are occasionally observed here too. This is due to differences in the timing of septum transversum development. In the chick septum transversum development is delayed such that at the time of proepicardial outgrowth a large communication exists between the pericardial cavity and the coelomic cavity. If proepicardial cells were released directly into the pericardial cavity, they would be lost through the incomplete septum transversum (Hiruma and Hirakow, 1989).

The direct adhesion of proepicardial cells to the naked surface of the myocardium suggests the existence of a mechanism of recognition and attachment. Several mechanisms have been proposed. Neural Cell Adhesion Molecule (NCAM), a membrane-bound glycoprotein that plays a role in cell-cell and cell-matrix adhesion, is expressed in both the epicardium and the myocardium (Lackie et al., 1991; Watanabe et al., 1992). However, mice deficient for NCAM shown no epicardial defects (Cremer et al., 1997). Similarly, discrete patches of the naked myocardium have been found to express fibronectin, another membrane-bound glycoprotein that plays a role in cell-cell and cell-matrix adhesion (Kalman et al., 1995). The adhesion of free floating cells is accompanied by a strong increase in fibronectin expression at the epicardium/myocardium interface (Tidball, 1992). Again, however, mice deficient for fibronectin show no epicardial defects (George et al., 1993).

Although little is known about the mechanism of initial attachment of proepicardial cells, two molecules have been implicated in the long-term attachment of the epicardium to the myocardium. Mice deficient for either of the cell-surface

glycoproteins Vascular Cell Adhesion Molecule (VCAM-1) (Kwee et al., 1995), or integrin alpha-4 (itga4) (Yang et al., 1995) show similar abnormalities in epicardium development. Both mutants show a normal phase of attachment of proepicardial cells to the myocardium. However, the epicardium soon falls away and disappears, leading to death via pericardial haemorrhaging. This phenotype is consistent with the fact that VCAM-1 is a known ligand of itga4 (Lobb et al., 1995), and VCAM-1 is known to be expressed in the developing myocardium, and itga4 in the epicardium (Pinco et al., 2001).

Regardless of which method of migration is used, the pattern of epicardial migration over the surface of the heart is consistent between all species studied. First the epicardium progresses around the AV canal, followed by the left ventricle, ventral surface of the atria, the right ventricle, and finally the roof of the atria and the OFT (Fransen and Lemanski, 1990; Komiyama et al., 1987; Vrancken Peeters et al., 1995). Although the pattern of migration is conserved between species, it is much more patchy in the mouse compared to the chick as seen with Retinaldehyde Dehydrogenase (RALDH2) antibody staining (Moss et al., 1998; Xavier-Neto et al., 2000). This is probably due to the more random method of proepicardial attachment seen in the mouse compared with the chick.

The epicardium does not cover the entire surface of the heart. It has been shown in both chick and mouse that the epicardium stops at the junction between the myocardial and mesenchymal regions of the OFT (Manner, 1999; Perez-Pomares et al., 2003). It is not known why the epicardium does not cover the entire length of the OFT, nor why it stops at the junction between the myocardial and mesenchymal regions of the OFT.

1.5 Generation Of Mesenchyme Via Epithelial To Mesenchymal Transition

As the epicardium covers the embryonic myocardium, a subepicardial space develops between the two layers. The development of the subepicardial space was first described in the dogfish (Muñoz-Chápuli et al., 1996), but has since been shown to be the same in a mammalian species, the Syrian hamster (*Mesocricetus auratus*), and the

chick (Perez-Pomares et al., 1997). The subepicardial space is first seen around the AV and CV canals, and later around the surface of the ventricles. There is very little subepicardial space around the atria where the epicardium adheres tightly to the myocardium. The subepicardial space is soon populated with mesenchymal cells. It was previously thought that these mesenchymal cells migrated across from the proepicardium along with the epicardial cells themselves (Manner, 1992). It is now known that these cells are generated via an epithelial to mesenchymal transition (EMT) of cells of the epicardium (Perez-Pomares et al., 1998b). Cells that are produced in this way are known as Epicardium-Derived Cells (EPDCs).

During their formation, EPDCs acquire mesenchymal characteristics allowing them to separate from neighbouring cells of the epicardium, reorganise their cytoskeleton, breakdown the basement membrane and underlying extra-cellular matrix, and acquire a migratory capacity (Hay, 1995). The EMT begins in the AV and CV canals, and later in other areas of the ventricular epicardium. Very little EMT is observed around the atria (Perez-Pomares et al., 1998b).

The exact mechanism that initiates epicardium EMT is poorly understood. Since epicardium EMT is first observed around the AV and CV canals, it was thought that it might be initiated by the same signals that initiate another EMT that takes place in this area - the formation of valvuloseptal mesenchyme (Markwald et al., 1996). In this case, members of the Bone Morphogenetic Protein (BMP), and Transforming Growth Factors-β (TGF-β) families are essential for EMT (Nakajima et al., 2000; Romano and Runyan, 2000). It was shown that addition of Noggin, a BMP antagonist, or an antiTGF-β2 antibody inhibited valvuloseptal EMT *in vitro*. The situation with the epicardium, however, is less clearly understood. Here the Fibroblast Growth Factor (FGF) family has been shown to be important. FGF-1, 2 and 7 have been shown to stimulate epicardium EMT *in vitro*, while TGF-β1, 2 and 3 inhibit it (Morabito et al., 2001). Conversely TGF-β1 and TGF-β2 have been shown to stimulate EMT of an *in vitro* proepicardial culture (Compton et al., 2006; Olivey et al., 2006). Perhaps contact with the myocardium causes a different response from proepicardial cells to TGF-β signals. The BMP family have not been shown to be important for epicardial EMT,

however it has been suggested that stimulation by FGFs is only possible after an initial BMP activation signal (Munoz-Chapuli et al., 2002).

Once epicardium EMT has been initiated, the zinc finger-containing transcription factors of the snail family, *Snail* and *Slug*, become important. *Snail* was first identified in *Drosophila,* where it was shown to be essential for mesoderm formation (Grau et al., 1984). Analysis of *Snail* expression in both *Xenopus* and mouse has confirmed a role in mesoderm formation (Nieto et al., 1992; Sargent and Bennett, 1990; Smith et al., 1992). *Slug* has been shown to be important for the EMT event that occurs at the formation of mesoderm during gastrulation, and on migration of the neutral crest from the neural tube in chick (Nieto et al., 1994). *Slug* has also been shown to be essential for EMT of the endocardium during endocardial cushion formation (Romano and Runyan, 1999; Romano and Runyan, 2000), and has also been shown to be expressed in the epicardium and EPDCs (Carmona et al., 2000). *Slug* and *Snail* appear to operate by repressing the expression of cell adhesion molecules. *Slug* has been shown to repress desmoplakin and desmoglein, proteins associated with the desmosome cell adhesion complex (Savagner et al., 1997), whilst *Snail* represses E-cadherin, an epithelial cell-associated cell adhesion protein (Batlle et al., 2000; Cano et al., 2000).

Other zinc finger-containing transcription factors have been implicated in epicardium EMT. Ets-1 is known to be expressed in regions of the chick epicardium undergoing EMT (Macias et al., 1998). Ets-1 activates the expression of proteolytic enzymes that are important in the degradation of extracellular matrix (Wasylyk et al., 1993). The zinc finger transcription factor Wilms tumour 1 (WT1) appears not to be involved in epicardium EMT itself, however it has been shown that WT1 preferentially maintains a mesenchymal state of the epicardium over the differentiated, migratory state (Carmona et al., 2001) .

One final transcription factor that has been implicated in epicardium EMT is Friend of GATA2 (FOG2). FOG2 is expressed in the myocardium together with three of its cofactors, GATA4, 5 and 6 (Lu et al., 1999; Molkentin, 2000; Svensson et al., 1999; Tevosian et al., 1999). Mice deficient for FOG2 do not undergo epicardial EMT and are characterised by an absence of EPDCs, lack of coronary vasculature, and

ventricular hypoplasia (Tevosian et al., 2000). This suggests that FOG2 could be a component of a myocardial signal for the initiation of epicardial EMT.

1.6 Epicardium Derived Cells Adopt A Migratory State

In an *in vitro* assay, epicardial monolayers have been shown to invade a collagen matrix in the presence of FGF2, VEGF, or Epidermal Growth Factor (EGF) (Dettman et al., 1998). This suggests that the EPDCs resulting from epicardial EMT have invasive properties.

Epicardial chimeras have been used to track the fate of these invading EPDCs *in vivo*. This involves removing the proepicardium of a chick embryo and replacing it with a stage matched quail proepicardium. The fate of EPDCs can then be observed by staining with the quail specific antibody QCPN (Gittenberger-de Groot et al., 1998; Vrancken Peeters et al., 1999). QCPN positive cells were found in the myocardial wall and AV cushions (Gittenberger-de Groot et al., 1998), and both the smooth muscle cells and fibroblasts of the coronary vasculature (Gittenberger-de Groot et al., 1998; Vrancken Peeters et al., 1999). It has also been suggested, through lineage analysis data, that EPDCs contribute to the endothelium of the coronary vasculature (Perez-Pomares et al., 1998b). These findings imply a cellular contribution of the epicardium to numerous regions of the developing heart.

1.7 A Role In Coronary Vasculature Development

The main contribution of the epicardium to the developing heart is to the coronary vasculature. As a result, it is this area that has received the most scientific investigation. The coronary vasculature consists of blood vessels that transport gases to and from the myocardium. Although blood fills the cardiac chambers, the myocardium is so thick that it requires coronary blood vessels to deliver blood deep into the myocardium. This holds true for higher vertebrate species such as mouse and chick, but not for amphibians as will be discussed later.

Historically it was thought that the coronary vasculature was an outgrowth of the aorta, and therefore the coronary vasculature endothelium and smooth muscle was simply the angiogenic continuation of the aortic endothelium and smooth muscle. This view has since been challenged and proved to be incorrect. It was found that coronary endothelial precursors are organised within the subepicardial space, where a vascular plexus forms independently of, and prior to connection to, the aorta in a vasculogenic process (Bogers et al., 1989; Waldo et al., 1990).

Vasculogenesis occurs in two phases. The first involves the assembly of angioblasts and mesodermal endothelial precursors. During the second phase the endothelial tubes recruit mesenchymal cells and induce them to differentiate into pericytes and smooth muscle cells. Because the coronary vasculature arises via vasculogenesis, the precursors of the coronary endothelium, fibroblasts, and smooth muscle cells must be present in the subepicardial mesenchyme. Proepicardial chimera experiments have established that EPDCs are the progenitors of both the coronary smooth muscle and fibroblasts (Gittenberger-de Groot et al., 1998; Vrancken Peeters et al., 1999). The progenitors of the coronary endothelium, however, are less clear.

Two conflicting theories exist regarding the origin of the coronary endothelium. The first proposes that the angioblasts necessary for vasculogenesis migrate to the subepicardial space from the liver (Manner, 1992). The second proposes the angioblasts differentiate form EPDCs (Perez-Pomares et al., 1998b). The first theory is supported by the observation that a quail donor proepicardium only contributes to the coronary endothelium of a chick recipient if it was implanted together with a piece of adjacent donor liver (Poelmann et al., 1993). However, in some examples of proepicardial chimeras, the recipient chick proepicardium is not completely removed. This results in a mosaic epicardium comprising of both quail donor and chick recipient epicardium cells (Perez-Pomares et al., 1998b). This leads to chick mesenchyme beneath the chick epicardium, and quail mesenchyme beneath the quail epicardium. The endothelial layer of the coronary vasculature that developed in these examples was also a mosaic of both chick and quail cells.

The second theory is also supported by the observation that the labelling of the chick proepicardium with fluorescent tracer molecules and retroviruses shows a direct contribution to the coronary endothelium (Perez-Pomares et al., 2002a). Also Vascular Endothelial Growth Factor Receptor 2 (VEGFR2), the earliest known vascular marker, is coexpressed with the epicardial marker cytokeratin, in subepicardial mesenchyme cells (Perez-Pomares et al., 1998a).

This is a particularly interesting finding when considered with the discovery of a bipotential vascular precursor cell derived from embryonic stem cells and selected by its expression of VEGFR2 (Yamashita et al., 2000). When cultured with Platelet-Derived Growth Factor BB (PDGF-BB) these cells differentiate into smooth muscle cells. When cultured in the presence of VEGF they differentiate into endothelial cells. When exposed to both growth factors, they differentiate into mixed cultures of endothelial cells surrounded by smooth muscle cells. This has lead to the suggestion that EPDCs could be the pluripotent progenitors of the coronary vasculature. The epicardium is know to express VEGFR2 (Perez-Pomares et al., 1998a) and PDGFRβ (Shinbrot et al., 1994), the high affinity receptors for those growth factors shown to induce a bipotential vascular precursor in vitro (Yamashita et al., 2000). A model for this process has been proposed as follows (Munoz-Chapuli et al., 2002): BMPs and FGFs from the myocardium stimulate epicardial EMT and the generation of subepicardial mesenchyme. Early EPDCs would be induced to differentiate into endothelial cells by the high levels of VEGF being secreted by the myocardium (Tomanek et al., 1999) and epicardium. These cells would organise into a primary vascular plexus, which would then recruit subsequent EPDCs to differentiate into smooth muscle cells through the production of PDGF-BB from the endothelium (Folkman and D'Amore, 1996). This model is summarised in figure 1-1.

Recently the actin monomer binding protein Thymosin β4 (Tβ4) has been shown to be important for the differentiation of the coronary vasculature from EPDCs (Nicola et al., 2007; Smart et al., 2007). Mice deficient for Tβ4 show impaired cardiac vasculogenesis which leads to a reduction in cardiomyocyte survival, which in turn results in a reduced compact layer and disrupted myocardial architecture. The process of EMT was not disrupted in these mice, but following EMT the cells failed to

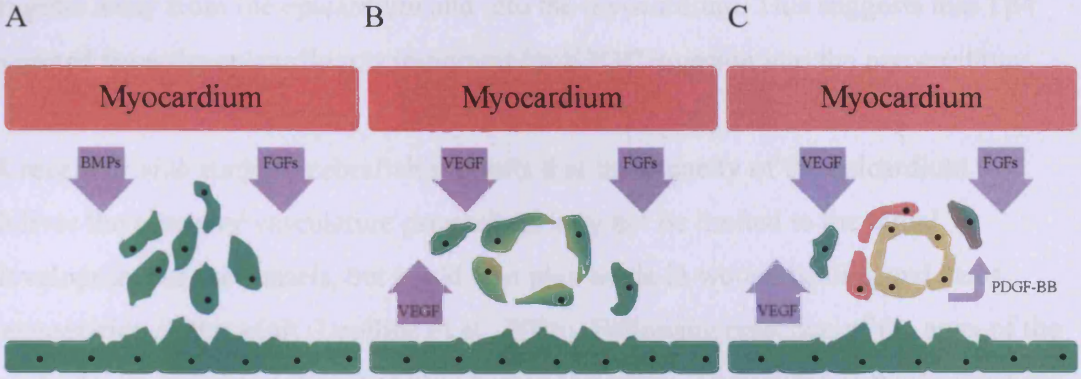

Figure 1-1. Role of the epicardium in coronary vasculature development.
(A)- BMPs and FGFs from the myocardium stimulate epithelial to mesenchymal transition of the epicardium (green) to produce EPDCs. (B)- VEGF secreted by both the myocardium and epicardium stimulates early EPDCs to differentiate into vascular endothelial cells (tan) and from a primary vascular plexus. (C)- subsequent EPDCs would be stimulated to differentiate into smooth muscle cells (red) by endothelium-secreted PDGF-BB.

migrate away from the epicardium and into the myocardium. This suggests that Tβ4 secreted from the epicardium is important for EPDC invasion into the myocardium.

A recent *in vivo* study in zebrafish suggests that the capacity of the epicardium to deliver the coronary vasculature progenitors may not be limited to the initial development of the vessels, but could also play a role in wound healing and heart regeneration in the adult (Lepilina et al., 2006). Following resection of the apex of the ventricle, an epicardial layer rapidly covered the injury. The source of this epicardium could have been the stimulation of surrounding quiescent adult epicardial cells. Alternatively the epicardium could have come from a progenitor population. In support of this theory, the response of the epicardium to injury mimicked the pattern of epicardial covering of the heart during embryonic epicardium formation. The epicardium not only covered the injury but also generated mesenchymal cells via EMT, a subpopulation of which invaded the regenerating myocardium and differentiated into new vascular tissue. The EMT was thought to be initiated by FGF signalling. FGF17b was found to be up regulated in the myocardium surrounding the injury whilst EPDCs expressed the FGF receptors FGFr2 and FGFr4. Blocking FGF signalling led to incomplete regeneration. The finding that the epicardium plays a role in adult heart regeneration following trauma is an interesting one. It should be noted however that zebrafish has a unique heart regeneration capacity (Poss et al., 2002) and as such these findings might be specific to this species.

1.8 A Role In Myocardium Development Modulation

The second most studied role of the epicardium is its role in modulating myocardium development. The first indication of this role was found during an *in vitro* analysis of a primary myocardial cell culture (Eid et al., 1992). Here it was found that myocardial cells undergo a process of dedifferentiation, where they change their structure, function, and gene expression profile. When the myocardial cells were co-cultured with epicardial cells, this process was significantly delayed and they maintained their contractility for longer. The first functional *in vivo* evidence of this role was seen following blocking of proepicardial outgrowth in chick embryos (Manner, 1993).

Experimental embryos failed to form the epicardium, which resulted in a thin ventricular compact layer, and round, disorganised cardiomyocytes.

During heart development in both mouse and chick, the primary phase of ventricular compaction coincides with an invasion by EPDCs into the myocardium (Carmona et al., 2001; Gittenberger-de Groot et al., 1998). The EPDCs that invade the ventricular myocardium maintain the expression of the transcription factor WT1. This is in contrast to the EPDCs that differentiate into the coronary vasculature where WT1 is switched off (Perez-Pomares et al., 2002b). Mice deficient for WT1 show severe malformations of the genitourinary system, but die perinatally from heart failure caused by ventricular hypoplasia, characterised by a thin ventricular wall and a failure to form the compact layer (Kreidberg et al., 1993). The epicardium in these mice was found to develop normally, and some EPDCs were generated, but much fewer than in wild type mice. Because WT1 is expressed exclusively in the epicardium and the myocardium-invading EPDCs, it appears that ventricular compaction is dependent on myocardial invasion by EPDCs.

The exact nature of the signal between the epicardium and underlying myocardium is poorly understood but retinoic acid and erythropoietin appear to be important (Stuckmann et al., 2003). The retinoic acid synthesising enzyme RALDH2 is known to be expressed in the epicardium and EPDCs in both mouse and chick (Moss et al., 1998; Perez-Pomares et al., 2002b; Xavier-Neto et al., 2000). The EPDCs that invade the myocardium also express RALDH2, however expression diminishes over time and is downregulated on differentiation of the EPDCs (Perez-Pomares et al., 2002b). The importance of retinoic acid is seen in mice deficient for the retinoic acid receptor RXRα. These mice show a ventricular hypoplasia phenotype identical to the mice deficient for WT1 (Kastner et al., 1994; Sucov et al., 1994). This would suggest that retinoic acid produced by the epicardium and EPDCs is the signal that induces ventricular compaction. However, the addition of retinoic acid, alone or in combination with erythropoietin, to a culture of myocardial cells is not sufficient for myocardial proliferation and compaction. Only in a coculture of myocardial and epicardial cells has retinoic acid and erythropoietin been found to induce myocardial proliferation (Stuckmann et al., 2003). Also, mice with a myocardial-specific deletion

of the RXRα gene show no abnormalities (Chen et al., 1998; Tran and Sucov, 1998). These findings suggest that retinoic acid does not act directly on the myocardium.

Because EPDCs also express RXRα, it has been proposed that retinoic acid is important for the maintenance of an autocrine loop that keeps the EPDCs in an undifferentiated state. This would allow the EPDCs to continue signalling to the myocardium. FGF9 appears to be one component of this loop. Retinoic acid can induce the expression of FGF9 in epicardial cell culture (Lavine et al., 2005). $FGF9^{-/-}$ mice died at birth due to hypoplastic lungs and an enlarged, dilated heart (Colvin et al., 2001), whilst at E12.5, $FGF9^{-/-}$ hearts were found to be much smaller than wild-type littermates, had a thin ventricular wall and reduced trabeculation. An identical phenotype has been described in $RALDH2^{-/-}$ (Mic et al., 2002) and $erythropoietin^{-/-}$ (Wu et al., 1999) mice. The embryonic myocardium has been shown to express the FGF receptors FGFR1 and FGFR2c (Lavine et al., 2005), both of which can be activated by FGF9 (Ornitz et al., 1996). These findings, together with the above observation that retinoic acid does not signal directly to the myocardium, suggest FGF9 is required by the myocardium for normal heart development, and its secretion by the epicardium is activated by an autocrine positive feedback loop of epicardium-secreted retinoic acid. These findings are summarised in figure 1-2.

1.9 A Role In Cardiac Conduction System Development

The physical proximity between the final destination of migrating EPDCs and the location of Purkinje fibre differentiation, has led to a suggestion that EPDCs are important for correct development of the Purkinje network (Eralp et al., 2006; Gittenberger-de Groot et al., 1998). Retroviral tagging experiments have shown that the periarterial Purkinje fibres differentiate from cardiomyocytes in close proximity to the coronary vasculature (Gourdie et al., 1995; Hyer et al., 1999), whereas the subendocardial Purkinje network differentiates close to endocardial cells. It has been suggested that these differentiation sites implicate an inductive role of periarterial and subendocardial EPDCs in the recruitment of cardiomyocytes into the Purkinje network (Gittenberger-de Groot et al., 2003; Gourdie et al., 2003).

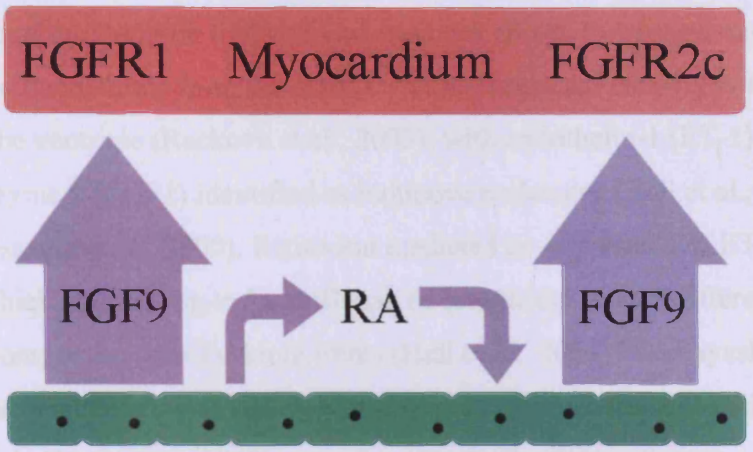

Figure 1-2. The role of the epicardium in myocardium development modulation.

FGF9 signaling, through FGF receptors 1 and 2c, is required by the myocardium for correct development of cardiac muscle. FGF9 secretion by the epicardium (green) is maintained by an autocrine positive feedback loop of epicardium-secreted retinoic acid (RA).

Differentiation of the Purkinje fibres *in vivo* has been shown to be regulated by haemodynamic fluctuations from the coronary vasculature and endocardial lining of the lumen of the ventricle (Reckova et al., 2003), with endothelin-1 (ET-1) and ET-converting enzyme 1 (ECE1) identified as inductive molecules (Hall et al., 2004; Takebayashi-Suzuki et al., 2000). Retroviral mediated co-expression of ET-1 and ECE1 in the chick, was shown to be sufficient to ectopically induce differentiation of adjacent cardiomyocytes into Purkinje fibres (Hall et al., 2004; Takebayashi-Suzuki et al., 2000). Due to EPDCs being widely distributed throughout the myocardium (Gittenberger-de Groot et al., 1998), even the ectopically differentiating cardiomyocytes could be influenced by adjacent EPDCs.

By mechanically inhibiting proepicardial outgrowth via the insertion of eggshell membrane, or genetically inhibiting epicardial EMT via retroviral expression of antisense Ets1/2, transcription factors whose down regulation has been shown to inhibit epicardium development (Lie-Venema et al., 2003), the role of EPDCs in Purkinje fibre development has been assessed in the chick (Eralp et al., 2006). The effect of these procedures is variable, ranging from complete inhibition of an epicardial contribution to heart development, which results in early lethality, to a very subtle effect where no gross abnormalities can be seen. By selecting embryos that survive beyond HH39, it was possible to study only those embryos where gross heart structure and the coronary vascular system were normal, thus ensuring any Purkinje network malformations could not be the result of coronary vascular malformations.

Nevertheless, Purkinje fibre malformations were observed in both the mechanically and genetically inhibited embryos. The most severe malformations were observed in the subendocardial Purkinje fibres. The Purkinje cells of control embryos were aligned in continuous, fibre-like strands. The Purkinje cells of inhibited embryos were abnormally large, rounded, and had failed to differentiate into a coherent Purkinje fibre network. This suggests that EPDCs are important for induction and/or organisation of the subendocardial Purkinje network. The molecular mechanism of EPDCs on Purkinje fibre differentiation is not known, but a direct paracrine effect has been proposed whereby EPDCs cooperate with endothelial cells in the differentiation of cardiomyocytes into conductive tissue (Eralp et al., 2006).

One possible model of the role of EPDCs in Purkinje fibre differentiation is shown in figure 1-3. Here a two hit hypothesis is proposed whereby an unidentified EPDC-secreted factor causes adjacent cardiomyocytes to become induction-competent cardiomyocytes. The second hit comes from endocardium-secreted ET-1 which has been stimulated by haemodynamic fluctuations. A similar mechanism is also possible in the case of periarterial Purkinje cells. In this case ET-1 would be secreted by the vascular endothelial cells. It is probable that the unidentified EPDC-derived factor is a transcription factor that activates transcription of the ET-1 receptor in the induction-competent cardiomyocytes.

1.10 A Role In Valve Development

Quail-chick chimera studies have shown that EPDCs invade the endocardium-derived mesenchyme of the AV cushions (Gittenberger-de Groot et al., 1998; Manner, 1999). This has led to a suggestion that EPDCs play a role in the formation of the AV valves (Gittenberger-de Groot et al., 1998). In support of this suggestion, AV valve malformations have been observed in numerous studies where the proepicardium has been blocked or excised, or epicardium development otherwise inhibited in the chick (Eralp et al., 2005; Gittenberger-de Groot et al., 2000; Perez-Pomares et al., 2002b; Poelmann et al., 2002). Not all studies concur however. Whilst one group reported the AV cushions were usually absent and did not fuse resulting in a common AV canal (Eralp et al., 2005; Gittenberger-de Groot et al., 2000; Poelmann et al., 2002), another group reported the AV cushions were abnormally large but no fusion defects were evident (Perez-Pomares et al., 2002b). The inconsistencies in these findings could be due to variation in the success of eliminating the contribution from the proepicardium. A recent study employed a more efficient technique to eliminate the proepicardium (Manner et al., 2005). Using photoablation the proepicardium was completely removed from 15 chick embryos. Only one had AV valve malformations. It therefore, remains unclear whether the EPDCs play a role in AV valve formation. Quail-chick chimera experiments demonstrate an early cellular contribution of EPDCs to the valves (Gittenberger-de Groot et al., 1998; Manner, 1999), however, the cellular contribution of EPDCs to the mature mouse AV valves has been shown to be minor (de Lange et al., 2004).

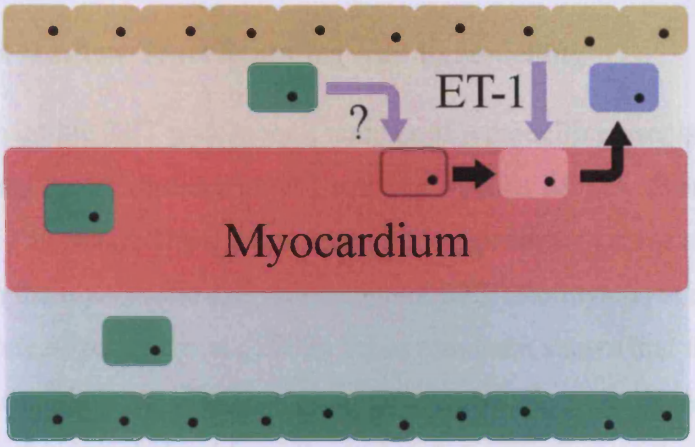

Figure 1-3. Role of EPDCs in conduction system development.
Purkinje cells (blue) develop in subendocardial domains where EPDCs (green) are also found. Purkinje cells are induced via two inductive hits. Firstly an unidentified EPDC-derived factor causes adjacent cardiomyocytes to become induction-competent cardiomyocytes. Haemodynamic fluctuations then cause the endocardium (tan) to secrete ET-1 that acts as the second hit causing the induction-competent cardiomyocytes to differentiate into Purkinje cells.

1.11 A Role In Outflow Tract Sculpting And Remodelling

During development the OFT undergoes a number of remodelling events and it has been suggested that the epicardium plays a role in a number of these events. Most, but not all, of the OFT is covered by the epicardium. The epicardium stops abruptly at the junction between the myocardial and mesenchymal OFT (Komiyama et al., 1987; Manner, 1999; Perez-Pomares et al., 2003). It has also been shown that the epicardium covering the most distal region of the chick OFT, is not derived from the proepicardium, rather it is derived from the pericardial epithelium in the vicinity of the aortic sac (Perez-Pomares et al., 2003).

One of the first remodelling events to occur is shortening of the OFT myocardium (Ya et al., 1998). This has been shown to be achieved by cardiomyocytes of the OFT undergoing apoptosis (Watanabe et al., 1998; Watanabe et al., 2001). The OFT epicardium also shortens during this time, again via apoptosis (Cheng et al., 2002; Rothenberg et al., 2002). OFT apoptosis was found to be disrupted in chick embryos that had undergone a proepicardial block (Rothenberg et al., 2002), suggesting that the epicardium plays some role in OFT remodelling.

Certainly a temporal relationship has been identified between development of the epicardium and the appearance of apoptosis within the underlying OFT myocardium in chick (Schaefer et al., 2004). Apoptosis within the OFT is initiated only a few stages behind it being covered by the epicardium. Cells from the OFT epicardium undergo an EMT but the resultant EPDCs do not enter the OFT myocardium prior to apoptosis occurring. Therefore whatever triggers OFT myocardium apoptosis does not require direct contact between EPDCs and cardiomyocytes.

Two models have been proposed to account for these findings: 1) EPDCs or the epicardium itself are secreting pro-apoptotic factors and 2) the epicardium is inducing hypoxia within the OFT myocardium. These models are summarised in figure 1-4. No direct evidence exists for the secretion of pro-apoptotic factors, however growth factor signalling between the epicardium and the myocardium is known to occur (Morabito et al., 2001). The epicardium surrounding the OFT is much thicker than

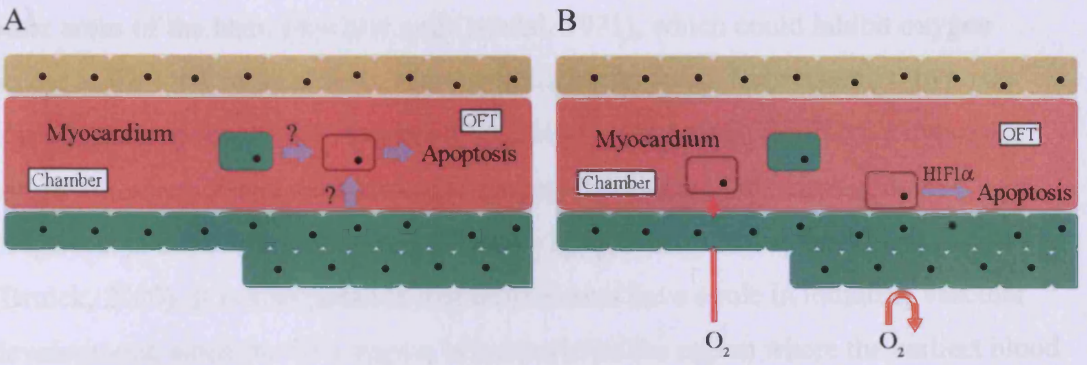

Figure 1-4. Two models for the role of the epicardium and EPDCs in OFT sculpting and remodelling. (A)- proapoptotic factors are being secreted by the epicardium and/or the proepicardium. (B)- the epicardium covering the OFT is significantly thicker than at other areas of the heart. This could prevent oxygen diffusion with the underlying myocardium. The resulting hypoxia could cause cardiomyocytes to secrete HIF1α and initiate apoptosis within the myocardium.

other areas of the heart (Rychter and Ostadal, 1971), which could inhibit oxygen access to the OFT myocardium, thereby initiating hypoxia. Subsequently, hypoxia could initiate apoptosis via Hypoxia-Inducible Factor 1 alpha (HIF1α), a hypoxia sensitive transcription factor known to be expressed in the OFT myocardium (Sugishita et al., 2004) and known to induce apoptosis under oxygen deprivation (Bruick, 2000). It is also possible that these events have a role in initiating vascular development, since the OFT region is known to be the region where the earliest blood and lymphatic vessels form (Rychter and Ostadal, 1971) and the vasculogenic mitogen VEGF, which is expressed in the myocardium (Lagercrantz et al., 1998), is a known target of HIF1α (Forsythe et al., 1996).

1.12 Genes Expressed In The Epicardium And Proepicardium

1.12.1 Tbx18

T-box genes are members of a large gene family that encodes transcription factors characterised by a conserved N-terminal DNA-binding domain known as the T-box (Kispert and Hermann, 1993; Kispert et al., 1995). Experimental evidence from many model systems has demonstrated an important role for T-box genes in mesendoderm formation, patterning, and organogenesis. This importance is emphasised by a number of known mutations in T-box genes linked to hereditary human disorders (Papaioannou, 2001; Smith, 1999).

A number of T-box genes have been shown to play important roles in many aspects of heart development. Loss of Tbx1 in the mouse for example, is associated with abnormal growth and septation of the OFT, and interventricular septation and conotruncal alignment defects (Jerome and Papaioannou, 2001). Similarly, loss of Tbx2 in the mouse is associated with AV canal and OFT septation defects (Harrelson et al., 2004). Mutations in the human Tbx5 gene cause Holt-Oram syndrome which is characterised by many heart defects including atrial and ventricular septal defects, tetralogy of Fallot, hypoplastic left heart and conduction abnormalities (Basson et al., 1997; Li et al., 1997). A similar phenotype is found in Tbx5 heterozygous mice (Bruneau et al., 2001). Finally loss of Tbx20 in the mouse is associated with failed

cardiac looping, hypoplastic heart, and lack of cardiac chamber differentiation (Cai et al., 2005; Singh et al., 2005a; Stennard et al., 2005; Takeuchi et al., 2005).
Two T-box genes have been implicated in epicardium development. Tbx5 has been shown to be expressed in the developing epicardium of human (Hatcher et al., 2000) and mouse (Bruneau et al., 1999). Tbx5 has also been reported in the epicardium of *Xenopus laevis* (Horb and Thomsen, 1999). The evidence for this however is not convincing. Tbx5 was reported in the 'epicardium' as early as stage 35. This is long before epicardium development actually begins in *Xenopus* as will be shown later in this thesis. Tbx18 has also been shown to be expressed in the developing epicardium of mouse (Kraus et al., 2001) and chick (Haenig and Kispert, 2004), and around the 'heart and septum transversum region' in zebrafish (Begemann et al., 2002). Sections of the zebrafish heart region were not shown so the precise area of cardiac expression is unknown. Tbx5, unlike Tbx18, is also strongly expressed in the myocardium of the heart and so it was thought Tbx5 would be of little use as a marker of the epicardium in this study.

Conservation between species of the Tbx18 amino acid sequence has been shown to be very high. Mouse Tbx18 shares 100% identity within the T-box region, and 94.5% overall, with the human equivalent. Within the mouse T-box family, Tbx18 is most closely related to the Tbx8/14/15 gene, with 92.8% identity over the T-box region (Kraus et al., 2001).

With the exception of a few species differences, the expression pattern of Tbx18 in the mouse (Kraus et al., 2001), chick (Haenig and Kispert, 2004), and zebrafish (Begemann et al., 2002) are very similar. In all species expression is first observed at the onset of somitogenesis in the somitic and presomitic mesoderm. Expression around the heart region was first observed in the caudo-lateral wings of splanchnic mesoderm that comprise the developing septum transversum. Expression was seen in the proepicardium and developing epicardium. Other areas of expression included the genital ridge, paraxial head mesenchyme, mouth and olfactory epithelium, developing palette, and the limb bud.

Mice deficient for Tbx18 have been generated in order to investigate its role in development (Bussen et al., 2004). The primary phenotype that was observed was an

abnormal vertebral column caused by defective somite patterning. Heterozygous mice appeared normal and were fertile. Homozygous mice died shortly after birth. The mice were characterized by a shortened body and severe malformations of the vertebral column and thoracic cavity. The lungs failed to inflate properly resulting in lethal respiratory failure. Interestingly no gross morphological defects in the cardiovascular system and limbs were reported.

Another area where Tbx18 appears to be important is development of the urogenital system. In the same mouse line as above, several aspects of distal ureter development were found to be disrupted (Airik et al., 2006). Many of the prospective ureteral mesenchymal cells delocalised to the surface of the kidneys. The remaining ureteral mesenchymal cells showed reduced proliferation and failed to differentiate into smooth muscle cells, but instead became ectopic fibrous and ligamentous tissue. The lack of ureteral smooth muscle resulted in a short ureter that was unable to carry urine to the bladder.

Recently Tbx18 has been implicated in the formation of the venus pole of the heart (Christoffels et al., 2006). Here it was shown that the venous pole myocardium is made up of Nkx2.5 positive cardiomyocytes only until E9.5 at which point these cells are taken up into the atria and venous valves. Therefore the sinus horns - the precursors of the right superior and inferior caval vein, the coronary sinus and sinus venarum - do not develop until after E9.5. The mesenchymal precursors of the sinus horns do not express Nkx2.5, but they do express Tbx18. The hearts of $Tbx18^{-/-}$ embryos appeared grossly unaffected. However, histological sections showed that at E10.5 mutant embryos had failed to form the left sinus horn, and by E14.5 the veins within mutant hearts were thinner and abnormally positioned.

1.12.2 Epicardin

Epicardin (also known as capsulin, pod1, and Transcription Factor 21) is a member of the basic helix-loop-helix (bHLH) transcription factor family. They are so named because of the structure of their functional domain - two segments capable of forming amphipathic alpha helices, separated by a loop region of variable length. Immediately

N-terminal to the HLH domain is a basic domain that mediates DNA binding (Murre et al., 1989). Many cell type-specific bHLH transcription factors have been described and shown to control cell fate specification, differentiation and morphogenesis during vertebrate development (Jan and Jan, 1993; Kadesch, 1993).

The developmental expression pattern of epicardin has been described in the mouse (Hidai et al., 1998; Lu et al., 1998) and chick (von Scheven et al., 2006). In the mouse expression was detected in the proepicardium at E9.5. By E10.5 expression was detected in mesoderm cells surrounding the foregut, stomach and hindgut. Expression was also seen in the spiral septum within the OFT, the endocardial cushions of the heart, and the epicardium, especially around the AV canal. By E11.5 expression was prominent in the mesoderm surrounding the oesophagus and trachea, and also the urogenital sinus. By E12.5 expression was detected in the mesenchyme of the lung, metanephros and the mesenchyme surrounding the gonads. As can be seen from this expression pattern, epicardin is primary expressed in the mesodermal cells that surround the epithelium of tubular structures. These tubular structures are generally organs within the gastrointestinal, respiratory, genitourinary, and cardiovascular systems. Epicardin expression in the chick was very similar to that described for mouse.

The epicardin developmental expression pattern has also been described in *Xenopus laevis* (Simrick et al., 2005). Specific expression was first observed in the branchial arches at stage 26 and in the glomus by stage 28. At stage 40.5 expression was described in the presumptive epicardium and all the components of the pronephros. RT-PCR revealed expression could first be detected at stage 13, followed by a gradual increase in expression from stages 16.5 to 26.5, then maintenance of this concentration until stage 35. No stages beyond stage 35 were examined via RT-PCR.

Epicardin expression levels in the adult have also been described in mouse (Lu et al., 1998), and *Xenopus laevis* (Simrick et al., 2005). Using RT-PCR strongest expression was seen in the *Xenopus* rectum and spleen, with slightly weaker expression in the duodenum, heart, kidney, lung, pancreas, skin, liver, and skeletal muscle. A similar pattern was found in the mouse using northern blot. However, unlike *Xenopus*, no epicardin expression was seen in skeletal muscle.

The most important role of epicardin during development appears to be in kidney and lung organogenesis. Epicardin$^{-/-}$ mice die shortly after birth from hypoplastic lungs and kidneys (Quaggin et al., 1999). The metanephroi were characterised by an increase in mesenchyme surrounding the ureteric bud tips and disrupted formation of the nephrons. Normally differentiation of the tubular epithelium of the metanephros results in the formation of the functionally distinct regions of the nephron - the proximal tubule, loop of Henle, and distal nephron. This differentiation process never occurred in null mice as seen by the absence of proximal tubule epithelium. These phenotypes suggest epicardin is important for an interaction between mesenchymal and epithelial cells that occurs in the nephron, and for terminal differentiation of the tubular epithelium. A related phenotype was found in the branching morphogenesis of the lung. This is a process that requires interactions between the epithelium and underlying mesenchyme. An increase in bronchiolar epithelium was observed again suggesting epicardin is important to epithelial and mesenchymal interactions.

Epicardin deficiency has also been shown to disrupt gonad development and sex differentiation (Cui et al., 2004). The external genitalia of male mice were indistinguishable from the grossly normal female genitalia. On internal examination, the gonads of both males and females showed vascular abnormalities and the male specific coelomic blood vessel was absent from genetically male mice. A reduction in endothelial cell migration from the mesonephroi to the gonads was observed. This could explain the absence of the coelomic vessel and its branches in the testis as the coelomic vessel is known to originate from endothelial cells that migrate into the testis from the mesonephroi (Brennan et al., 2002). A reduction in gonadal pericytes was also observed in both male and female gonads. These are intimately associated with mesonephroi endothelial cells, are known to express epicardin (Cui et al., 2004), and are important for vasculogenesis within the gonads (Benjamin et al., 1998) and so probably account for the vascular abnormalities observed here.

In another epicardin null mouse spleen formation was found to be severely disrupted (Lu et al., 2000). The spleen primordium failed to develop beyond a group of splanchnic mesoderm precursor cells and eventually underwent apoptosis. The phenotype of epicardin mutant mice suggested that epicardin acts within a

subpopulation of splanchnic mesodermal cells to control an essential early step in spleen organogenesis.

1.12.3 Wilms tumour 1

The WT1 gene encodes a zinc finger DNA-binding protein that can act as an activator or repressor of transcription depending on the cellular context. The human WT1 gene was cloned from a Wilms tumour cell line (Huang et al., 1990), and by the creation of a physical map of chromosomal region 11p13 which is deleted in individuals with Wilms tumour (Rose et al., 1990).

Mutations within the WT1 gene have been identified in several solid tumour diseases including Wilms tumor-aniridia-genitourinary anomalies-mental retardation syndrome (WAGR syndrome) (Pelletier et al., 1991) Denys-Drash syndrome (Hastie, 1992), and Frasier syndrome (Barbaux et al., 1997). The most common disease resulting from a mutation in the WT1 gene is Wilms tumour, or nephroblastoma. It is one of the most common solid childhood tumours prevalent in around 1 in 10,000 children, and accounts for 8% of all childhood cancers (Breslow and Beckwith, 1982). The primary clinical features associated with Wilms tumour are genitourinary disorders, whilst the additional features of mental retardation and anomalous genitalia seen in other WT1-associated disorders, are probably caused by other genes (Schumacher et al., 1997).

A mutation has been introduced into the mouse WT1 gene (Kreidberg et al., 1993). The mutation resulted in embryonic lethality in homozygotes. Internal examination of mutant embryos showed a failure of kidney and gonad development. The cells of the metanephric blastema were found to have undergone apoptosis, the ureteric bud had failed to grow out from the Wolffian duct, and the inductive events that lead to formation of the metanephric kidney had not occurred.

The severity of the phenotype of WT1 deficient mice has made it difficult to study the role of WT1 in kidney development. However, the recent use of an *in vitro* kidney organ culture and siRNA has allowed this role to be studied (Davies et al., 2004). WT1 was found to induce the mesenchymal to epithelial transition (MET) necessary

for the formation of the nephrons. It has long been known that disruption to this process is the primary cause of Wilms tumours (Dressler and Douglass, 1992).

WT1 is expressed within the podocytes of the kidney throughout life. By combining a WT1 knockout mouse with an inducible human WT1 yeast artificial chromosome (YAC), the effect of variable doses of WT1 in the podocytes have been examined (Guo et al., 2002). WT1 null mice with one or two copies of the human WT1 YAC did not develop the embryonic lethal defects seen in homozygous WT1 knockout mice. Where only one copy of the YAC was present all mice died within 20 days of birth from glomerulosclerosis, an accumulation of mesangial matrix in the glomerular basement membrane. Where two copies of the YAC were present only 26% of mice died before 150 days from end-stage renal disease. Interestingly the podocyte specific gene nephrin (Lenkkeri et al., 1999) was shown via semi-quantitative RT-PCR to be reduced to 14% of wild type levels where only one copy of the YAC was present and 68% of normal levels when two copies were present. Expression of another podocyte specific gene podocalyxin (Lenkkeri et al., 1999), was also reduced. These findings suggest nephrin and podocalyxin act downstream of WT1.

The YAC strategy described above was used in an earlier experiment that identified a role for WT1 in epicardium development (Moore et al., 1999). The epicardium of WT1 null mice did not form correctly resulting in large gaps in the epicardium at the cranial end of the heart and absence of the epicardium over the ventral surface of the aorta. The presence of two copies of the human WT1 YAC rescued these phenotypes. Interestingly the WT1 null mice also showed a failure in diaphragm formation. The diaphragm is derived in part from the septum transversum. Perhaps WT1 is important for migration and proliferation of cells derived from the septum transversum.

The epicardial defect described above for WT1 knockout mice is remarkably similar to the defect described for the cell adhesion molecule itga4 knockout mice (Yang et al., 1995). A recent study has shown via quantitative RT-PCR that itga4 expression is reduced to 43% of normal levels in mice deficient for WT1 (Kirschner et al., 2006), suggesting WT1 is necessary for normal expression of itga4 in the epicardium.

Finally WT1 has been shown to be coexpressed in the epicardium and sub-epicardial

blood vessels with the high-affinity neurotrophin receptor TrkB (Wagner et al., 2005). TrkB was shown to be greatly reduced in the hearts of WT1 knockout mice, whilst activation of WT1 in an inducible cell line significantly increased TrkB expression. Transgenic experiments showed a WT1 consensus binding motif identified in the Ntrk2 (the gene that encodes TrkB) promoter was required to drive expression of a reporter gene in the epicardium and developing coronary vasculature of the embryonic mouse heart. Mice with a disrupted Ntrk2 gene had a reduction in the number of intramyocardial blood vessels. These findings suggest that transcriptional activation of the TrkB neurotrophin receptor gene by WT1 is important for normal development of the coronary vasculature.

Xenopus laevis WT1 has been cloned and its expression profile analysed (Carroll and Vize, 1996; Semba et al., 1996). Expression was first observed at stage 20 in two crescent shaped patches posterior to the head and ventral to the somites. The specific expression was seen in the general region in which the pronephros will form at stages 21-22, just ventral to somites 3 and 4, but does not precisely correspond to it. A crescent of expression extends around the dorsal border of the future anlage of the pronephric tubules and pronephric duct but does not stain the anlage itself. Histological sections revealed this area of expression corresponded to the future glomus. A similar pattern of expression was seen until stage 38 to 39 at which time expression was seen in the heart region. The precise areas of cardiac expression were not described and no stages beyond stage 39 were examined.

The role of WT1 in *Xenopus* kidney development has been investigated by ectopic injection of mRNA (Wallingford et al., 1998). *Xenopus* WT1 was injected into the presumptive pronephric region of 32-cell embryos. Embryos were raised to tadpole stages and analysed. Ectopic expression of WT1 resulted in restricted formation of the pronephric tubule anlage. This resulted in a reduction of tubule size and complexity compared to control tadpoles. Due to mRNA being injected into specific blastomeres to target pronephros formation, no heart phenotypes were described.

1.13 Why Investigate Epicardium Development In The Frog?

The frog heart has a number of structural differences that make it a good model for investigating the epicardium. Due to its simpler three-chambered structure and its spongy myocardium, the amphibian heart tissue receives sufficient oxygen via direct diffusion from the blood in the heart chambers and hence is devoid of coronary vasculature. Using the amphibian *Xenopus laevis* as a model will allow circumvention of previous biases towards defining a role for the epicardium in coronary vasculature formation. *Xenopus laevis* embryos are also readily manipulated experimentally, and are resilient to induced cardiac perturbations until late stages of development since cardiac function is not necessary until swimming tadpole stage. Frog embryos therefore have the potential to provide a simple experimental model to study the role of the epicardium in the relatively neglected areas of myocardium development modulation, OFT sculpting and remodelling, valve formation and conduction system formation.

Xenopus is an excellent system for studying early developmental events, however the use of *Xenopus* for research into later developmental events such as organogenesis, is not as popular as other vertebrate systems. Recent techniques such as transgenesis (Kroll and Amaya, 1996) and morpholino oligonucleotides (MOs) (Heasman, 2002), have made the study of organogenesis in *Xenopus* more accessible. Also the use of the diploid species *Xenopus tropicalis* has introduced the possibility of genetic studies of organogenesis in *Xenopus* (Hirsch et al., 2002). *Xenopus* is frequently used as a model to study heart development, and since the epicardium is known to be crucial for many aspects of heart development in other species, it is important that we understand the role of the epicardium in this species.

1.14 Aims And Objectives

The aims of this thesis were to: (1) establish the presence of the epicardium in the anuran amphibian *Xenopus laevis* and describe its structure in the adult; (2) describe the physical process of epicardium formation in *Xenopus laevis*; (3) identify the early embryological origins of the epicardium; (4) identify molecular markers of the epicardium; (5) investigate the effect of loss of function of these candidate genes in

order to understand their role in epicardium development, and therefore the wider role of the epicardium in heart development.

2 Materials And Methods

2.1 *Xenopus laevis* Frogs And Embryos

Female *Xenopus laevis* were induced to lay by the injection of 50 units of human chorionic gonadotropin (hCG) (Sigma) into the dorsal lymph sac on day 1, and 500-800 units, depending on size, on day 7. On day 8, eggs were harvested by gently squeezing the abdomen of an induced female. Eggs were collected in a Petri dish. Males were killed in 0.4% ethyl 3-aminobenzoate methanesulfonate (MS222) (Sigma) pH 7. Testes were dissected into 4°C L15 medium and stored at 4°C. Eggs were fertilized with macerated testis, left for 5 minutes, then flooded with 0.1x Normal Amphibian Medium (NAM) (Slack and Forman, 1980) containing 50μg/ml gentamicin (Sigma). Fertilised eggs were left for 2 hours before being de-jellied in 2% cysteine (Sigma) in 0.1x NAM pH 8. Embryos were staged according to the Normal Table of *Xenopus laevis* development (Nieuwkoop and Faber, 1994).

2.2 *Xenopus tropicalis* Frogs And Embryos

Female *Xenopus tropicalis* were induced to lay by the injection of 10 units of hCG into the dorsal lymph sac on day 1, and 100 units on day 2. On day 1, males were also injected with 100 units of hCG. On day 2 plus 4 hours, eggs were harvested by gently squeezing the abdomen of an induced female. Eggs were collected in a Petri dish containing 0.4x Marc's Modified Ringers (MMR) (Ubbels et al., 1983). Males were killed in 0.2% MS222 pH 7. Testes were dissected into room temperature L15 medium supplemented with 10% calf serum, and stored at 14°C. The 0.4x MMR was removed and the eggs were fertilised with macerated testis. The fertilised eggs were left for 4 minutes than flooded with 0.05x MMR containing 50μg/ml gentamicin. Fertilised eggs were de-jellied in 2% cysteine in 0.05x MMR pH 7.6 - 8. Embryos were staged according to the Normal Table of *Xenopus laevis* development (Nieuwkoop and Faber, 1994).

2.3 Fixation

Embryos were fixed in MEMFA at room temperature for 2 hours on a rocking platform. Tadpoles beyond the feeding stage were first anaesthetised in 0.02% MS222 before being fixed in MEMFA for 4 hours on a nutator. Where dissection of the pericardial cavity was required, fixed tadpoles were dehydrated to 100% ethanol, dissected, and then returned to MEMFA for a further 2 hours. All fixed tadpoles were dehydrated in 3 changes of 100% ethanol and stored at -20°C until needed.

2.4 Histology

2.4.1 Wax Sectioning

Fixed embryos were dehydrated through a graded series of ethanol for 5 minutes each followed by three 5-minute washes in 100% ethanol. Embryos were cleared in Histoclear (Raymond A Lamb) overnight. Embryos were than incubated in 50% Histoclear:50% Fibrowax (Raymond A Lamb) for 1 hour at 60°C, followed by similar incubations in 60%, 70%, 80%, 90% and finally 2 incubations in 100% Fibrowax. Embryos were placed in moulds, embedded in Fibrowax, and stored at 4°C before sectioning.

[The following procedures were carried out by Wendy Hatton, Histology Service, NIMR] Embedded samples were fixed onto wooden blocks with molten Fibrowax. Ribbons were cut on a Leica microtome and floated out on a 40°C waterbath. Sections were scooped out onto SuperFrost Plus Slides (Menzel-Gläser), and were allowed to dry horizontally on a Raymond A Lamb Slide drier at 45°C. Samples were dewaxed for 10 minutes each in 2 changes of Histoclear and immediately mounted under coverslips (Menzel-Gläser) in Permount mounting medium (Fisher).

2.4.2 Plastic Sectioning

Fixed embryos were dehydrated as described above. Embryos were preinfiltrated with a 50:50 mixture of 100% ethanol and Technovit 7100 base liquid (Heraeus) for 2 hours. Embryos were then infiltrated overnight with Technovit 7100 base liquid

containing 1g of hardening powder per 100ml. Embryos were then placed in moulds and embedded in infiltration solution containing 1ml hardening solution per 15ml. Before the solution hardened, a microtome chuck was placed in each mould. On hardening, the bond between the chuck and sample was sufficient to allow sectioning with no further processing.

Blocks were sectioned on a Leica SM2500 microtome. Sections were floated out on a 40°C water bath and scooped out with SuperFrost Plus slides. Slides were allowed to dry horizontally on a Raymond A Lamb slide drier at 50°C. If no counterstaining was required, sections were mounted under coverslips with Eukitt Mounting Medium (O. Kindler, Freiburg, Germany).

2.4.3 Mallory's Trichrome Staining

[Mallory's Trichrome Staining was performed by Wendy Hatton, Histology Service, NIMR] 10μm Fibrowax sections of an adult male *Xenopus laevis* heart on SuperFrost Plus slides were dewaxed in Histoclear, rinsed in 100% ethanol and rehydrated to PBS through an ethanol gradient. Sections were then stained for 4 minutes in iron haematoxylin, rinsed in running tap water for 3 minutes, stained for 3 minutes in 8.5mM acid fuchsin (dissolved in water), then stained in aniline blue/orange G staining solution for 2 changes of 20 minutes each. Stained sections were then dehydrated in a graded series of ethanol, cleared in Histoclear and mounted under coverslips in Permount.

2.4.4 Haematoxylin And Eosin Staining

Dried plastic sections on SuperFrost Plus slides were immersed in haematoxylin solution, Gill No. 2 (Sigma-Aldrich) for 2 minutes, and then rinsed in 10 changes of tap water. Sections were immediately immersed in eosin Y solution (Sigma-Aldrich) for 2 minutes, and again rinsed in 10 changes of tap water. Slides were left to dry horizontally on a Raymond A Lamb slide drier at 50°C, and then mounted under coverslips with Eukitt Mounting Medium.

2.4.5 Feulgen Staining

[Feulgen Staining was performed by Wendy Hatton, Histology Service, NIMR] 10μm Fibrowax sections of stage 47 tadpoles on SuperFrost Plus slides were dewaxed in Histoclear, rinsed in 100% ethanol and rehydrated to H_2O through an ethanol gradient. Sections were rinsed in 1M HCl at room temperature for 1 minute, followed by 8 minutes in preheated 60°C HCl. The sections were again rinsed in 1M HCl at room temperature for 1 minute. Sections were then transferred to Schiff's Reagent for 45 minutes to 1 hour. Sections were then rinsed 3 times in bisulphite solution for 2 minutes each. Finally sections were rinsed in water, dehydrated in a graded series of ethanol, cleared in Histoclear and mounted under coverslips in Permount.

2.5 Scanning Electron Microscopy

Tadpoles were fixed in Karnovsky Fixative overnight. Tadpoles beyond the feeding stage were first anaesthetised in 0.02% MS222 before being fixed in Karnovsky Fixative overnight. Tadpoles were rinsed in 0.2M sodium cacodylate buffer and dissected to expose the surface of the heart. Dissected embryos were then returned to Karnovsky Fixative for 2 hours. Tadpoles were again rinsed in cacodylate buffer, and dehydrated through an ethanol series. [The following procedures were performed by Liz Hirst, Electron Microscope Laboratory, NIMR] Tadpoles were critical point dried from CO_2 and fixed onto SEM chucks with Araldite (Huntsman Advanced Materials). The Araldite was coated in silver conductive paint and the entire sample sputter coated with gold to 20nm in an EMScope SC500 sputter coater. The samples were visualised at an accelerating voltage of 10kV in a Joel-35 CF microscope.

2.6 Transcription And Injection Of Lineage Tracer RNAs

The plasmid pCS2-nβ-gal contains the coding sequence of a nuclear localized form of the enzyme β-galactosidase and was a gift from Ralph Rupp (Ludwif Maximilians Universität, Munich). Plasmid pCS2-DsRed1 contains the sequence of the fluorescent reporter protein DsRed1 with a codon-useage optimised for mammalian expression (Clontech). Both plasmids were linearised using the enzyme *ApaI* and capped *in vitro* transcriptions were performed using the SP6 mMessage mMachine kit (Ambion) as

described in section 2.20. Synthesized RNA was purified using Chroma Spin-100 columns (Clontech). Procedures described in section 2.21 were used to inject *Xenopus* embryos with 200pg of the DsRed1 and nuclear β-galactosidase RNAs.

2.7 X-gal Staining Of Whole Tadpoles

Stage 47 tadpoles were fixed for one hour in a modified MEMFA solution that contained only half the normal concentration of formaldehyde (1.85% v/v). Tadpoles were then transferred to Wash Solution for ten minutes, followed by Wash Solution containing 2μg/ml proteinase K for two hours, then Wash Solution alone for a further ten minutes. Tadpoles were then placed in X-gal Developing Solution for 2 hours at 37°C in the dark. After the X-gal stain had developed, the tadpoles were washed twice in TTw for ten minutes each, followed by full strength MEMFA for one hour. Tadpoles were washed twice in TTw before photography.

2.8 Episcopic Fluorescent Image Capturing

Stage 42 tadpoles were fixed in MEMFA as described in section 2.3 and dehydrated to 95% alcohol. Samples were infiltrated overnight with two changes of JB4 plastic resin (Polysciences) containing 2.75mg/ml eosin and 1mg/ml Orasol Black dye. The plastic was polymerised according to manufacturer's instructions and samples were oriented in the plastic before polymerisation was complete. Plastic blocks were sectioned on a Leica SM2500 microtome - 2 micron sections were taken. Serial images of the block surface were captured using a Jenoptik C14 cooled colour CCD camera using a modified Zeiss Axiotech compound microscope positioned over the block photostop position. Illumination was achieved using Leica GFP3 excitation and emission filter sets. Image data sets were converted to greyscale after removal of the red and blue channels. The greyscale range was optimised using Adobe Photoshop and data scaled to give cubic voxels (as determined from graticule measurements). Image data was visualised by 3D volume rendering, using Osirix 2.6 on a Mac Pro workstation.

2.9 Antisense RNA Probe Synthesis

Antisense RNA *in situ* hybridisation probes were made against the following genes:

TARGET	*VECTOR*	*ANTISENSE PROBE*		*ORIGIN*
		CUT	*RNA Pol*	
Tbx18	pCR4-TOPO	NotI	T3	Accession number: BJ048587 Amplification (*Xl* gDNA) F GATAGAAAGAGATGTTCTTGTAAGGGAG R ACTCAGCATGTGGTCGATCAAGCCTTGCAC Cloned into PCR4-TOPO (Invitrogen)
WT1	pCMVSPORT6	NotI	Sp6	Accession number: CF270874 IMAGE: 3548862
Epicardin	pCMVSPORT6	NotI	Sp6	Accession number: CF270487 IMAGE: 5512805
Podocalyxin	pCMVSPORT6	SalI	T7	Accession number: BX847258 IMAGE: 4057588
Nephrin	pCMVSPORT6	SalI	T7	Accession number: BX854330 IMAGE: 4964461
MLC2	pXMLC2	EcoRI	T7	Accession number: Z33999 (Chambers et al., 1994)
XHex	pCMVSPORT6	NotI	Sp6	Accession number: BC059320 IMAGE: 4965399

Table 2-1. Templates for antisense RNA probes used for in situ hybridisation.

10μg of template DNA was linearised by restriction enzyme digestion, extracted with 1 volume of phenol then 1 volume of 1:1 phenol:chloroform. The DNA was precipitated by adding sodium acetate to 0.3M, and 2.5 volumes of 100% ethanol. The reaction was left at -20°C for at least 20 minutes. The precipitate was recovered by centrifugation at 12,000x g for 15 minutes. The pellet was washed in 70% ethanol and resuspended at 0.5mg/ml in TE. A transcription mix was assembled on ice as follows:

H_2O	20	µl
0.1M DTT	5	µl
rNTP-Dig Mix	10	µl
RNasin (40U/µl) (Promega)	1	µl
Template DNA (0.5µg/µl)	5	µl
10x Transcription Buffer	5	µl
RNA Polymerase (20U/µl)	4	µl
Total	50	µl

The reaction was incubated at 37°C for 4 hours. 2 µl of 1U/µl RQ-1 RNase-free DNase (Promega) was added and incubated for a further 20 minutes at 37°C. RNA was purified using Chroma Spin-100 columns (Clontech). The columns were pre-spun at 700x g for 5 minutes. The reaction was loaded and spun for a further 7 minutes at 700x g. Purified RNA was collected in a microfuge tube.

2.10 Whole-Mount *In Situ* Hybridisation

Albino and wild type embryos were fixed in MEMFA for 2 hours and stored in 100% ethanol. Embryos were rehydrated through 5-minute washes in 75% ethanol, 50% ethanol, 25% ethanol, and 3 five-minute washes in TTw. Embryos were permeabilised by incubating for 15 minutes in TTw containing 2µg/ml Proteinase K. The embryos were washed three times in 0.1M triethanolamine for 5 minutes each. To the third wash was added 2.5µl/ml acetic anhydride and a further 2.5µl/ml acetic anhydride was added after 5 minutes. Triethanolamine and acetic anhydride were removed by two 5-minute washes in TTw. Embryos were then refixed in MEMFA for 20 minutes followed by five 5-minute washes in TTw. Embryos were transferred to 1ml of TTw and 250µl RNA hybridisation buffer was added. Once the embryos had settled to the bottom (about 15 minutes) they were transferred into RNA hybridisation buffer for 10 minutes at 60°C, followed by an overnight incubation in fresh RNA hybridisation buffer at 60°C. After this prehybridisation, the solution was replaced with preheated (60°C) RNA hybridisation buffer containing digoxygenin-coupled probe at 1µg/ml and incubated at 60°C overnight.

Excess probe was removed by two twenty-minute washes in 2x SSC at 37°C. This was then replaced with 2x SSC containing 20μg/ml RNase A and 10μg/ml RNase T1 and incubated at 37°C for 30 minutes. Excess RNase was removed by washing once in 2x SSC for ten minutes, then twice in 0.2x SSC for 1 hour each at 60°C. The embryos were prepared for antibody incubation by washing once for 10 minutes in preheated TTw at 60°C followed by 1 ten-minute wash in TTw at room temperature. Embryos were blocked in TBT for 15 minutes followed by 60 minutes in TBT plus 20% heat-treated lamb serum. Embryos were then incubated overnight at 4°C in TBT plus 20% heat-treated lamb serum, containing 1/2000 dilution of alkaline phosphatase-conjugted anti-digoxygenin antibody (Roche).

Excess antibody was removed by washing 5 times for 60 minutes in TBT. The embryos were prepared for the chromogenic reaction by washing twice for 15 minutes in alkaline phosphatase buffer. The solution was then changed to alkaline phosphatase buffer containing 5-bromo-4-chloro-3-indolyl phosphate/nitroblue tetrazolium (NBT/BCIP) (Roche). Staining was monitored until it appeared optimal. The reaction was stopped by washing for 5 minutes each in TTw, 25% ethanol, 50% ethanol, 75% ethanol, and 100% ethanol. The reverse gradient of washes was then performed followed by 60-minute fixation in MEMFA, and two final 5-minute washes in TTw.

Where necessary, wild type embryos were bleached in glass vials containing Bleaching Solution. The vials were placed on a light box. Embryos were monitored until bleaching was complete (usually within 30 minutes to 3 hours). Embryos were photographed in agarose-coated dishes containing TTw. For viewing internal staining, embryos were first dehydrated through 5-minute washes in 25% ethanol, 50% ethanol, 75% ethanol, and 100% ethanol. To clear embryos, the ethanol was replaced with Clearing Solution.

2.11 Immunohistochemistry

The 4A6 and 3G8 antibodies (Vize et al., 1995) were kindly provided by Elizabeth Oliver-Jones (University of Warwick).

Albino embryos, or wild type embryos, were fixed in MEMFA for 2 hours and stored in 100% ethanol. Embryos were rehydrated through 5-minute washes in 75% ethanol, 50% ethanol, 25% ethanol, and 3 five-minute washes in TTw. Embryos were then washed in TTw containing 10% goat serum for 1 hour, followed by an overnight incubation at 4°C in TTw containing the appropriate antibody. The 3G8 antibody was used at 1:40 and the 4A6 antibody at 1:2.

Excess antibody was removed by washing in TTw four times for 2 hours each. The embryos were than incubated overnight at 4°C in TTw containing a 1:1000 dilution of anti-mouse IgG Horseradish Peroxidase (HRP) secondary antibody (Amersham Biosciences). Embryos were then washed in TTw four times for 2 hours each. Immunodetection of HRP was carried out using a DAB staining kit (Vector).

The reaction was stopped by washing for 5 minutes each in TTw, 25% ethanol, 50% ethanol, 75% ethanol, and 100% ethanol. The reverse gradient of washes was then performed followed by 60-minute fixation in MEMFA, and two final 5-minute washes in TTw. Wild type embryos were bleached if necessary in glass vials containing Bleaching Solution as described above. Embryos were cleared if necessary and photographed as described above.

2.12 RNA Extraction From Embryos

Excess buffer was removed from embryos, and Trizol reagent (Invitrogen) was added at volumes of 200µl per 5 embryos. Embryos were vortexed and homogenised until no cell clumps were visible, incubated at room temperature for 5 minutes, and frozen at -80°C to improve cell lysis. Samples were thawed, 20µl of chloroform added per 100µl Trizol, vortexed and incubated at room temperature for 5 minutes. Samples were then centrifuged at 12,000x g for 15 minutes at 4°C. The upper aqueous layer was retained and isopropanol was added at 50µl per 100µl of Trizol. Samples were vortexed briefly, incubated at room temperature for 10 minutes, and centrifuged at 12,000x g for 10 minutes at 4°C. The supernatant was removed and 75% ethanol was added at 100µl per 100µl of Trizol. Samples were vortexed briefly, and centrifuged at 7,500x g for 5 minutes at 4°C. The 75% ethanol was removed and the pellet was air-

dried briefly (but not until completely dry as this reduced solubility). RNA was dissolved in DEPC-H_2O at 0.1-0.5μg/μl (~25μl per embryo) incubated at 56°C for 10 minutes and stored at -80°C.

2.13 Deoxyribonuclease I Treatment Of RNA

DNase I and DNase I Inactivation Reagent (Ambion) were used according to manufacturer's instructions. Briefly, 0.1 volumes of 10x DNase I buffer, and 1μl of DNase I were added to the RNA sample, mixed gently and incubated at 37°C for 60 minutes. DNase I Inactivation Reagent was resuspended and added at 0.1 volumes, or 2μl, whichever was greater. The reaction was incubated at 37°C for 5 minutes with frequent mixing. The reaction was centrifuged at 10,000x g for 2 minutes, the supernatant retained and stored at -80°C.

2.14 Reverse Transcription (RT) Reaction

An RT-premix was assembled on ice as follows:

DEPC-H_2O	0.75	μl
5x First Strand Buffer	2	μl
2.5mM dNTP Mix	2	μl
0.1M DTT	1	μl
RNAsin 40U/μl (Promega)	0.25	μl
100μM Random Primers (Invitrogen)	1	μl
Total	7	μl

The necessary amount of premix for minus reverse transcriptase controls was set aside and supplemented with 1μl DEPC-H_2O per 7μl. 1μl 200U/μl SuperScript III RNase H- Reverse Transcriptase (Invitrogen) was added per 7μl of the remaining RT-premix. 8μl aliquots of plus RTase and minus RTase were transferred to 0.2ml PCR tubes. 2μl of RNA was added to each tube. Also a tube containing mock RNA was included. Reactions were transferred to a pre-cooled (4°C) thermal cycler and

incubated for 30 minutes at 55°C. The reactions were diluted as necessary and stored at -20°C.

2.15 Quantitative RT-PCR

Primers used for quantitative RT-PCR were as follows:

PRIMER	*SEQUENCE*
Tbx18 forward	ACTTACAAACTCAGCAAGTGAAAGCT
Tbx18 reverse	GCTGCTTGTCATGCCAACAT
WT1 forward	AAAGACTGCGAGAGGCGATTT
WT1 reverse	GACGCCTGTGTGTGCCTCCTT
Epicardin forward	AGTCCACTGGGCACCATCA
Epicardin reverse	CCTGGCATTGGCTGCATT
GAPDH forward	GCAGAAGCCGGCCAAGT
GAPDH reverse	GGGCCCTCTGATGCAGTCT
Podocalyxin forward	TGGTTAAGCATGCCTCTAATAATCA
Podocalyxin reverse	GCATCCATAAATAGCTGCCAATGAG
Nephrin forward	TCCACCAAATGCTCCGATTAT
Nephrin reverse	AATGCAGATGAGCTTCAGTGTTTC

Table 2-2. Sequences of primers used for Quantitative RT-PCR.

Primers were designed using PrimerExpress software (PE Biosystems). Primers were designed against a *Xenopus laevis* epicardin EST (accession number CF270487), full length *Xenopus laevis* WT1 (Carroll and Vize, 1996) (accession number XLU42011), a *Xenopus laevis* Tbx18 EST (accession number BJ048587), full length *Xenopus laevis* GAPDH (Klein et al., 2002) (accession number BC043972), full length *Xenopus laevis* nephrin (Gerth et al., 2005) (accession umber AY902238), and a *Xenopus laevis* podocalyxin EST (accession number CB558235).

A PCR master-mix was assembled on ice as follows:

2x SYBR Green (ABgene)	162.5	µl
Primer 1 (1.5µM)	32.5	µl
Primer 2 (1.5µM)	32.5	µl
H_2O	65	µl
Total	292.5	µl

The master mix was mixed gently and 90µl was aliquoted into three microfuge tubes labelled +RT, -RT, and No Template Control. To these were added 10µl of plus RTase RT reaction, 10µl of minus RTase RT reaction, and 10µl of H_20 respectively. These were then mixed gently and were plated onto a 96-well plate (ABgene) in triplicates of 25µl. The plate was sealed with Clear Seal Diamond sealing film (ABgene), centrifuged briefly, and loaded into an ABI PRISM® 7000 Sequence Detection System. PCR cycles were as follows: 50°C for 2 minutes, 95°C for 15 minutes, followed by 40 cycles of 15 second denaturing at 95°C, and 60 seconds of annealing/extension at 60°C.

2.16 Quantitative RT-PCR Calibrations And Calculations

Gene expression was calculated using the ΔΔCT method (Applied Biosystems) where CT is the threshold cycle, and ΔΔCT is normalised for amount of input cDNA by comparison with an endogenous reference (GAPDH) and target levels relative to a calibrator sample (GeneTools Standard Control MO).

Before using the ΔΔCT method a validation experiment was performed to ensure the efficiencies of the target and endogenous reference amplicons are approximately equal. A series of five 5-fold dilutions of cDNA were used for the calibration reactions. Log10 of relative RNA was plotted against ΔCT (CT of target normalised against CT of endogenous reference). If the amplicon efficiencies were equal, the slope of the graph would be 0. However, values within +/- 0.1 are considered acceptable. The amplicon efficiencies of all target genes versus endogenous reference fell within these limits and so the ΔΔCT method of analysis was appropriate.

2.17 Genomic DNA Extraction

Single *Xenopus laevis* tadpoles were homogenized using a micropestle in a microfuge tube containing 0.5ml of homogenisation buffer. 2.5µl of proteinase K (20mg/ml) was added to the homogenate and incubated overnight at 55°C. DNA was extracted once with 1 volume of aqueous phenol, once with 1 volume of 1:1 phenol:chloroform, and once with 1 volume of chloroform. The reaction was precipitated by adding ammonium acetate to 2M, and 0.6 volumes of isopropanol. The precipitate was recovered by centrifugation at 12,000x g for 5 minutes. The pellet was washed in 70% ethanol and resuspended in 100µl of TE. RNase A was added to 10µg/ml and RNase T1 to 10µg/ml, and incubated at room temperature for 30 minutes. The reaction was precipitated by adding ammonium acetate to 2M, and 0.6 volumes of isopropanol. The precipitate was recovered by centrifugation at 12,000x g for 5 minutes. The pellet was washed in 70% ethanol and resuspended in 20µl of TE.

2.18 Morpholino Oligonucleotides

Translation inhibition morpholino oligonucleotides (MOs) were designed by Gene Tools against *Xenopus laevis* WT1, and *Xenopus tropicalis* Tbx18 and epicardin. The WT1 MO was designed against the full length cDNA (Carroll and Vize, 1996) (accession number XLU42011). Tbx18 has not been cloned in either *Xenopus* species. Blast searches were carried out using mouse Tbx18 to identify the *Xenopus tropicalis* orthologue. Tbx18 was found to be located on contig 39 of scaffold 76 of the Joint Genome Institute *Xenopus tropicalis* genome assembly version 3.1 (http://genome.jgi-psf.org/Xentr4/Xentr4.home.html). A *Xenopus tropicalis* EST spanning the translational start site of epicardin (DN071293) was found on the Sanger Institute *Xenopus tropicalis* EST Project (http://www.sanger.ac.uk/Projects/X_tropicalis/). This was found to be identical to the translational start sight of *Xenopus laevis* epicardin (accession number AY660871) so one MO would be sufficient to knockdown the gene in both species.

TARGET	*SEQUENCE*
Tbx18	ATCGCCTCTTCTCTGCCATCCCGGT

WT1	TCATATCCCGGACATCAGACCCCAT
Epicardin	CGGTGGACATGATCTGTTATGCTGC
GeneTools Standard Control	CCTCTTACCTCAGTTACAATTTATA

Table 2-3. Sequences of morpholino antisense oligonucleotides.

MOs were resuspended in 300µl of water. The MO solution was cleaned through a G25 spin column (Amersham Biosciences) and stored at -20°C in 10µl aliquots at 8ng/nl.

2.19 Morpholino Oligonucleotide Control Constructs

In order to test the specificity of the MOs, control constructs were made. Oligonucleotides corresponding to the MO recognition sequence plus AgeI and NcoI compatible ends (italics in table 2-4) were purchased from Eurogentec. These were annealed and ligated into a pCS2-EGFP reporter vector digested with AgeI and NcoI. The oligonucleotides were designed to ensure the ATG of the MO target was in frame with the ATG of EGFP. Another set of oligonucleotides was purchased which were identical to the first except they contained 5 silent mutations within the MO recognition sequence (underlined in table 2-4). The constructs were linearised with ApaI at the 3' end, and *in vitro* translated.

OLIGO	*SEQUENCE*
Tbx18 forward	*CCGGT*CGGAACCGGGATGGCAGAGAAGAGGCGATC
Tbx18 reverse	*CATGG*ATCGCCTCTTCTCTGCCATCCCGGTTCCGA
WT1forward	*CCGGT*CAGATGGGATCTGATGTGCGGGATATGAATGC
WT1 reverse	*CATGG*CATTCATATCCCGCACATCAGATCCCATCTGA
Epicardin forward	*CCGGT*GCAGCATAACAGATCATGTCCACCGC
Epicardin reverse	*CATGG*CGGTGGACATGATCTGTTATGCTGCA
Tbx18 Δ forward	*CCGGT*CGGAACCGGGATGGCTGAAAAAGACGCTC
Tbx18 Δ reverse	*CATGG*AGCGTCTTTTTTCAGCCATCCCGGTTCCGA
WT1Δ forward	*CCGGT*CAGATGGGCTCCGACGTTCGAGATATGAATGC

WT1 Δ reverse	*CATGG*CATTCATATCTCGAACGTCGGAGCCCATCTGA
Epicardin Δ forward	*CCGGT*GTAGTATGACAGATCATGTCTACTGC
Epicardin Δ reverse	*CATGG*CAGTAGACATGATCTGTCATACTACA

Table 2-4. Sequences of oligonucleotides used to make MO control constructs.

2.20 Capped RNA Synthesis

Capped RNA was synthesised using an mMessage mMachine kit (Ambion). A reaction was set up as follows:

DNA Template (1μg/μl)	1	μl
2x NTP/CAP	10	μl
10x Reaction Buffer	2	μl
Enzyme Mix	2	μl
H_2O	5	μl
Total	20	μl

The reaction was gently mixed and incubated at 37°C for 2 hours. The reaction was then spun through a Chroma Spin-100 column (Clontech). RNA was measured on a NanoDrop ND1000 Spectrophotometer and diluted to 400pg/nl

2.21 Injections

Dejellied embryos at the correct stage of development were injected with GC100F-15 glass needles (Harvard) pulled on a Kopf 750 needle puller. Embryos were injected in an agarose lined dish containing 4% Ficoll in 0.75x NAM. Shortly after injection, embryos were transferred to dishes containing 0.1x NAM. *Xenopus tropicalis* embryos were maintained at 22-25°C and *Xenopus laevis* at 18-22°C.

100pg of MO control RNA was injected into 1 cell of 2-cell embryos. Once the embryos had reached the 4-cell stage, the MO was injected into 1 cell on the same side as the RNA was injected. Injecting separately in this manner ensures any reaction

between the MO and the control RNA occurs *in vivo.* It also allows the selection of the healthiest embryos.

MOs were injected at concentrations of between 0.5 and 16ng (in 2nl). In some experiments the MO was supplemented with 10,000-molecular weight rhodamine-dextran (Sigma) to a final volume of 1ng/nl.

2.22 Morpholino Oligonucleotide Rescue Constructs

Full length cDNAs corresponding to *Xenopus laevis* WT1 and epicardin were kindly provided by Peter Vize (University of Calgary) and Andre Brandli (Swiss Federal Institute of Technology, Zurich) respectively.

Because the MOs used were translation inhibition MOs, simply injecting wild type RNA would not rescue the knockdown phenotype because the MO would also target the rescue RNA. To avoid this problem, 5 silent mutations were introduced into the MO recognition sequence using a QuickChange Site Directed Mutagenesis kit (Stratagene). A set of primers for each construct was designed using the QuickChange Primer Design Program (http://www.stratagene.com/sdmdesigner/default.aspx).

OLIGO	*SEQUENCE*
WT1 mis forward	CTTTGGCAGATCCCAGATGGGATCGGACGTACGTGATATGAATCTGTTGCCTCCA
WT1 mis reverse	TGGAGGCAACAGATTCATATCACGTACGTCCGATCCCATCTGGGATCTGCCAAAG
epicardin mis forward	TGAGAAGGAGTAGTATGACAGATCATGTCTACTGGTTCTCTCA
epicardin mis reverse	TGAGAGAACCAGTAGACATGATCTGTCATACTACTCCTTCTCA

Table 2-5. Sequences of oligonucleotides used to induce point mutations in the cDNA sequence of Xenopus laevis WT1 and epicardin.

A PCR reaction was assembled on ice as follows:

10x Reaction Buffer	5 _l
dsDNA Template (25ng/_l)	1 _l

Primer 1 (125ng/_l)	1	_l
Primer 2 (125ng/_l)	1	_l
dNTP Mix	1	_l
PfuTurbo DNA Polymerase (2.5 U/_l)	1	_l
H_2O	40	_l
Total	50	_l

The reaction was then cycled on a PTC-100 Peltier Thermal Cycler according to the following parameters:

1x	95°C	30 seconds
25x	95°C	30 seconds
	60°C	1 minute
	68°C	6 minutes

1_l of DpnI restriction endonuclease (10U/_l) was then added to the reaction and incubated at 37°C for 1 hour. This digested the methylated parental DNA but left the newly synthesized, mutated DNA in tact. The DNA was then transformed into chemically competent cells and correct clones selected by restriction analysis.

2.23 Solutions

SOLUTION	*RECIPE*
10x Transcription Buffer	400mM Tris-HCl (pH7.5), 60mM $MgCl_2$, 20mM spermidine HCL, 50mM NaCl
20x SSC	3M NaCl, 0.3M Sodium Citrate
Alkaline Phosphatase Buffer	100mM Tris-HCl (pH 9.5), 50mM $MgCl_2$, 100mM NaCl, 0.1% (v/v) Tween20, 2mM Levamisol
Aniline Blue/Orange G Staining Solution	6.8 mM aniline blue, 44 mM orange G, 3.5 mM phosphotungstic acid

Bisulphite Solution	0.5% $K_2S_2O_5$, 0.05% HCl
Bleaching Solution	1% (v/v) H_2O_2, 5% (v/v) formamide, 0.5x SSC
Clearing Solution	1 part benzyl alcohol:2 parts benzyl benzoate
dNTP Mix	10mM each: dATP, dGTP, dCTP, dTTP, dilute in DEPC-H_2O
Ferri/ferrocyanide Stock Solution	10ml: PBS, containing 1.06g potassium ferrocyanide (yellow, Sigma P-9387), 0.82g potassium ferricyanide (red, Sigma P8131)
First Strand Buffer	250mM Tris-HCl (pH 8.3) 375mM KCl, 15mM $MgCl_2$, 0.1M DTT
Homogenisation Buffer	1% SDS, 10mM EDTA, 20mM Tris-HCl (pH 7.5), 100mM NaCl
Karnovsky Fixative	6% glutaraldehyde, 4% paraformaldehyde in 0.2M sodium cacodylate
Marc's Modified Ringers (MMR) (Ubbels et al., 1983)	0.1M NaCl, 2mM KCl, 1mM $MgSO_4$, 2mM $CaCl_2$, 5mM HEPES (pH 7.8), 0.1mM EDTA
MEMFA	0.1M MOPS (pH 7.4), 2mM EGTA, 1mM $MgSO_4$, 3.7% (v/v) formaldehyde
Normal Amphibian Medium (NAM) (Slack and Foreman, 1980)	110mM NaCl, 2mM KCl, 1mM $Ca(NO_3)_2$, 1mM $MgSO_4$, 0.1mM EDTA, 1mM $NaHCO_3$, 2mM Na_3PO_4
RNA Hybridisation Buffer	50% formamide, 5x SSC, 1% (w/v) Torula RNA,

	1x Denharts, 0.1% Tween20, 5mM EDTA
rNTP-Dig Mix	10mM each: rATP, rGTP, rCTP, 7.5mM rUTP, 2.5mM DIG-11-rUTP (Boehringer Mannheim)
Schiff's Reagent	200ml: H_2O containing 1g basic fuchsin, 2g $K_2S_2O_5$, 2ml conc. HCl, (activated charcoal)
TBT	200mM NaCl, 50mM Tris-HCl (pH7.5), 2% (w/v) BSA
TE	10mM Tris-HCl (pH 7.5), 1mMEDTA
TTw	200mM NaCl, 50mM Tris-HCl (pH 7.5), 0.1% (v/v) Tween20
Wash Solution	500ml: PBS containing 1ml 1M $MgCl_2$, 2.5ml 2% deoxycholate, 5ml 2% NP40
X-gal Developing Solution	50ml: Wash Solution, containing 2ml 25mg/ml X-gal, 1ml ferri/ferrocyanide stock solution

3 Results: Structure Of *Xenopus laevis* Heart And Epicardium

3.1 Introduction

3.1.1 The Amphibian Epicardium

Little is currently known about the epicardium in amphibians. A small amount of evidence exists for the formation of the epicardium in the urodele amphibian, the axolotl (*Ambystoma mexicanum*) (Fransen and Lemanski, 1989; Fransen and Lemanski, 1990; Fransen and Lemanski, 1991). Here SEM was used to examine the surface of the developing tadpole heart. The myocardial surface was seen to be naked until stage 39, when mesothelial cells were released from the septum transversum into the pericardial cavity. These were seen attached and flattened to the ventricular myocardium. By stage 40 the posterior (caudal) surface of the looped ventricle was in direct contact with the septum transversum on the right side of the pericardial cavity. The epicardial layer first covered the surface of the ventricle, and then extended towards the atria and OFT. The embryonic heart was covered by the epicardium by stage 43, however the epicardium appeared to spread over the myocardium not as a complete sheet but as discrete patches. These findings were used as a starting point for this investigation into the structure and development of the epicardium in the anuran amphibian, *Xenopus laevis*.

The staging system in axolotl is not directly comparable to *Xenopus laevis*. Two separate staging systems are often used (Bordzilovskaya et al., 1989; Schreckenberg and Jacobson, 1975). Both of these systems were used in the above studies with Schreckenberg and Jacobson (1975) used to stage embryos up to stage 40, and Bordzilovskaya et al (1989) used to stage embryos above this stage. The axolotl heart was reported to be 'S' shaped at stage 40, whereas in *Xenopus* the heart is 'S' shaped prior to this at around stage 35/36 (Mohun et al., 2000).

3.1.2 Anurans Versus Urodeles

As can be seen from the description above, a small amount of data exists about the development of the epicardium in the urodele amphibian, the axolotl. However, the

axolotl is not the favoured amphibian species for developmental biology research. The anuran species *Xenopus laevis* has been the preferred amphibian species for over 50 years, whilst the axolotl has become almost obsolete (Nieuwkoop, 1996). The advantages of *Xenopus* over the axolotl include the ability to obtain eggs all year round by a simple hormone injection, a shorter generation time, and now the ability to perform genetic experiments in the diploid species *Xenopus tropicalis*. The morphogenetic understanding of *Xenopus* however, is not nearly as advanced as it is for the axolotl. It is therefore important that we understand the morphogenetic development of structures such as the epicardium before we can take advantage of the many benefits of *Xenopus*.

3.1.3 Aims Of This Chapter

This chapter will describe the structure of the heart and epicardium of an adult *Xenopus laevis*. The embryonic development of the epicardium will also be described, including the structure, size and location of the proepicardium, the method of proepicardial attachment, and the timing of proepicardial outgrowth.

3.2 Results

3.2.1 Structure Of Adult Xenopus laevis Heart And Epicardium

In order to establish whether an epicardial layer could be detected in the anuran species *Xenopus laevis*, serial transverse sections through the ventricular region of an adult *Xenopus laevis* heart were made. A heart was removed from an adult male frog and embedded in wax. 10μm sections were made and stained with Mallory's Trichrome Stain.

Figure 3-1(A) shows a transverse section through the caudal apex of the ventricle where no distinct lumen is visible. The structure of the ventricle can be seen to be very spongy with many extended trabeculae. Figure 3-1(B) shows a more rostral transverse section through the ventricle. The compact layer of the myocardium has been marked by a red bar. The compact layer is the portion of the myocardium

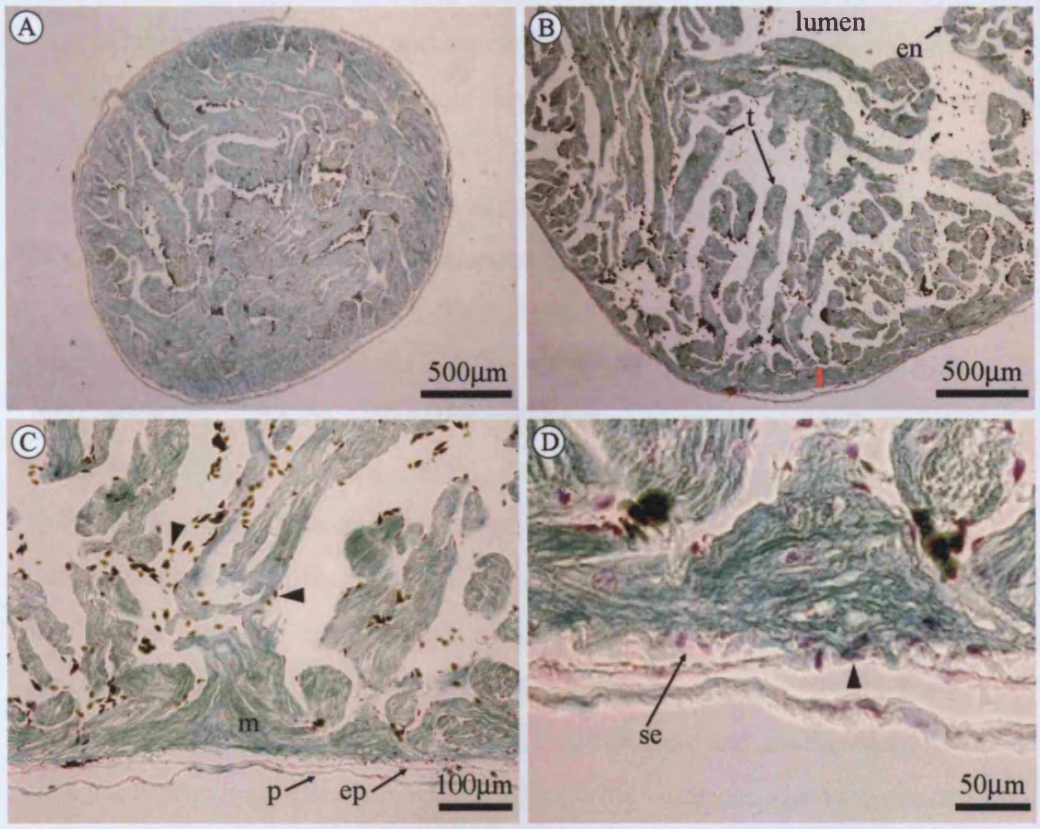

Figure 3-1. Structure of adult *Xenopus laevis* heart and epicardium.

Transverse sections through the ventricle of an adult *Xenopus laevis* heart. Sections are stained with Mallory's Trichrome Stain, muscle is stained green. (A)- section through the apex of the ventricle. Note the sponge-like appearance of the myocardial muscle. No lumen is visible at the apex of the ventricle. (B)- section through a more rostral plane of the ventricle. A more pronounced lumen can be seen. Numerous extended trabeculae (t) create intertrabecular spaces (lacunae). The inner layer of the heart, the endocardium (en) can be seen lining the trabeculae. The compact layer of the ventricle (red bar) is much reduced in comparison to species with a smooth-walled myocardium. (C)- close-up of the pericardial region of the heart. Arrowheads mark erythrocytes dispersed throughout the lacunae. An additional layer can be distinguished between the pericardium (p), the protective sac which ensheathes the heart, and the myocardium (m) – this is the epicardium (ep). (D)- high magnification image of (C). The epicardium is sometimes closely associated with the myocardium (arrowhead), whilst at other regions a sub-epicardial space (se) exists between the epicardium and the myocardium.

responsible for contraction, and appears to be much thinner compared with the compact layer of higher species. In this section the finger-like trabeculae are even more apparent. Also at this level a more distinct lumen can be seen. Although not a true lumen as would be found in mammalian and avian hearts, it is nonetheless an area where the lacunae are less frequent, allowing the free flow of blood out of the ventricle. An endothelial layer, the endocardium, covers the trabeculae and is in direct contact with the blood. Figure 3-1(C) shows a section of the heart at a higher magnification. Here the pericardium, the protective sac in which the heart is ensheathed, can be seen surrounding the heart. This is a tough fibrous sac that prevents the heart from expanding excessively due to overfilling with blood. In addition another cell layer, comprised of simple squamous cells can be seen between the pericardium and the myocardium. This corresponds to the epicardium as described in other species. Many individual erythrocytes (which, unlike mammalian erythrocytes, are nucleated) can be seen dispersed around the lacunae. Figure 3-1(D) is a yet higher magnification section through the ventricle. Here the pericardium can again be seen to ensheathe the heart. Here the epicardium is sometimes in close association with the myocardium (arrowhead). At other areas a subepicardial space can be seen between the myocardium and the epicardium.

3.2.2 When Does Epicardium Development Occur?

In order to establish at what stage in development the epicardium begins to form, SEM was used to analyse the cardiac surface of a series of *Xenopus laevis* tadpoles. As a starting point, data on epicardium formation in chick and mouse embryos was used. A number of studies have examined the formation of the epicardium using SEM in the mouse (Komiyama et al., 1987) and in the chick (Hiruma and Hirakow, 1989). These studies showed the proepicardium is first visible at embryonic day 9.5, and HH14 respectively.

Figure 3-2 shows the key events of heart development in the mouse. From this it can be seen that proepicardium outgrowth occurs at about the time when looping of the heart is nearing completion. Figure 3-3 shows the key events of heart development in the chick. Again it can be seen that the reported time of proepicardial outgrowth

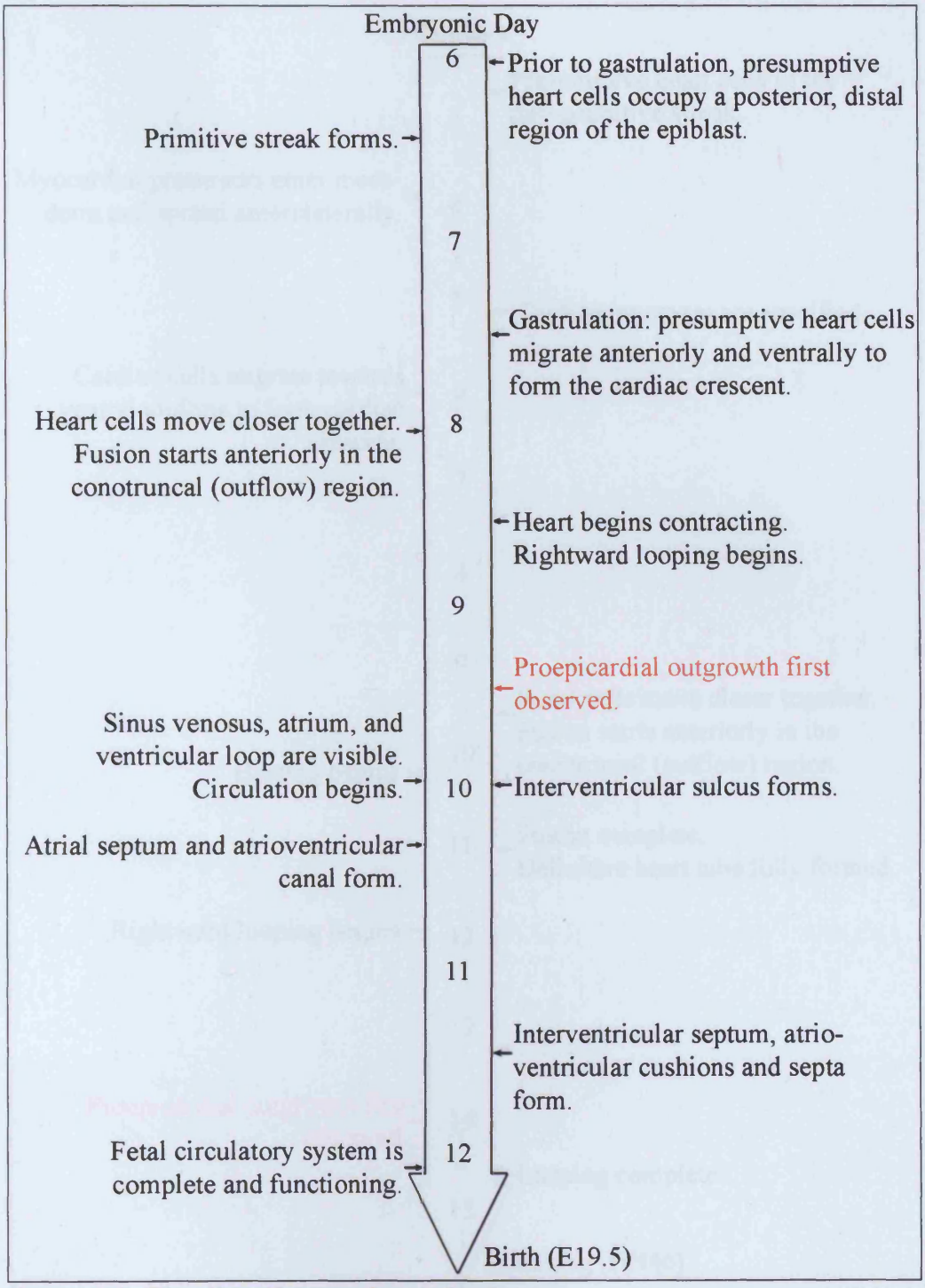

Figure 3-2. Timeline of mouse heart development.

Proepicardial outgrowth is first observed in the mouse at around E9.5. This corresponds to the time when the heart is at an advanced stage of looping. (DeRuiter et al., 1992; Kaufman and Navaratnam, 1981; Komiyama et al., 1987; Rugh, 1968)

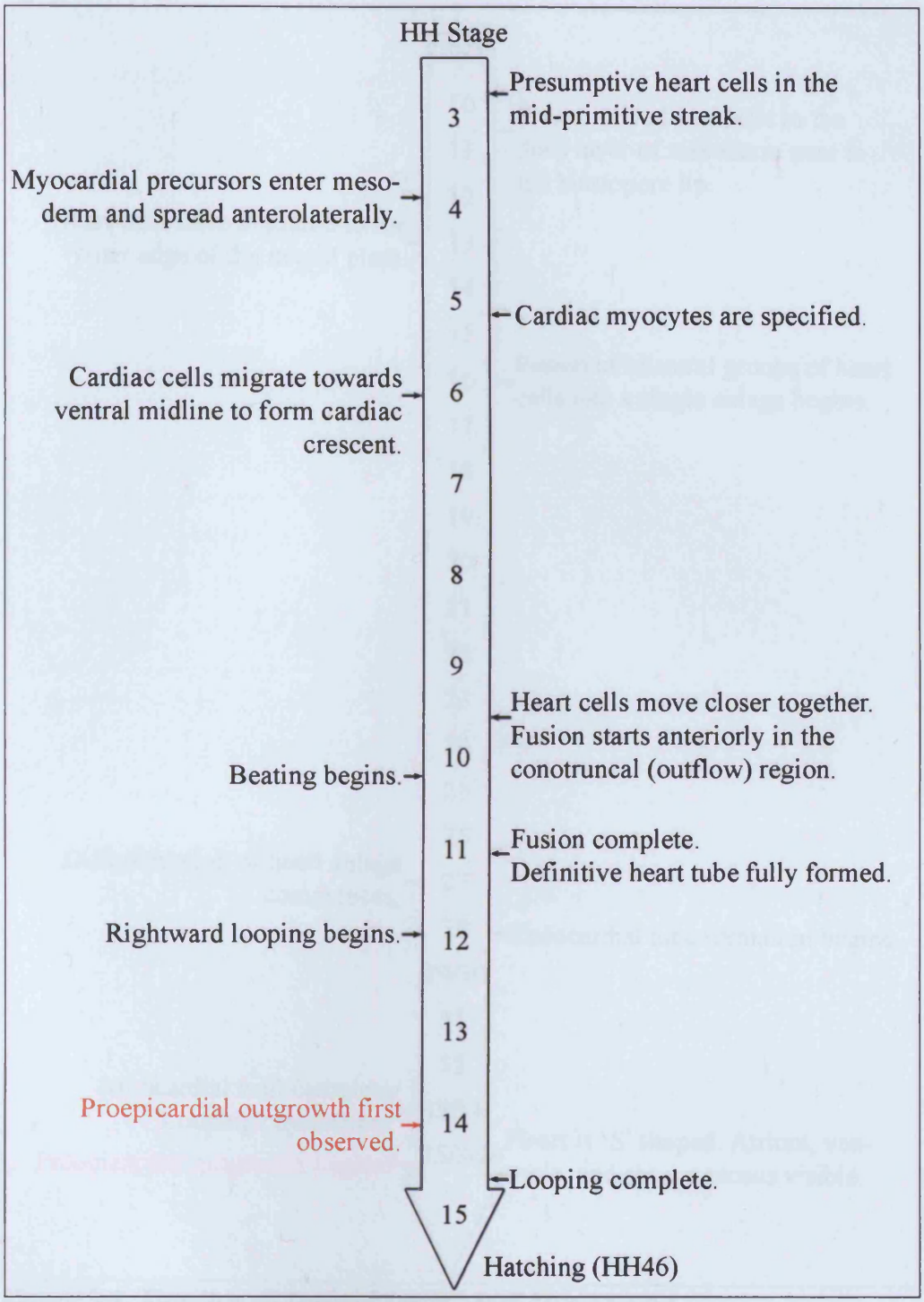

Figure 3-3. Timeline of chick heart development.

Proepicardial outgrowth is first observed at around HH14. This corresponds to the time when the heart is at an advanced stage of looping. (De Haan, 1965; Gonzalez-Sanchez and Bader, 1990; Hamburger and Hamilton, 1992; Hiruma and Hirakow, 1989; Viragh et al., 1989)

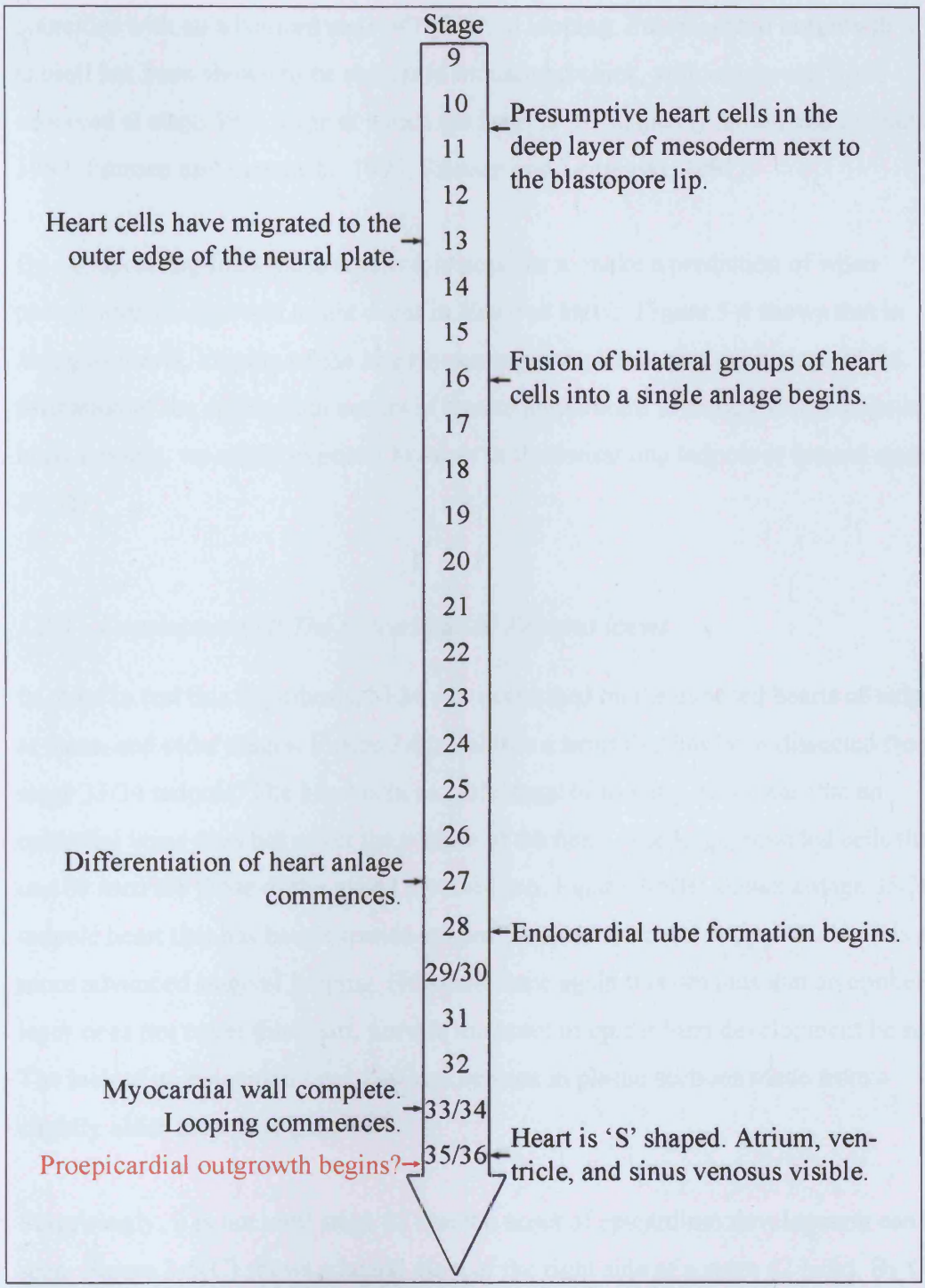

Figure 3-4. Timeline of *Xenopus laevis* heart development.

By extrapolating the information shown in figures 2 and 3, it is possible to predict that proepicardial outgrowth will begin when the heart is at an advanced stage of rightward looping. This corresponds to around stage 35/36. (Mohun et al., 2000; Nieuwkoop and Faber, 1994; Sater and Jacobson, 1990)

coincides with an advanced state of rightward looping. Proepicardial outgrowth in the axolotl has been shown to be similar to mouse and chick, with outgrowth first observed at stage 39, a stage at which the heart is 'S' shaped (Fransen and Lemanski, 1989; Fransen and Lemanski, 1990; Fransen and Lemanski, 1991).

By extrapolating from these results it is possible to make a prediction of when proepicardial outgrowth might occur in *Xenopus laevis*. Figure 3-4 shows that in *Xenopus laevis*, looping of the heart is nearing completion at around stage 35/36. If formation of the epicardium occurs in anuran amphibians at an equivalent stage of heart looping, we might expect it to occur in the swimming tadpole at around stage 35/36.

3.2.3 Development Of The Epicardium In Xenopus laevis

In order to test this hypothesis, SEM was performed on the exposed hearts of tadpoles at these, and older stages. Figure 3-5(A) shows a heart that has been dissected from a stage 33/34 tadpole. The heart is in an early stage of looping. It is clear that an epithelial layer does not cover the surface of the heart. The large, rounded cells that can be seen are those of the naked myocardium. Figure 3-5(B) shows a stage 35/36 tadpole heart that has been exposed but not removed from the body. This heart is at a more advanced stage of looping. However, once again it is obvious that an epithelial layer does not cover this heart, nor can the onset of epicardium development be seen. The lack of an epicardial layer can also be seen in plastic sections made from a slightly older tadpole (figure 3-6).

Surprisingly, it is not until stage 42 that the onset of epicardium development can be seen. Figure 3-5(C) shows a lateral view of the right side of a stage 42 heart. By this stage of development the tadpole heart has many of the structures present in the adult heart, such as a muscular ventricle, the atrial septum, and the spiral and AV valves are beginning to form. A population of cells can be seen in the left of the figure, adjacent to the septum transversum/liver region. These cells represent the proepicardium and have attached to the heart at the junction between the ventricle and OFT, from where they are beginning to spread out and cover the surface of the heart. The approximate

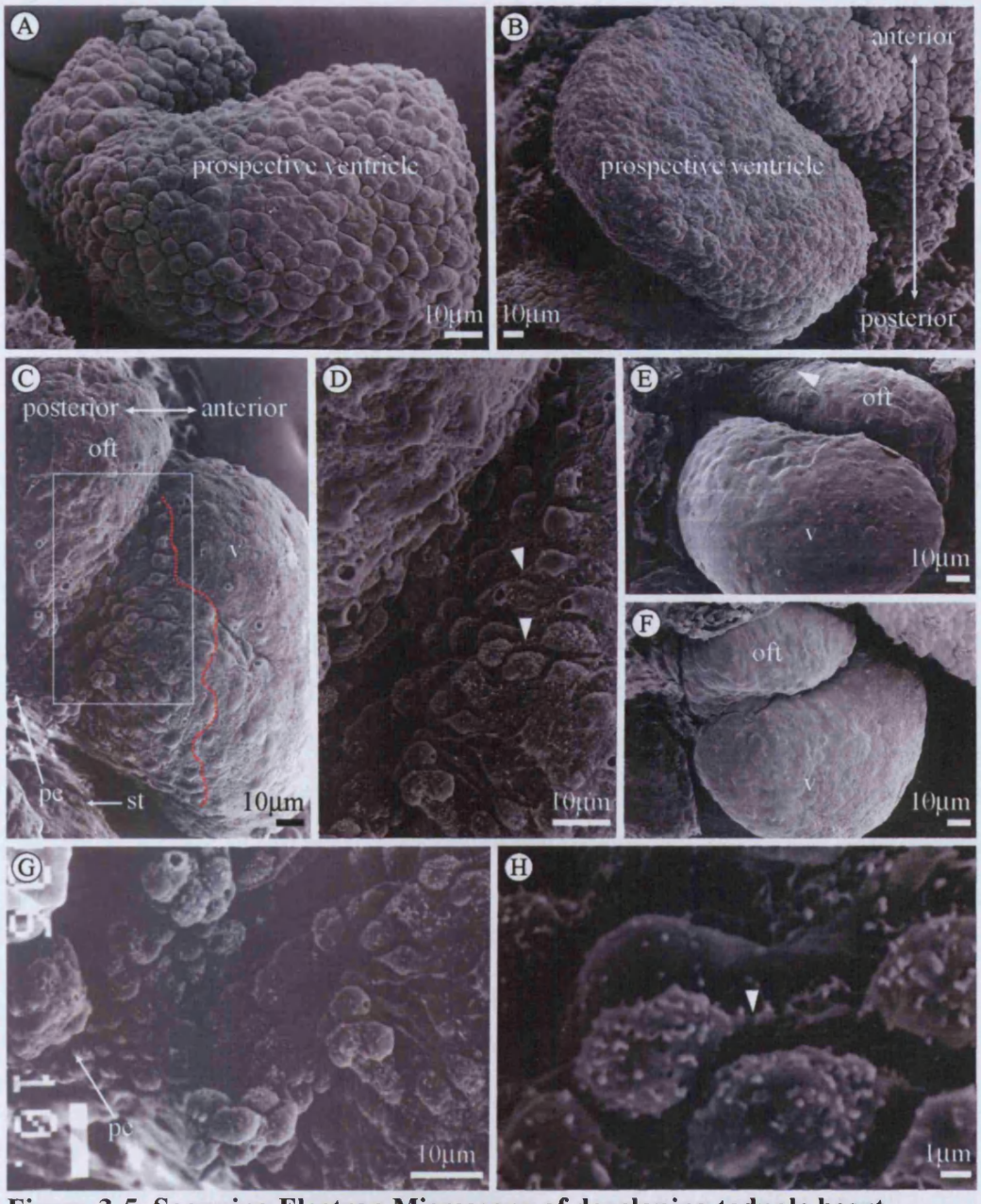

Figure 3-5. Scanning Electron Microscopy of developing tadpole heart.

(A)- ventral view of a stage 33/34 heart that has been dissected from the tadpole. The heart is starting to loop, and the large rounded appearance of the myocardial cells can be clearly seen. (B)- ventral view of a stage 35/36 heart. The heart is at a more advanced stage of looping. The cells, however, appear rounded and do not look like an epithelial layer - this is the naked myocardium. (C)- lateral view of the right side of a stage 42 heart. The origin of the epicardium, the proepicardium (pe), can be seen adjacent to the septum transversum (st). Proepicardial cells can be seen migrating towards the heart, attaching at the junction between the outflow tract and the ventricle, and starting to spread out over the surface of the heart. The

Figure 3-5. SEM of developing tadpole heart continued -
approximate boundary of migration has been marked by a red line. (D)– close-up of boxed region of (C). The migrating epicardial cells project filopodia (arrow heads). These guide the epicardial cells across the surface of the heart. A higher magnification image of the migrating epicardial cells and their filopodia (arrowhead) can be seen in (H). (E)– posterior view of a stage 46 heart. Here the epicardial cells have flattened to form a cohesive epithelial layer. A change in the appearance of the cells can be seen on the outflow tract (arrowhead). This is the limit of the epicardium. (F)– anterior view of a stage 46 heart showing the surface of the heart is covered by the epicardium. (G)- a high magnification image of the proepicardium attaching to the myocardial surface of the ventricle.

---

boundary of the migrating epicardium has been indicated with a red line. A higher magnification image of the proepicardium can be seen in figure 3-5(G). Figure 3-5(D) shows a close up of the AV junction region. The epicardial cells have projected filopodia, which are necessary for migration. Once the epicardial cells have covered the entire surface of the heart, they flatten and take on the appearance of an epithelial layer. A higher magnification image of a migrating epicardial cell and its filopodium can be seen in figure 3-5(H). Figures 3-5(E) and (F) show posterior and anterior views of stage 46 hearts respectively. Here it can be seen that the surface of the heart is covered by the now flat, smooth epicardium. This new layer can also be seen on plastic sections taken from an equivalently staged tadpole (figure 3-8). Interestingly, the epicardium does not extend up the entire length of the OFT. The limit of the epicardium is shown in figure 3-5(E), and can be seen as a change of cell structure from smooth, epithelial cells, to the more rounded myocardial cells as seen in figures 3-5(A) and (B).

3.2.4 Histological Analysis Of Epicardium Development

SEM is an excellent method for analyzing the surface appearance of the heart and epicardium, however, it gives limited information about the cellular architecture of the heart. In order to obtain such data serial sections of tadpoles embedded in plastic were made. These were stained with haematoxylin and counterstained with eosin.

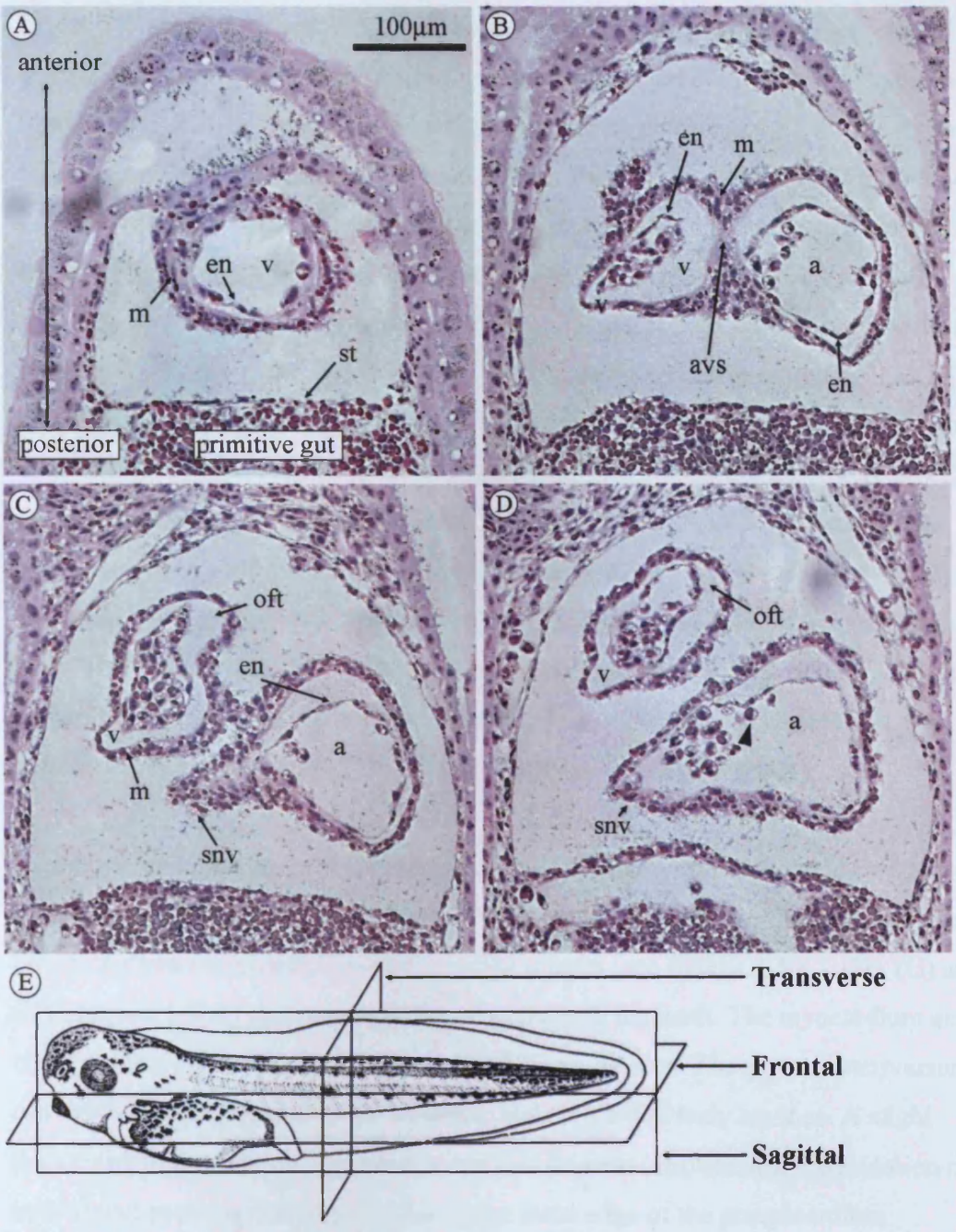

Figure 3-6. Frontal sections through a stage 37/38 heart.

(A) to (D)- sections through the ventricle and atrium. At this stage in development the epicardium has not started to develop. The septum transversum (st) can be seen separating the coelomic body cavity from the cardiac body cavity. The endocardial (en) and myocardial (m) layers of both the ventricle (v) and atrium (a) can be seen. The AV septum (avs) can be seen in (B). By this stage the heart is pumping blood around the body as shown by the erythrocytes in the heart (arrowhead in (D)). The sinus venosus (snv) and the outflow tract (oft) can also be seen in (C) and (D). (E)- diagram showing the three section planes used in this thesis.

Figure 3-6 shows a selection of frontal sections taken from a single series through a stage 37/38 heart. A key to the section planes used throughout this thesis is shown in figure 3-6(E). At this stage, no epicardial layer can be detected by SEM (see figure 3-5(B)). Figure 3-6(A) is the most ventral section, progressing dorsally to figure 3-6(D). Figure 3-6(A) is a section through the apex of the ventricle. The myocardium and endocardium of the ventricular apex can be seen. The septum transversum can be seen separating the coelomic body cavity from the pericardial body cavity. In more dorsal sections the atrium of the heart can be seen. The endocardium and myocardium of both the atrium and the ventricle can be seen in figure 3-6(B). It can also be seen here that AV septation has occurred. In the further dorsal section shown in figure 3-6(C) the OFT and sinus venosus can be seen. Finally, in figure 3-6(D), the most dorsal section, more of the OFT and sinus venosus can be seen, also individual erythrocytes can be seen which indicates that the heart is at this stage pumping blood around the body. In all of the sections taken through the heart at stage 37/38 is neither a mature epicardium, nor indeed the initiation of epicardium development evident. This is consistent with results from SEM at a similar stage (see figure 3-5(B)).

In order to examine the process of proepicardium outgrowth, sagittal and frontal sections were taken through the heart region of stage 42 tadpoles, the stage at which proepicardium outgrowth is evident in SEM images (see figures 3-5(C), (D), (G) and (H)). Figure 3-7(A) shows a sagittal section through the heart. The myocardium and endocardium of the ventricle, atrium and OFT can be seen. The septum transversum can again be seen separating the coelomic and pericardial body cavities. A slight thickening of the septum transversum can also be seen (arrowhead). Examination of subsequent sections indicates that this is the outer edge of the proepicardium.

Progressing further through the heart, the proepicardium can be seen as a cone-shaped projection from the septum transversum towards the heart (figure 3-7(B)). In some sections individual proepicardial cells can be seen detaching from the proepicardium and migrating towards the naked myocardium (figure 3-7(C)). The area of attachment of these cells appears to be the junction between the ventricle and the atrium.

An alternative view of proepicardium outgrowth and migration can be seen in figures 3-7(D) to (F). These are frontal sections through a stage 42 tadpole heart. Again the

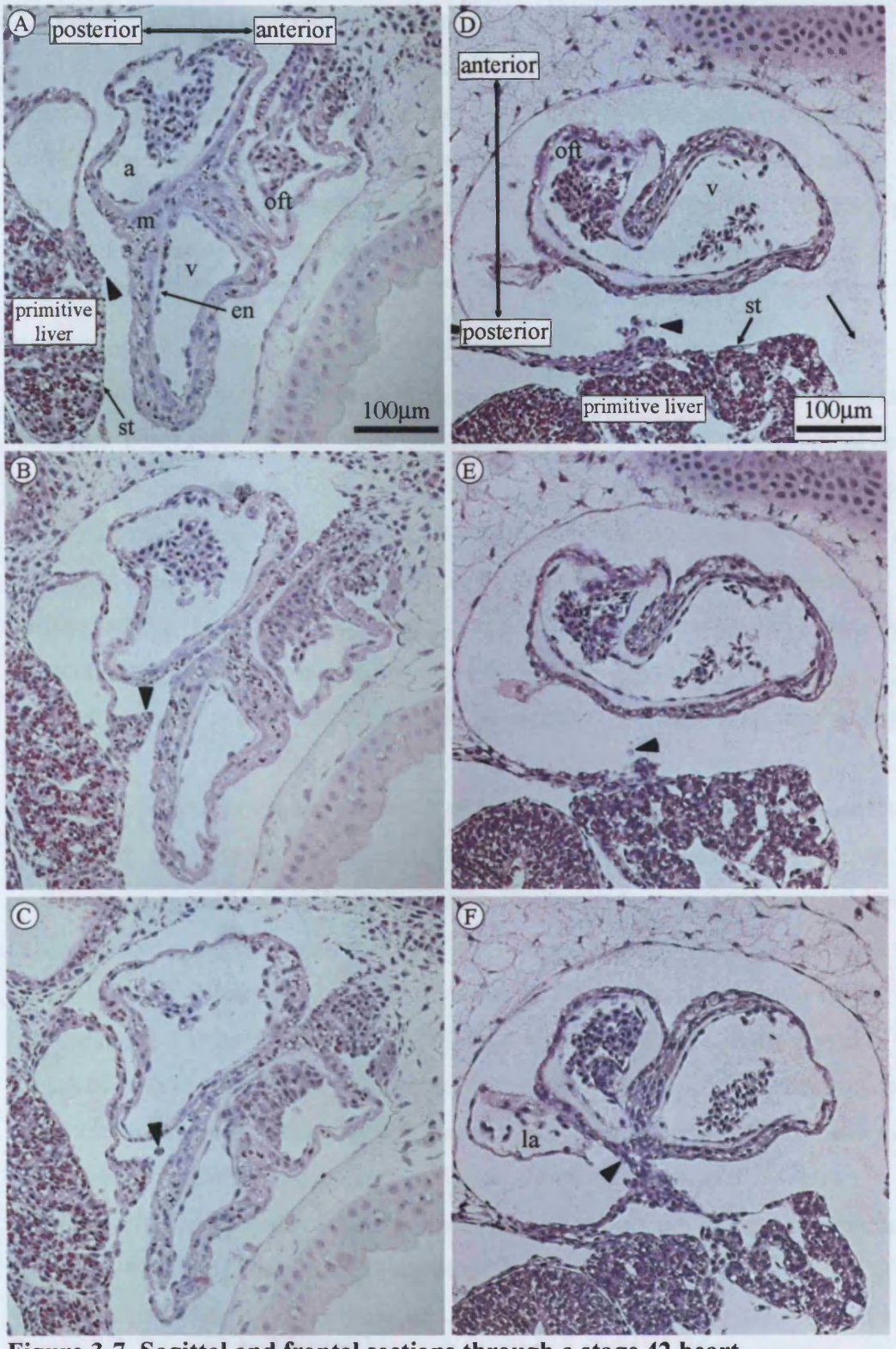

Figure 3-7. Sagittal and frontal sections through a stage 42 heart.

(A) to (C)- sagittal sections through the heart. At this stage in development the proepicardium (arrowheads) has started to grow out from the septum transversum (st). The proepicardium appears as a cone shape projecting towards the junction between the ventricle and the atrium. Individual epicardial cells can be seen mi-

Figure 3-7. Sagittal and frontal sections through a stage 42 heart continued - grating across to the heart (arrowhead in (C)). (D) to (F)- frontal sections through the heart. Again the proepicardium can be seen projecting from the septum transversum towards the heart. (F) shows the proepicardium has actually contacted the heart (arrowhead) and epicardial cells are beginning to migrate over the heart. Interestingly the septum transversum is incomplete at this stage (arrow in (D)).

---

proepicardium can first be seen as a thickening of the septum transversum. Progressing more dorsally through the region, the proepicardium can again be seen to be a cone shaped protrusion. Figure 3-7(E) indicates an individual proepicardial cell that has detached from the proepicardium and is migrating towards the heart. In figure 3-7(F) the proepicardium has actually attached to the heart and proepicardial cells are migrating across to attach to the surface of the heart at the junction between the atrium and the ventricle. It is also interesting that at this stage the septum transversum is incomplete, and a large communication exists between the right side of the pericardial cavity and the coelomic cavity, as indicated by an arrow on figure 3-7(D).

By stage 46 the tadpole heart comprises of separate left and right atria, the ventricle, and complete spiral and AV valves. At this stage, earlier SEM analysis has shown that a smooth epithelial layer covers the surface of the heart. Figures 3-8(A) to (D) show sections from a single frontal section series through a stage 46 heart. By this stage the single ventricle is heavily trabeculated (arrows on figure 3-8(A)) and has a very similar internal structure to the adult frog heart. The endocardial and myocardial layers of both the ventricle and OFT can be seen, however, unlike in earlier sections a third additional layer, the epicardium, can also be seen. The epicardium is usually in close association with the myocardium. In some locations, such as those shown in figures 3-8(C) and (D), there is a space between the epicardium and the myocardium. Figures 3-8(E) and (F) show high magnification views of the epicardium region of a stage 46 heart. Here the epicardium can clearly be seen as a distinct layer from the myocardium. Also the subepicardial space shown in figure 3-8(F) appears to contain mesenchymal cells.

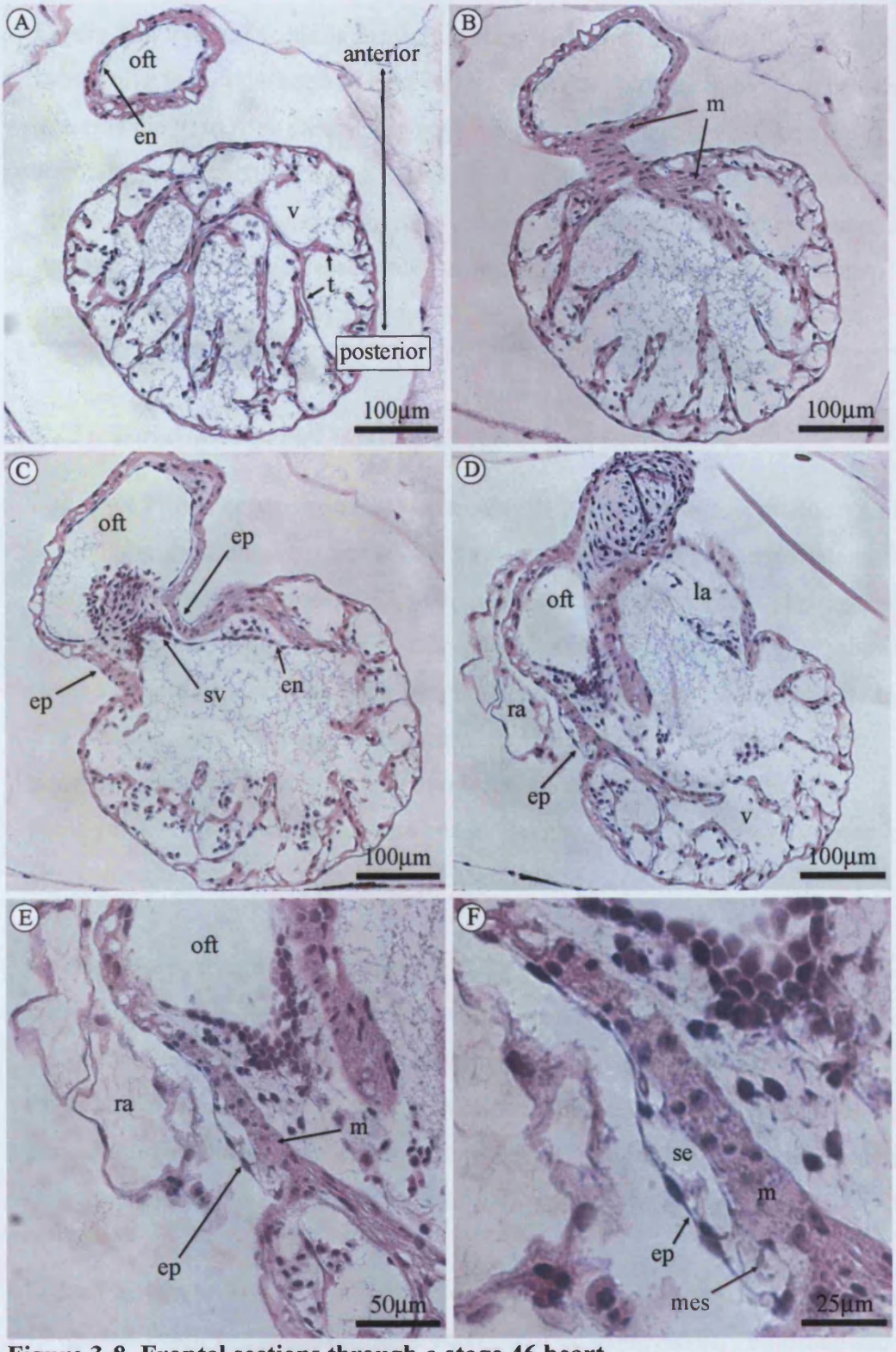

Figure 3-8. Frontal sections through a stage 46 heart.

(A) and (B)- sections through the ventricle and outflow tract. By this stage in development the heart is showing extensive trabeculation (t). The myocardium (m) and the endocardium (en) of the ventricle (v) and the outflow tract (oft) can be seen. (C) and (D) show sections through a more dorsal area of the heart. Here the

Figure 3-8. Frontal sections through a stage 46 heart continued -
spiral valve (sv) in the outflow tract can be seen. The epicardium (ep) can be seen covering the heart. It is particularly apparent around the junction between the ventricle and the outflow tract. (E) and (F) show high magnification images of the epicardium area. The epicardium can be clearly distinguished from the myocardium. A region of subepicardial space (se) can be seen in (F) which appears to contain subepicardial mesenchyme cells (mes).

3.2.5 Three-Dimensional Modeling Of Epicardium Development

Episcopic Fluorescence Image Capturing (EFIC) is a technique that produces serial section images in a manner that retains their alignment and precise registration. Such data is ideally suited for use in 3D modeling of complex morphological structures (Weninger et al., 2006; Weninger and Mohun, 2002). Figures 3-9(A) to (F) show section images captured using this technique. Stage 42 tadpoles were embedded in JB4 plastic resin containing 2.75mg/ml eosin and 1mg/ml Orasol Black. 2_m transverse sections were taken on a horizontal microtome and the block was photographed after each section was taken. The image data sets were converted to greyscale after removal of the red and blue channels.

As can be seen from figures 3-9(A) to (F), the resolution achieved using this technique is not as high as can be achieved using conventional histology. However, the resolution is sufficiently high to distinguish the major chambers of the heart, the trabeculation within the ventricle, blood cells within the atria and the ventricle, the pericardium, and also other organs such as the liver and intestine. The real benefit of capturing data in this way however, is the ability to generate 3D models.

Figures 3-9(G) to (I) show a 3D reconstruction of such a section series through a stage 42 tadpole heart. The greyscale range was optimised using Adobe Photoshop and the data was scaled to give cubic voxels. Image data was then 3D volume rendered using Osirix 2.6.

The proepicardium can be seen growing out from the septum transversum/liver region

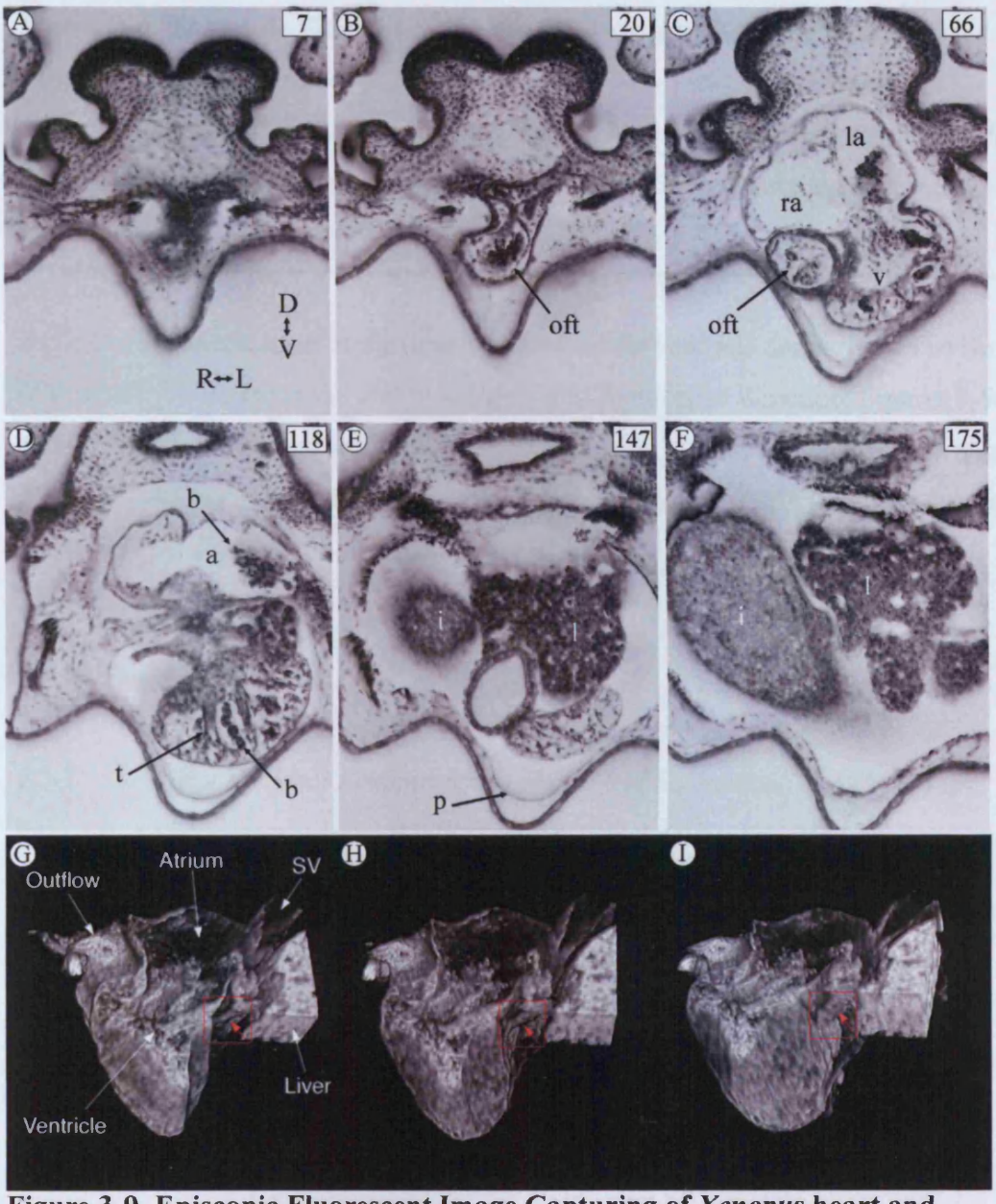

Figure 3-9. Episcopic Fluorescent Image Capturing of *Xenopus* heart and proepicardium. (A)-(F)- 2μm transverse sections were taken through a stage 42 tadpole embedded in plastic resin containing eosin and Orasol Black dye. The orientation of the heart is shown as viewed from the anterior aspect with dorsal to the top and the right cardiac side to the left as shown in (A). Section numbers are shown in the top right of each panel. The outflow tract (oft), right atrium (ra), left atria (la), and ventricle (v) can be seen. Blood cells (b) can be distinguished within the atria (a) and between the trabeculations (t) of the ventricle. (E) and (F)- the liver (l) and intestine (i) can be seen in the more posterior sections. (G) to (I)- 3D rendering of section series through a stage 42 heart captured via episcopic fluores-

Figure 3-9. Episcopic Fluorescent Image Capturing of *Xenopus* heart and proepicardium continued –

cence image capturing. The proepicardium (red arrows) can be seen growing out from the septum transversum/liver region and attaching to the heart at the atrioventricular junction.

---

and attaching to the heart at the junction between the ventricle and atrium. The benefit of a virtual 3D model is the ability to rotate it in any desired direction. Figures 3-9(H) and (I) have been rotated so the proepicardium can be viewed from alternative angles. Much of the liver and other surrounding tissues have also been digitally removed to allow clearer visualisation of the area of interest.

3.3 Discussion

3.3.1 Structure Of Adult Xenopus laevis Heart And Epicardium

The structure of the adult frog heart shown in figure 3-1 reveals two important differences between it and the hearts of higher vertebrates. Firstly the gross structure of the frog heart is almost sponge-like in appearance due to the large number of extended trabeculae. By having these the amphibian heart can operate at a mechanical advantage compared to higher species. This is because the trabecular network creates many inter-trabecular spaces (lacunae), which act as small heart compartments within the large ventricle. Because the lacunae are very small, much less pressure is needed to pump the blood through the heart, thus increasing contractile efficiency compared with species with a smooth-walled myocardium such as mammals (Johansen, 1965). In this respect, the internal structure of the frog ventricle is similar to that described for zebrafish (Hu et al., 2000; Hu et al., 2001).

Secondly it can be seen that the compact layer (as demarcated by the red bar in figure 3-1(B)) of the frog ventricle is very thin in comparison to that described in mammalian and avian species (Hu et al., 1991; Taber et al., 1992). The reason for this is likely to be twofold. Firstly since lower vertebrate hearts have a higher pumping efficiency than mammalian and avian hearts due to the presence of the lacunae, they

do not need to generate the same pressures as those found in these species, and thus do not require such thick compact layers. Secondly, since the frog heart has only one ventricle, there is some mixing of oxygenated and deoxygenated blood. Although mixing is minimised by the trabeculae and the presence of the spiral valve (Delong, 1962; Haberich, 1965), the pressure exerted on the heart by the blood itself is lower than in a completely closed system, and so a large compact layer is not required.

Importantly, these two observations most likely account for why the amphibian heart has no need for coronary vasculature. The spongy nature of the myocardium, caused by the lacunae, allows the muscle to receive sufficient oxygen via direct diffusion with the blood in the lacunae. Similarly, the compact layer of the ventricle is sufficiently thin to allow direct diffusion with the blood in the chamber.

3.3.2 Timing Of Proepicardial Outgrowth And Epicardium Development

Proepicardial outgrowth in mouse and chick begins when the heart is in an advanced state of rightward looping. The heart of a *Xenopus laevis* tadpole is at an advanced state of rightward looping at around stage 35/36. This was predicted to be the stage at which proepicardium outgrowth would begin in *Xenopus laevis*. However, as can be seen from figures 3-5(B) and 3-6, proepicardium outgrowth cannot be observed until after stage 37/38 and is not in fact detected in *Xenopus laevis* until around stage 42.

A possible explanation for the difference between anuran amphibians and mammals or birds may be the different mechanisms by which the ventricular myocardium receives oxygen in these species. The fact that birds and mammals have developed larger, more complex hearts, with a four-chambered closed system, has meant they have had to develop a coronary vascular system. This is because the thickness of the left ventricle, to deal with the increased pressure of the oxygenated blood, prevents direct diffusion between the blood and muscle. Also the right chambers of the heart are only ever exposed to deoxygenated blood so are unable to acquire oxygen directly.

An important role of the epicardium in mammalian and avian heart development is to

supply the progenitors of the coronary vasculature. This could explain why the epicardia of these higher species develop at an earlier stage in cardiogenesis. However, the fact that *Xenopus laevis* does develop an epicardium, albeit later, suggests that the epicardium plays other roles in frog heart development consistent with suggestions of an epicardial role in myocardium development modulation, conduction system formation, valve formation, and OFT sculpting and remodelling in other vertebrate species.

3.3.3 Epicardium Development In Xenopus laevis

The precise structure of the proepicardium varies between species and the data presented here shows the proepicardium of *Xenopus laevis* is located asymmetrically. Figure 3-5(C) shows a SEM image of the right side of a stage 42 *Xenopus laevis* tadpole heart. It can clearly be seen that the proepicardium is located to the right of the sagittal plane. Equivalent images were produced of the left side of the heart and neither the proepicardium nor migrating epicardium were observed. This is similar to published data for the chick (Ho and Shimada, 1978).

Further similarities exist between proepicardial outgrowth and method of proepicardial attachment in chick and frog. The data presented here suggest that both of the known methods of proepicardial attachment (free floating cell aggregates and direct attachment of a proepicardial bridge) are utilised in *Xenopus laevis* heart development. The coexistence of both methods of attachment has also been described in the chick although the direct attachment of the proepicardium protrusions is thought to be of far greater importance (Manner, 1992; Nahirney et al., 2003).

It has been suggested that direct attachment of the proepicardium to the myocardium is necessary in the chick due to the late closure of the septum transversum (Hiruma and Hirakow, 1989). A large communication exists in the chick between the pericardial cavity and the coelomic cavity at the time of proepicardial outgrowth. Cells that simply detach from the proepicardium and float across the pericardial cavity could be lost through the incomplete septum transversum. As can be seen from figures 3-7(D) to (E) this is also the case in *Xenopus laevis*. Here the septum

transversum is clearly incomplete. Interestingly it is the right side of the septum transversum that is yet to fully close. This could be significant since cells detaching from the right-sided proepicardium could easily be lost through this opening.

It is possible to make a crude guess at the dimensions of the proepicardium by using the thickness of the sections. The proepicardium spans 23 7μm sagittal sections and 19 7μm frontal sections giving it overall dimensions of approximately 161μm wide by 133μm high. This is consistent with data from the chick (Nahirney et al., 2003). Here the dimensions of the proepicardium at the onset of outgrowth (HH14) were reported as 150μm wide by 120μm high. The size of a HH14 chick embryo is very similar in size (approximately 7.5mm) to a stage 42 *Xenopus laevis* tadpole.

Once the proepicardial cells have attached to the myocardium they continue to spread out over the entire surface of the heart. A complete description of the pattern of epicardial spreading is not possible from the SEM and histological section data presented here. However, figure 3-5(C), and figure 3-7 show the first area of the heart to be covered by the epicardium is the AV and CV canals. This is consistent with observations in other species (Fransen and Lemanski, 1990; Komiyama et al., 1987; Vrancken Peeters et al., 1995) suggesting that the pattern of epicardial coverage might be conserved. Certainly the limit of the epicardium appears to be conserved. Figure 3-5(E) shows the epicardium does not cover the entire OFT and a similar finding has also been reported in mouse and chick (Komiyama et al., 1987; Manner, 1999; Perez-Pomares et al., 2003), where the limit of the epicardium is described as being the junction between the mesenchymal and myocardial OFT.

The mechanism by which the epicardial cells might spread can be seen in figures 3-5(C) and (D). The epicardial cells have filopodia which form focal adhesions with the myocardium, presumably anchoring them to the cell surface, and preventing them being swept away by the pericardial fluid. The filopodia also allow the epicardial cells to populate the entire surface of the heart. The epicardial cells migrate over the heart by extending their filopodia at the leading edge. Following attachment to the myocardium, contraction of actin filaments within the filopodia moves the cell forward. Filopodia have been observed on the advancing edge of the epicardium of

both the axolotl (Fransen and Lemanski, 1989; Fransen and Lemanski, 1990) and chick (Sejima et al., 2001), and are a well established component of epithelial cell migration (Wehrle-Haller and Imhof, 2002).

Once the epicardium covers the heart of both chick and mouse, a subepicardial space develops (Manner, 1999; Perez-Pomares et al., 2003), shortly followed by an EMT (Perez-Pomares et al., 1998b). The subepicardial space can also be observed in *Xenopus laevis* once the epicardium has covered the heart (figures 3-8(C) to (F)). It is also present in the adult heart (figure 3-1(D)). It is not known if the subepicardial space is important for the adult heart, nor do we know if the epicardium of *Xenopus laevis* undergoes an EMT. Since the primary role of the EMT is to generate the progenitors of the coronary vasculature (which *Xenopus* lacks), this would be an interesting question to address. Areas of subepicardial mesenchyme can be seen in stage 46 tadpoles (figures 3-8(E) and (F)) but whether this is epicardial or myocardial in origin is unknown.

There are numerous markers of EMT that could be used to investigate this further. N-cadherin, Vimentin, Fibronectin, Snail, Slug, Twist, Goosecoid, and Sox10 are proteins known to increase in abundance, whilst E-cadherin and cytokeratin are known to decrease in abundance (Lee et al., 2006). A decrease in E-cadherin, as visualised with the well characterised antibody against *Xenopus* E-cadherin (Choi and Gumbiner, 1989), coupled with an increase in Vimentin, as visualised with the 14h7 antibody against *Xenopus* Vimentin (Klymkowsky et al., 1987) available from the Developmental Studies Hybridoma Bank, could be used to visualise the process of EMT during epicardium development.

4 Results: Lineage Analysis Of *Xenopus laevis* Epicardium

4.1 Introduction

4.1.1 Fate Mapping In Xenopus

A fate map charts lineage relationships between parent and daughter cells through many cell divisions during the development of an embryo. It can therefore trace the origin of an organ or tissue back to distinct regions of the early embryo. It can also reveal common ancestor cells for apparently diverse groups of embryonic tissues. In addition, a good fate map provides knowledge of the coordinated cell movements that occur during embryogenesis. Defining the origin and movement of cells in an embryo (their ontogeny) is essential to understanding the sequence of influences and signals that they have experienced.

A reliable fate map exists for embryos of *Xenopus laevis* that has been compiled from many studies, and is well summarized by Lane and Sheets (Lane and Sheets, 2006) and Sive (Sive et al., 2000). *Xenopus* embryos display a highly regimented pattern of cell division and morphogenesis and because of this the origins of all major tissues and organs can be traced back to specific blastomeres of early cleavage stage embryos, or to particular regions of blastula or gastrula stage embryos. The *Xenopus* fate map is so well accepted that current debate centres on the terminology used to describe it, rather than on the lineage data itself (Lane and Sheets, 2006). Here the traditional definitions of the embryonic axes found in the cleavage stage embryo will be used to describe this study of epicardial origin (left-right, dorsal-ventral and animal-vegetal axes).

4.1.2 Current Understanding Of The Origin Of The Epicardium

The major, myocardial component of the heart originates from bilateral domains of lateral plate mesoderm located at the dorsal aspect of the embryo. That is, myocardial cells are descendents of the two dorsal blastomeres of the four-cell stage embryo and of the two dorsal-vegetal blastomeres at the 8-cell stage. Later in development this will translate to bilateral, vegetal regions of the dorsal marginal zone at blastula and

early gastrula stages. However, the resolution of the existing fate map is not sufficient to resolve the origin of the epicardium within the early embryo. The fact that the epicardial precursor cells are migratory, are few in number and they do not form a recognisable cardiac structure until late in tadpole development makes them particularly difficult to trace.

Studies in other vertebrate species have noted significant differences in the outgrowth of the proepicardial organ in mouse and chick embryos that relate to the origin and laterality of this tissue. In mouse embryos, the proepicardium forms from two regions of mesothelial cells, bilaterally located on the ventral-caudal wall of each side of the sinus venosus. These left and right-sided anlagen merge and apparently make an equal contribution to the developing proepicardium (Schulte et al., 2007; Viragh and Challice, 1981). In chick embryos however, only the right-sided anlagen undergoes rapid growth to form the proepicardium. The left-sided anlagen remains in a rudimentary state and ultimately disappears in chick (Ho and Shimada, 1978; Schulte et al., 2007). Preliminary experiments to address the different potential of the left and right anlagen in chick suggest that it is established early in development and could be linked to the specification of the left versus right-sided body axis. Since the left and right halves of the sinus venosus are known to originate from the left and right sides of the early embryo and, providing the observed anlagen truly are direct descendents of the sinus venosus, then it appears that the mouse epicardium has a bilateral fate map while the chick epicardial layer originates solely from the right side of the early embryo.

In the case of *Xenopus*, if the basic ontogeny of the epicardium could be determined, it would greatly improve the experimental accessibility of this cell layer. From a practical perspective, it would allow more precise targeting of the epicardium, and more accurate delivery of molecules to the cells of the forming epicardium. This could be particularly useful when examining the function of a gene that is normally required in multiple cell types during embryonic development. For example, MOs that interfere with the expression of an epicardial gene could be injected into those blastomeres that contribute to the epicardium while avoiding the blastomeres that form other tissues where that gene function is also necessary. Also, if *Xenopus* embryos have a unilateral origin of the epicardium as is observed in chick, the

injection strategy could be refined by delivery of MOs to only the right-sided blastomere in order to target all the epicardial progenitors.

4.1.3 Aims Of This Chapter

This chapter will describe experiments designed to address whether there is an equal contribution to the epicardial cell layer from the left and right-sided blastomeres of the early embryo in *Xenopus*. Also experiments to confirm that progeny of dorsal blastomeres (at the four-cell stage) and not ventral blastomeres form the epicardium, as is the case for other tissues of the heart, will be described.

4.2 Results

4.2.1 Injection Of Lineage Marker RNAs Into Xenopus Blastomeres

Two RNAs were used as the lineage markers in this experiment. The first encoded the red fluorescent protein, DsRed1, while the second encoded a nuclear-localized form of the enzyme β-galactosidase. The two RNAs were pooled together and injected at concentrations of 200pg of each RNA into the equatorial region of individual blastomeres of four-cell stage embryos. The equatorial region was targeted to ensure the highest concentration of RNA was delivered to regions of the blastomere that will ultimately produce mesodermal tissue. Only embryos with perpendicular cleavage furrows (cell boundaries) and clear dorsal-ventral patterns of pigment distribution were chosen for injection. The experiment was performed on two separate occasions and in each case, all four injection classes were performed on the same batch of embryos from a single fertilisation. The injected RNAs were chosen as lineage tracers in preference to fluorescent-Dextran beads or the horseradish peroxidase enzyme because stability and detection of the signal during late tadpole stages was paramount (Sive et al., 2000). The combined use of DsRed1 and nuclear β-galactosidase allows the detection of lineage-marked progeny cells by their fluorescence emission in living animals and also by blue X-gal staining methods that are suitable for subsequent histological examination.

Left-Dorsal Lineage

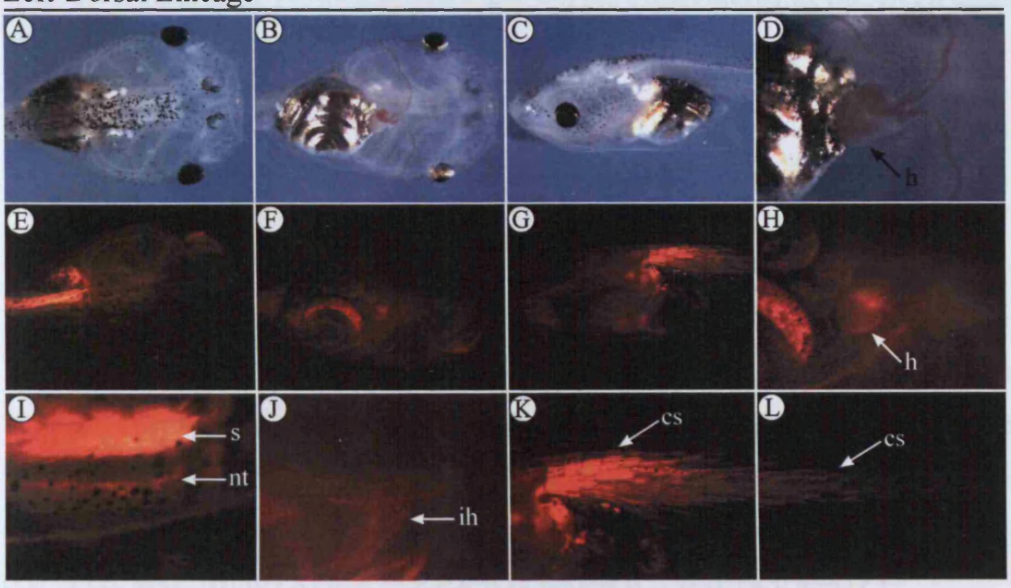

Right-Dorsal Lineage

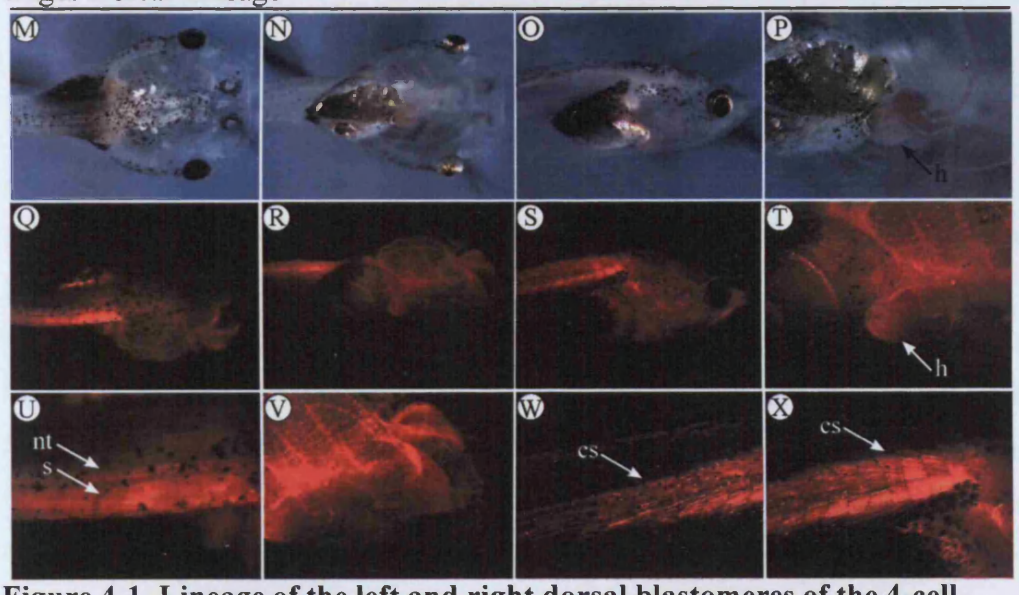

Figure 4-1. Lineage of the left and right dorsal blastomeres of the 4-cell embryo. Two stage 47 tadpoles display typical, restricted patterns of DsRed1 fluorescence that shows the lineage relationship of tissues to the two dorsal blastomeres of the 4-cell embryo. (A) to (L)- the fluorescence of the tadpole results from injection of 200pg of DsRed1 RNA (and also 200pg nuclear-localized b-galactosidase RNA) into the left-dorsal blastomere when the embryo was at the four-cell stage. (A) and (E)- brightfield and darkfield images show a dorsal view of the head and trunk. (B) and (F)- ventral view of the head and trunk. (C) and (G)- left-lateral view of the head and trunk. (D) and (H)- detail, ventral view of the heart (h). (I)- detail, dorsal view of the neural tube (nt) and somites (s). (J)-

Figure 4-1. Lineage of the left and right dorsal blastomeres of the 4-cell embryo continued -

facial muscle (ih). (K) and (L)- left-lateral views show that the DsRed1 signal is restricted to the central portion of the somites (cs) of the trunk and tail. (M) to (X)- the fluorescence of the second tadpole results from injection of the same RNAs into the right-sided dorsal blastomere at the four-cell stage. (M) and (Q)- dorsal view of the head and trunk. (N) and (R)- ventral view. (O) and (S)- right-lateral view. (P) and (T)- detail, ventral view of the heart. (U)- detail, dorsal view of the neural tube and somites. (V)- ventral view of the head showing the right interhyoid muscle. (W) and (X)- right-lateral views again show that DsRed1 is restricted to the central portion of the somites in the trunk and tail. Anterior is to the right in panels (A), (B), (D) to (F), (H) to (J), and (M) to (X) and to the left in panels (C), (G), (K), and (L).

4.2.2 Assessing Cell Lineage Using DsRed1 Fluorescence

Embryos were allowed to develop to stage 47, when the pattern of fluorescence emitted from the resulting DsRed1 protein was assessed in living tadpoles. At this point, the best tadpoles were selected that exhibited lineage-restricted patterns of DsRed1 fluorescence that were absolutely consistent with the known fate-map of the injected blastomeres (figures 4-1 and 4-2). The criteria used for selection of both the left and the right-dorsal blastomere injections were unilateral labelling of the skeletal muscles, particularly of the interhyoid muscle of the jaw (figures 4-1(J) and (V)) and the somites (figures 4-1(I) and (U)). As well as being one-sided, the somite fluorescence had to mark the central-most portion in the trunk and tail (figures 4-1(K), (L), (W) and (X)). There had to be obvious fluorescence in the heart myocardium (figures 4-1(H) and (T)) but none in the circulating red blood cells. For the embryos where the left or right-ventral blastomere was injected, tadpoles displayed unilateral labelling of the dorsal and ventral-most portions of the somites (figures 4-2(F), (G), (P) and (R)). Fluorescence had to be detected in circulating red blood cells but with no obvious signal in the heart myocardium (figures 4-2(I) and (N)). Additionally, sided labelling within the gut tube had to be noted (figures 4-2(H) and (Q)). Approximately half of the embryos originally injected, passed these stringent selection criteria.

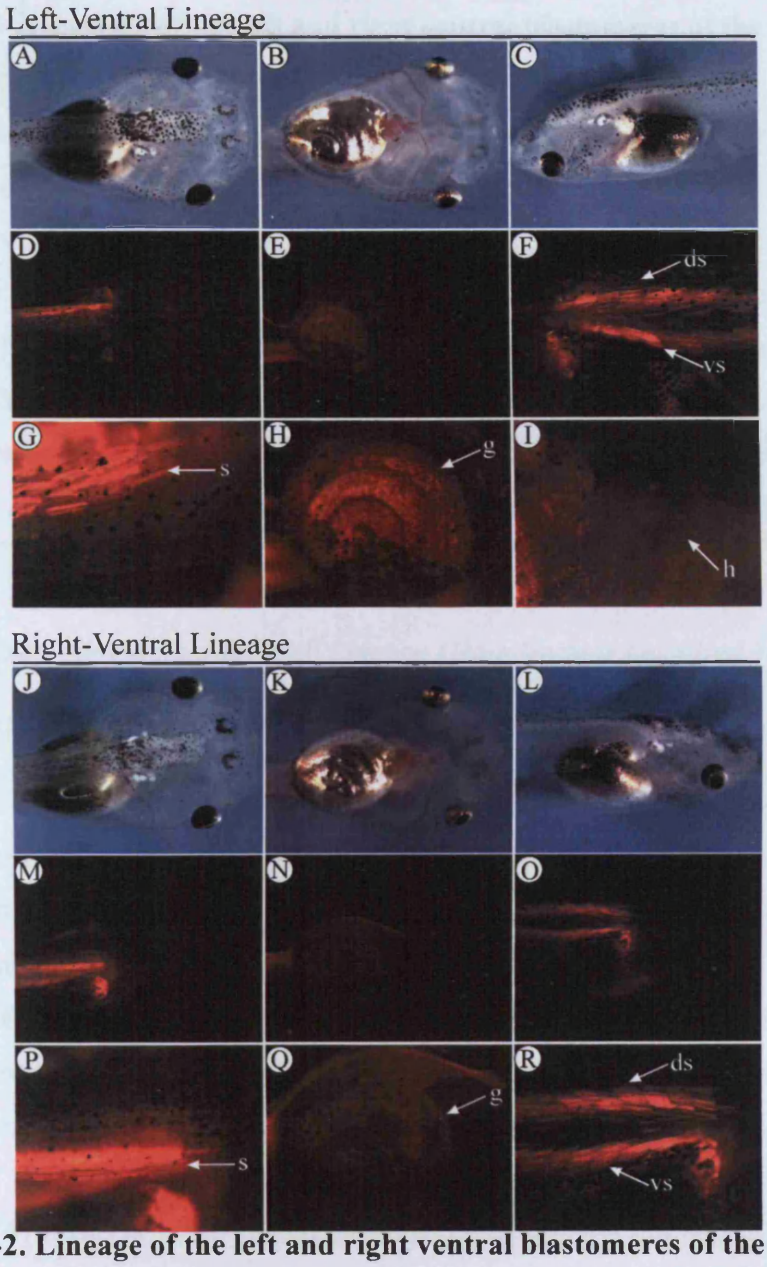

Figure 4-2. Lineage of the left and right ventral blastomeres of the 4-cell embryo. Two stage 47 tadpoles display typical, restricted patterns of DsRed1 fluorescence that shows the lineage relationship of the two ventral blastomeres of the 4-cell embryo. (A) to (I)- the fluorescence of the tadpole results from injection of 200pg of DsRed1 RNA (and also 200pg nuclear-localized b-galactosidase RNA) into the left-sided ventral blastomere when the embryo was at the four-cell stage. (A) and (D)- dorsal view of the head and trunk. (B) and (E)- ventral view. (C) and (F)- left-lateral view bright-field image and a detail, dark-field image shows DsRed1 is restricted to the dorsal (ds) and ventral (vs) portions of the somites. (G)- detail, dorsal view shows that no fluorescence is detected in the

Figure 4-2. Lineage of the left and right ventral blastomeres of the 4-cell embryo continued -

neural tissue (somites (s)). (H)- ventral view of the gut. (I)- ventral view shows the absence of DsRed1 in the heart (h). (J) to (R)- the fluorescence of the second tadpole results from injection of the same RNAs into the right-sided ventral blastomere at the four-cell stage. (J) and (M)- dorsal view of the head and trunk. (K) and (N)- ventral view. (L) and (O)- right-lateral view. (P)- detail, dorsal view shows fluorescence in somites but not neural tissue. (Q)- ventral view of the gut. (R)- right-lateral view shows DsRed1 again restricted to the dorsal and ventral portions of the somites. Anterior is to the right in all panels, except (C) and (F) where anterior is to left.

4.2.3 Examining Epicardial Cell Lineage Using Nuclear Localized β-galactosidase Activity

Tadpoles that passed the selection criteria were fixed and stained for β-galactosidase activity using X-gal substrate (figure 4-3). The nuclear localized blue stain that marked descendents of the injected blastomere developed rapidly in stage 47 tadpoles. The patterns of blue lineage stain obtained were identical to the results observed using DsRed1 fluorescence, with the additional benefit that the nuclear localisation of the stain allowed the identification of individual cells within the embryo (figures 4-3(E), (J), (L) and (N)).

At stage 47 it was possible to determine the origin of numerous epicardial precursor cells present on the outer surface of the tadpole heart. Beyond stage 47 however, the assay did not work satisfactorily. The failure of the stain beyond stage 47 is probably due to the gradual thickening of the epidermis during development which makes it more difficult for the X-gal substrate to penetrate. 10μm frontal, wax sections were used to analyse stage 47 tadpole hearts for the presence of X-gal stained cells (figures 4-4 to 4-6). Also a Feulgen, pink nuclear counterstain was used to reveal all (other) cell nuclei on the sections. The entire series of sections through the heart was photographed in order to obtain a complete picture of the cardiac cell fate map.

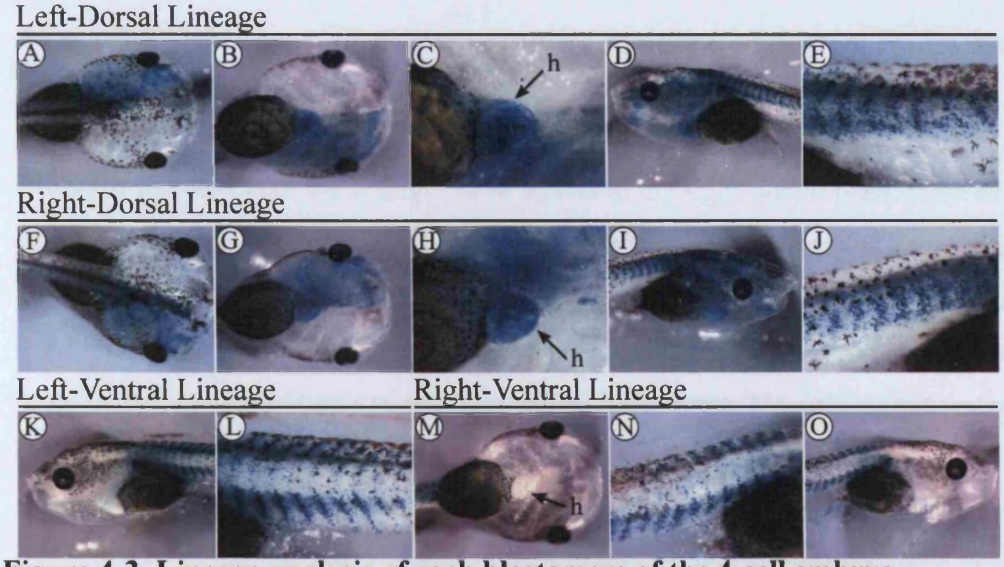

Figure 4-3. Lineage analysis of each blastomere of the 4-cell embryo.

The contribution of individual blastomeres of the four-cell stage embryo to tadpole tissue at stage 47 can be observed in detail by using a nuclear-localized form of the b-galactosidase enzyme as a lineage marker. (A) to (E)- the lineage relationship of the left-sided dorsal blastomere is shown by the blue X-gal stain of a tadpole, following injection of both DsRed1 and b-galactosidase RNAs when the embryo was at the four-cell stage. The correct lineage-restriction of the DsRed1 fluorescence was used to identify the best tadpoles for subsequent X-gal staining. (A)- dorsal view of the head and trunk. (B)- ventral view. (C)- detail, ventral view of the heart (h). (D)- left-lateral view. (E)- detail, left-lateral view of blue stain in the central portion of the somites. (F) to (J)- the lineage of the right-sided dorsal blastomere is shown by the blue X-gal stain of a tadpole, following injection of the two RNAs at the four-cell stage. (F)- dorsal view. (G)- ventral view. (H)- detail, ventral view of the heart. (I)- right-lateral view. (J)- detail, right-lateral view of blue stain in the central somite portion. (K) and (L)- the lineage of the left-sided ventral blastomere in a tadpole. (K)- left-lateral view. (L)- detail, left-lateral view of blue stain in the dorsal and ventral portions of the somites. (M) to (O)- the lineage of the right-sided ventral blastomere. (M)- ventral view. (N)- detail, right-lateral view of blue stain in the dorsal and ventral portions of the somites. (O)- right-lateral view. Anterior is to the right in panels (A) to (C), (F) to (J), and (M) to (O) and to the left in panels (D), (E), (K), and (L).

4.2.4 The Right-Dorsal Blastomere Provides A Major Contribution To Epicardial Precursors

Embryos injected with the lineage tracer RNAs in the right-dorsal blastomere at the four-cell stage gave tadpole hearts with characteristic arrangements of X-gal stained cell nuclei (figure 4-4). Within these hearts, the right side of the distal OFT (figures 4-4(A) and (B)) and the right atrium (figures 4-4(D) and (E)) are comprised exclusively of cells that are descendents of the right-dorsal blastomere. No right-dorsal progeny cells are located on the converse, left side of the distal OFT and left atrium. Within the myocardium of the ventricle and the proximal OFT, the region occupied by the right-dorsal blastomere descendents appears contorted into a posterior and dorsal position (figures 4-4(C) to (E)). This twisted pattern of right-sided laterality within the ventricular myocardium is consistent with previous fate map studies of the *Xenopus* heart (Gormley and Nascone-Yoder, 2003; Ramsdell et al., 2006). Therefore, the correct, right-dorsal fate map observed for the myocardium acts as an internal control that can validate the analysis of epicardial cell lineage.

When the outer surface of the heart ventricle is viewed in detail, numerous cell nuclei can be observed that have an elongated morphology compared with nuclei within the adjacent myocardium (fig. 4-4(F) to (J)). These adherent cells are found at all locations on the ventricle surface. Significantly, in the tadpole shown, all the adherent cells are stained blue, not pink, and so are derived from the right-dorsal blastomere of the early embryo. Based on the morphology, position and the developmental stage at which the analysis was performed, it can be assumed that these are cells of the epicardial layer. Similar histological analyses were performed on 10 tadpoles with right-dorsal lineage injection and an identical, right-dorsal blastomere contribution to the epicardial layer was observed in all 10 tadpoles.

4.2.5 Epicardial Precursors Are Not Derived From The Left-Dorsal Blastomere

Embryos injected with β-galactosidase RNA in the left-dorsal blastomere produced essentially the opposite pattern of lineage labelling within the stage 47 tadpole hearts (figures 4-5 and 4-6). The left side of the distal OFT (figures 4-5(A) and (B)) and the

Right-Dorsal Lineage

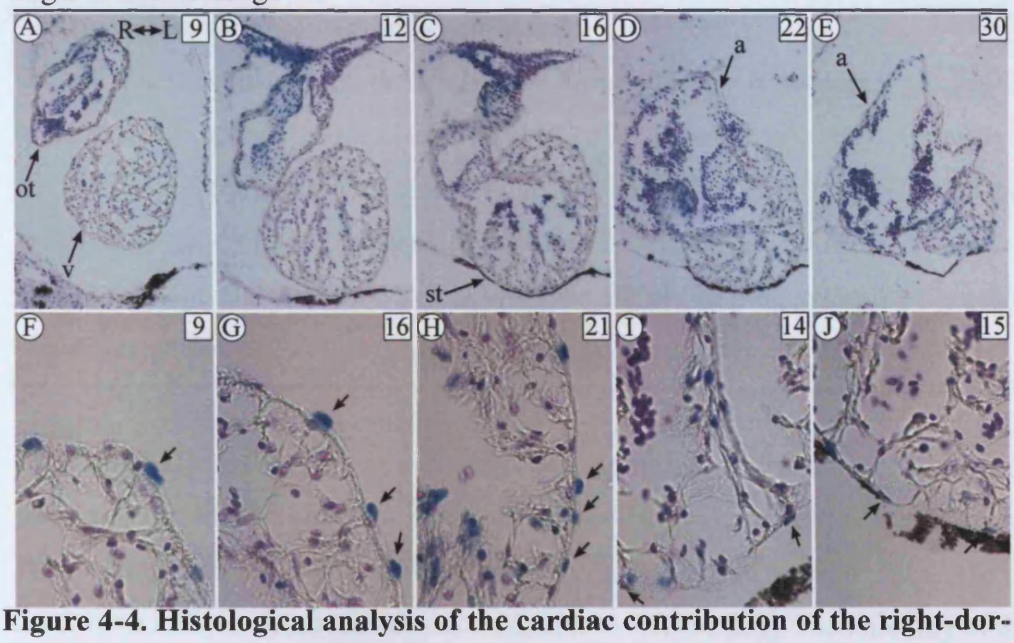

Figure 4-4. Histological analysis of the cardiac contribution of the right-dorsal blastomere of the 4-cell embryo. Histological analysis reveals the contribution of the right-sided dorsal blastomere of the four-cell stage embryo to the tadpole heart and in particular, to the epicardial layer. (A) to (E)- five representative frontal sections (10μm) marking progressively dorsal slices through the heart of a X-gal stained, right-dorsal lineage-labelled, stage 47 tadpole. The nuclei of progeny cells of the right-dorsal blastomere are stained blue and in addition, the sections have been counterstained to reveal all (other) cell nuclei in pink. Sections are numbered (top right of each panel), commencing from the ventral-most slice of the ventricle. The orientation of the heart is shown as viewed from the ventral side, with the right cardiac side on the left side of all images presented (denoted by the double headed arrow in figure (A)). Anterior is to the top, while the brown pigment cells of the posterior-located septum transversum (st) appear at the bottom. Right-dorsal progeny cells are located on the right side of the distal outflow tract (ot) and the right side of the atrial chamber region (a). Whereas in the myocardium of the ventricle (v), these blue cell nuclei occupy a more posterior and dorsal position (figures (C) to (E)) caused by rotation of the heart tube during cardiac chamber morphogenesis. Importantly many blue stained cells can be seen on the outer surface of the heart. (F) to (J)- detail images of sections that show the outer surface of the cardiac ventricle. Many blue cell nuclei are observed adhering to the ventricle (arrows) that have a different, elongated morphology, compared to

Figure 4-4. Histological analysis of the cardiac contribution of the right-dorsal blastomere of the 4-cell embryo continued -
the cell nuclei within the myocardial layer. These adherent right-dorsal progeny cells are distributed at anterior (figures (F) and (G)), left-sided (figure (H)), posterior (figure (I)) and right-sided locations (figure (J), and also (A), (C), and (D)) on the ventricle at stage 47 and are assumed to be cells of the epicardial layer. All the elongated, adherent cells observed in this heart stained as progeny of the right-dorsal blastomere.

---

left atrium (figures 4-5(E)) consist exclusively of left-dorsal blastomere descendents, while no stained cells are located on the right side of these regions of the heart. Within the ventricular myocardium, the region of left-dorsal lineage is contorted, and occupies a left-sided, anterior position (figures 4-5(A) to (D)). The laterality of the proximal OFT also appears twisted, with left-dorsal blastomere progeny occupying a ventral and not dorsal position (compare the OFT closest to the ventricle in Figure 4-5(B) -ventral side, with Figure 4-5(C) -dorsal side).

Detail views of the outer surface of the ventricle also show epicardial cells with the distinctive elongated nuclear morphology (figures 4-5(F) to (J)). In the heart presented, none of these adherent cells stained as descendents of the left-sided dorsal blastomere and so were coloured pink. Seven tadpoles with left-dorsal lineage injection were subjected to such histological analyses and in five of these, not a single blue stained epicardial cell was detected on the surface of the heart. Of the remaining two tadpoles, one had two blue stained cells adhering to the surface of the heart while the other had five, suggesting a very minor left-blastomere epicardial contribution.

To further demonstrate the absence of left-dorsal blastomere progeny among the epicardial cells, a tadpole was subjected to a grossly overdeveloped X-gal staining reaction (figure 4-6). Despite the very heavy blue lineage stain, the basic features of the left-sided fate map are present within the heart (figures 4-6(A) to (E)). Again, all cells that clearly adhere to the outer surface of the ventricle have pink stained nuclei and are not derived from the left-dorsal blastomere (figure 4-6(F) to (J)).

Left-Dorsal Lineage

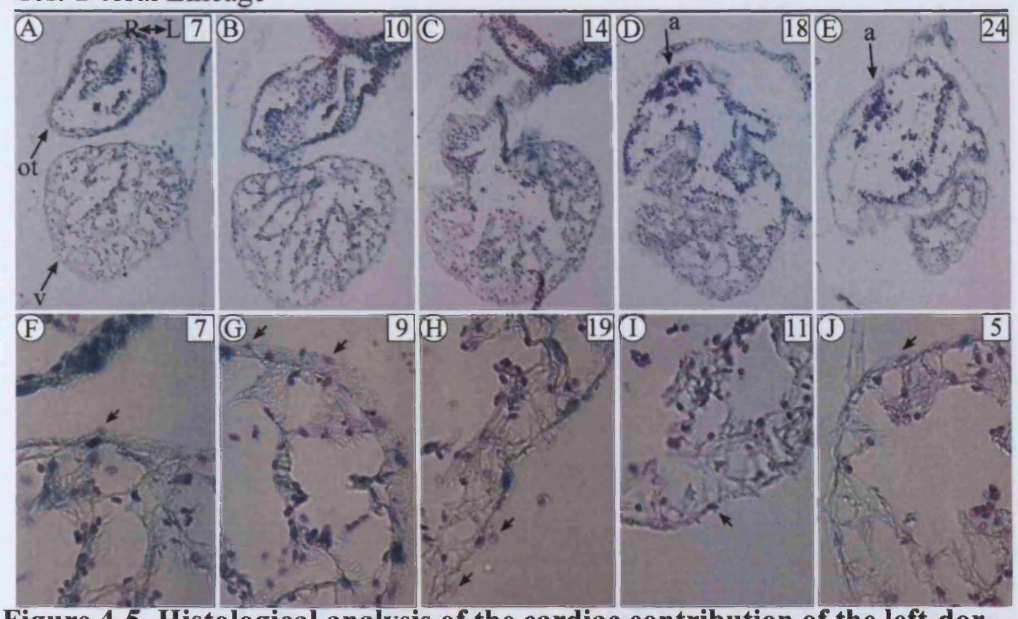

Figure 4-5. Histological analysis of the cardiac contribution of the left-dorsal blastomere of the 4-cell embryo. Histological analysis of the contribution of the left-sided dorsal blastomere of the four-cell stage embryo to the tadpole heart shows an absence of staining in the epicardial cells. (A) to (E)- five representative frontal sections (10μm) through the heart of an X-gal stained, left-dorsal lineage labelled, stage 47 tadpole. The order, orientation and pink nuclear counterstain of the sectons is the same as in figure 4-4. Left-dorsal progeny cells are located on the left side of the outflow tract (ot) and left atrial chamber region (a). In the myocardium of the ventricle (v), the blue cell nuclei occupy a more anterior-left and ventral position (figures (A) to (D)). (F) to (J)- detail images of sections that depict the outer surface of the ventricle. Those cells that clearly adhere to the surface of the ventricle (figures (G) and (H)), or have an obvious elongated nuclear morphology (figures (F), (G), (I), and (J)), have pink stained nuclei and not blue (arrows). Blue stained nuclei are occasionally found near the ventricle surface (figures (H) and (J)) but on close inspection, these have a rounded morphology and actually reside within the myocardial layer. Thus, none of the presumed epicardial cells identified in this heart are derived from the left-dorsal blastomere.

Left-Dorsal Lineage

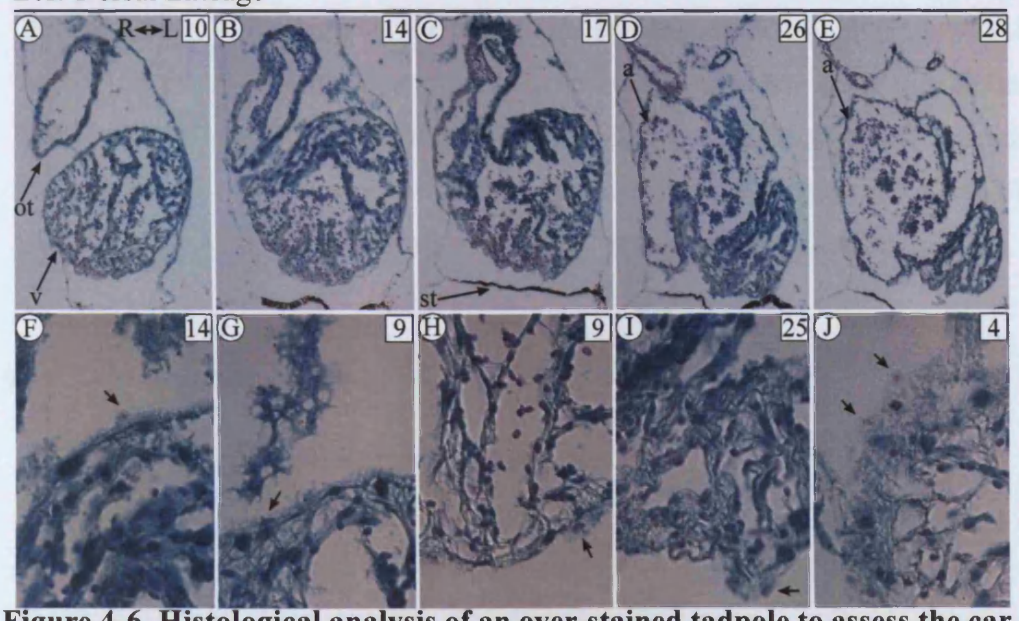

Figure 4-6. Histological analysis of an over-stained tadpole to assess the cardiac contribution of the right-dorsal blastomere of the 4-cell embryo. An example of a grossly over-stained stage 47 tadpole heart still shows an absence of contribution of the left-sided dorsal blastomere to the epicardial cells. The figure panels are arranged identically to figure 4-5. (A) to (E)- despite the very heavy X-gal lineage stain, the basic features of left-dorsal lineage stain are present. The left side of the outflow tract (ot) and left atrial chamber region (a), plus the anterior-left portion of the ventricular myocardium (v) are the progeny of the left-dorsal blastomere. (F) to (J)- cells that clearly adhere to the outer surface of the ventricle (arrows) have pink stained nuclei and not blue. These epicardial cells are not derived from the left-dorsal blastomere.

Finally, stage 47 tadpoles that resulted from left and right-sided ventral blastomere lineage injection were also subjected to X-gal staining and histological analysis. No staining of surface located, epicardial cells was observed in 8 out of 9 tadpole hearts that displayed typical patterns of right-ventral blastomere lineage in other tissues (data not shown). Also, the complete absence of epicardial cell staining was observed in 9 out of 9 tadpoles with left-ventral blastomere lineage injection (data not shown).

4.3 Discussion

The data presented here indicates that only right-sided blastomeres of the early *Xenopus* embryo make a contribution of cells to the forming epicardial cell layer. This unilateral epicardial origin is in keeping with studies using chick embryos that showed only a right-sided cluster of mesothelial cells grows out from the sinus venosus to form the proepicardial organ.

4.3.1 Other Possible Sources Of Positive Cells

It is assumed that the X-gal positive cells observed on the cardiac surface of experimental tadpoles are epicardial cells. However these are not the only migratory cells that make a contribution to the developing heart. Cardiac neural crest cells (Kirby et al., 1983) have been shown to make significant cardiac contributions, whilst macrophages are a population of migratory cells that can be found around the heart region at this time (Shepard and Zon, 2000). However, these cells are certainly bilateral in origin and so would not show a right sided origin as seen here. It can therefore be concluded that the positive cells observed on the cardiac surface of experimental tadpoles are epicardial cells.

4.3.2 Contribution From The Left

The data appears to categorically show that the epicardium is derived from the right side of the embryo and not the left. However, it is not possible to rule out a contribution from the left entirely. Firstly the number of tadpoles analysed for a left sided contribution (n=7) is too small to completely discount a left sided contribution.

Also in 2 of the tadpoles analysed, a small number of positive cells were observed on the surface of the heart.

There is also a possibility that the left side does contribute to the epicardium, but that this contribution occurs after stage 47. It was not possible to analyse whole tadpoles beyond this stage due to the thickening epidermis preventing penetration of the X-gal substrate. In order to observe any later contribution from the left, the staining reaction could be performed on sections of older tadpoles. However this would also increase the likelihood of problems associated with degradation and dilution of the ß-galactosidase RNA.

It appears that like in the chick the *Xenopus* epicardium is derived from the right side of the embryo and that any contribution form the left side to the *Xenopus* epicardium is likely to be very minor.

4.3.3 What is the Significance Of A Unilateral, Right-Sided Origin Of The Epicardium?

It might be expected that the significance of a unilaterally derived epicardium would be reflected in differences in structure and function between mammalian versus avian and anuran amphibian hearts. However, whilst the differences between amphibian versus higher vertebrate hearts have been described in detail in this thesis, differences between avian and mammalian hearts are not so apparent.

One aspect of heart development that is shared by *Xenopus* and chick, and differs from mammalian species, is the method of proepicardial outgrowth and attachment to the surface of the myocardium. Whilst the mouse sheds proepicardial cells directly into the pericardial cavity, both chick and *Xenopus* form a bridge from the proepicardium to the surface of the heart over which proepicardial cells migrate. The use of a bridge is necessitated by the incomplete formation of the septum transversum in *Xenopus* and chick at the time of proepicardial outgrowth. Once fully developed the septum transversum closes off the pericardial cavity from the coelomic cavity. If epicardial cells were shed directly into an 'open' pericardial cavity they could be lost

through the incomplete septum transversum. The unilateral origin of the epicardium in *Xenopus* and chick could therefore be a result of the incomplete development of the septum transversum. However, in the case of mouse and chick, the origin of the epicardium appears to have no effect on it's function.

5 Results: Genes Expressed In The Epicardium And Proepicardium Of *Xenopus laevis*

5.1 Introduction

5.1.1 Purpose Of Molecular Markers

In chapter 3 several techniques were used to describe the morphological process of epicardium formation in *Xenopus laevis*. The timing of epicardium formation, the location and approximate size of the proepicardium, and developmental progression were described in relation to what is known about epicardium development in other vertebrate species. However, in order for these tissues to be positively identified as the *Xenopus* epicardium and proepicardium, the expression of a number of molecular markers known to be expressed in the epicardium and proepicardium of other species would be beneficial.

5.1.2 Candidate Genes

Three genes have been shown to be expressed in the epicardium and proepicardium of other species. The T-box gene Tbx18 has been described in the epicardium of mouse (Kraus et al., 2001), chick (Haenig and Kispert, 2004) and zebrafish (Begemann et al., 2002). The bHLH transcription factor epicardin has been shown to be expressed in the epicardium of mouse (Hidai et al., 1998; Lu et al., 1998) and chick (von Scheven et al., 2006). Finally the zinc finger-containing transcription factor WT1 has been shown to be expressed in the epicardium of mouse (Moore et al., 1999) and chick (Carmona et al., 2001).

Unfortunately none of these genes are specific to the epicardium. Both epicardin and WT1 are described as being strongly expressed in the developing kidney, whilst Tbx18 has been described as being expressed in the somites, musculature of the head and the developing limbs.

5.1.3 Aims Of This Chapter

This chapter will describe the expression patterns of the above genes *in Xenopus laevis*. Particular attention will be paid to expression around the heart region. Anti-sense RNA *in situ* hybridisation probes were made and hybridised to embryos ranging from stage 20 to stage 44. In order for the *in situ* hybridisation reaction to work efficiently beyond stage 41, the outside layers of epidermis were removed from the tadpole to allow adequate probe penetration. Where significant staining was observed around the heart region histological sections were made in order to analyse this expression more accurately.

5.2 Results

5.2.1 Expression Pattern Of Wilms tumour 1 In Xenopus laevis

An *in situ* hybridisation probe was made from IMAGE clone 3548862 (accession number CF270874) that corresponds to *Xenopus laevis* WT1. This clone was obtained from the IMAGE consortium (http://image.llnl.gov/), and was identified using a BLAST (Basic Local Alignment Search Tool) (Altschul et al., 1990) search against the mouse WT1 orthologue (Buckler et al., 1991) (accession number NM144783).

Expression can first be observed at stage 22 in an anterior/dorsal region that corresponds to the pronephric anlage (figure 5-1(A)). By stage 26 expression can also be seen in the pronephric duct (figure 5-1(B)). By stage 33/34 expression within the pronephros is becoming restricted to the most dorsal compartment, the glomus (figure 5-1(C)). Expression remains in the glomus until at least stage 39 (figures 5-1(D) and (E)). A cleared stage 33/34 embryo reveals expression in the duct and glomus of the pronephros (figures 5-1(F) and (G)). Figures 5-1(H) and (I) show the duct specific antibody 4A6, and tubule specific antibody 3G8 respectively for comparison. At stage 40.5 expression can be seen in a region posterior to the heart (figures 5-1(J) to (L)). This region is present on the right side of the tadpole (figure 5-1(K)) but is absent from the left (figure 5-1(J)). A ventral view of the embryo confirms that this area of expression is located to the right of the sagittal plane (figure 5-1(L)).

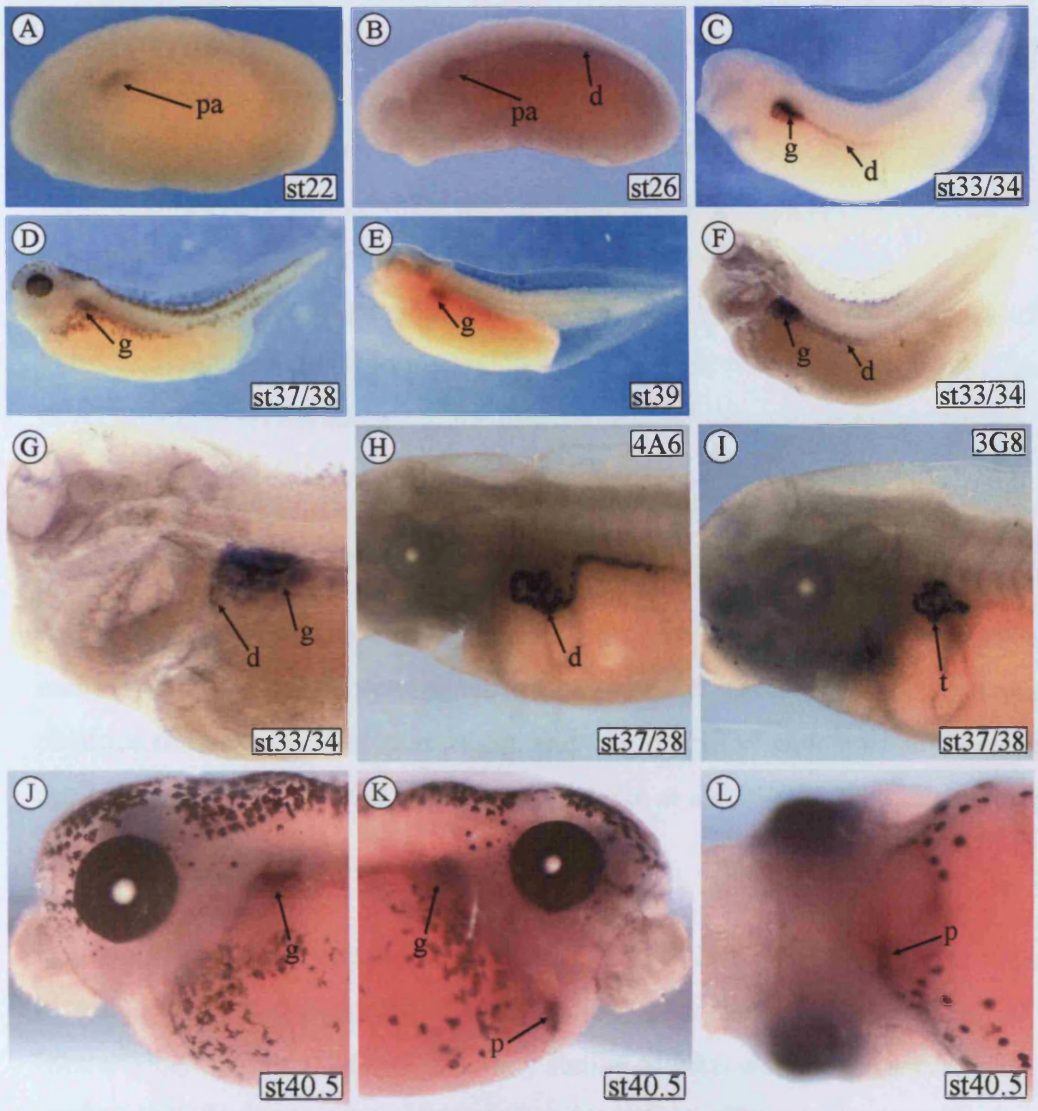

Figure 5-1. Wilms tumour 1 expression in *Xenopus laevis*.

(A)- left lateral view of a stage 22 embryo. Expression can first be seen in the pronephric anlagen (pa) on both sides of the embryo. (B)- By stage 26 expression can also be seen in the pronephric duct (d). (C)- by stage 33/34 pronehric expression is strongest in the glomus (g). (D) and (E)- expression remains in the glomus until after stage 39. (F) and (G)- a stage 33/34 embryo that has been cleared. Here expression can be seen in the pronephric duct (d) as well as the glomus. (H) and (I)- the 4A6 and 3G8 antibodies stain the pronephric duct and pronephric tubules respectively. (J) left, (K) right and (L) ventral- by stage 40.5 expression can be seen in the proepicardium (p), as well as the glomus. Expression in the proepicardium can be observed only on the right side, not the left.

An inherent problem when performing whole-mount *in situ* hybridisation to *Xenopus laevis* tadpoles is the unreliability of hybridisations performed after stage 41. By this stage the skin is composed of a double-layered epidermis of flattened cells and a thin layer of connective tissue, which appears to hinder probe penetration. In order to get around this problem, fixed embryos were dehydrated and the external layer of epidermis gently peeled away so as not to disturb the underlying structures. *In situ* hybridisation was then performed on the dissected embryos. WT1 expression was never observed on the surface of the heart in stage 45 tadpoles (data not shown).

5.2.2 Expression Pattern Of Epicardin In Xenopus laevis

An *in situ* hybridisation probe was made from IMAGE clone 5512805 (accession number CF270487) that corresponds to *Xenopus laevis* epicardin. This clone was obtained from the IMAGE consortium, and was identified using a BLAST search against the mouse epicardin orthologue (Quaggin et al., 1999) (accession number NM011545).

Expression was first observed via wholemount RNA *in situ* hybridisation at stage 23 in two ventral/anterior patches adjacent to the cement gland (figure 5-2(A)). Interestingly these patches are strikingly similar to what would be observed with a cardiac specific gene such as Nkx2.5 (Tonissen et al., 1994) at this stage. By stage 33/34 expression was also seen in the branchial arches (figures 5-2(B) and (C)). A ventral view of a stage 37/38 embryo shows weak expression around the liver region (figure 5-2(D)). Expression persists around the liver region until at least stage 39. Also at this stage expression can be seen in the urinary tract (figure 5-2(E)), and the pronephros (figures 5-2(E), (F) and (G)). Comparing a ventral view of a stage 39 embryo (figure 5-2(H)) with a ventral view of a similarly staged embryo that has been stained for the liver specific marker XHex (Newman et al., 1997) (figure 5-2(I)), it can be seen that epicardin is expressed around the outside of the liver. On clearing the embryos expression in the pronephros and liver can be seen more clearly (figures 5-2(J), (K) and (L)).

Between stages 40 and 41 a region of expression can be seen posterior to the heart

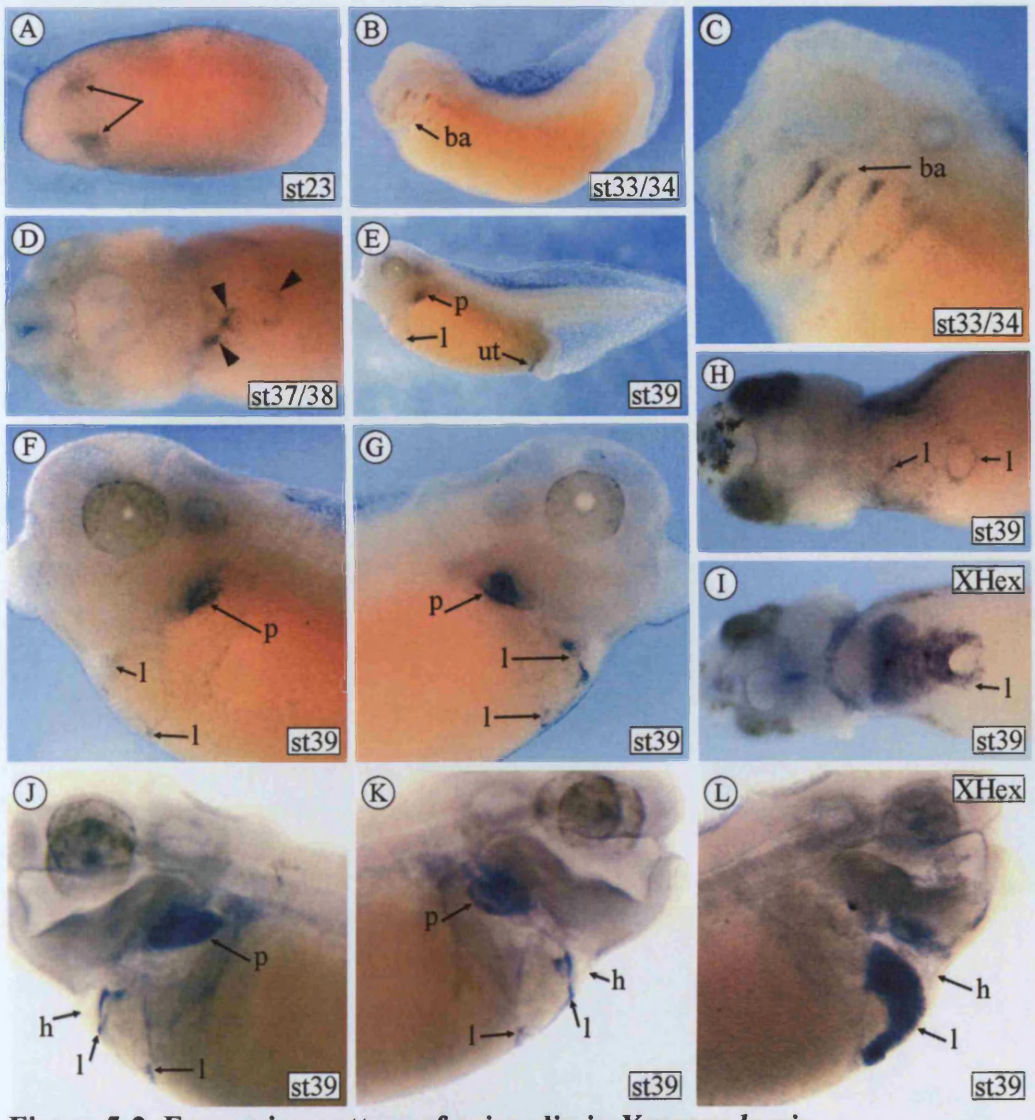

Figure 5-2. Expression pattern of epicardin in *Xenopus laevis*.

(A)- ventral view of stage 23 embryo. Expression can first be observed at stage 23 in two ventral/anterior patches. (B) and (C)- specific expression is first seen at stage 33/34 in the branchial arches (ba). (D)- ventral view of stage 37/38 embryo. Expression can be seen around the liver region (arrowheads). (E) to (H)- by stage 39 expression has gone from the branchial arches, but can be seen in the pronephros (p) and urinary tract (ut). Expression remains around the liver region (l). (I)- ventral view of expression of XHex, a liver specific marker. (J) and (K)-stage 39 embryo that has been cleared to allow viewing of internal staining. Expression can be seen in the pronephros and liver region. (L)-stage 39 embryo stained with XHex that has been cleared to show expression in the liver.

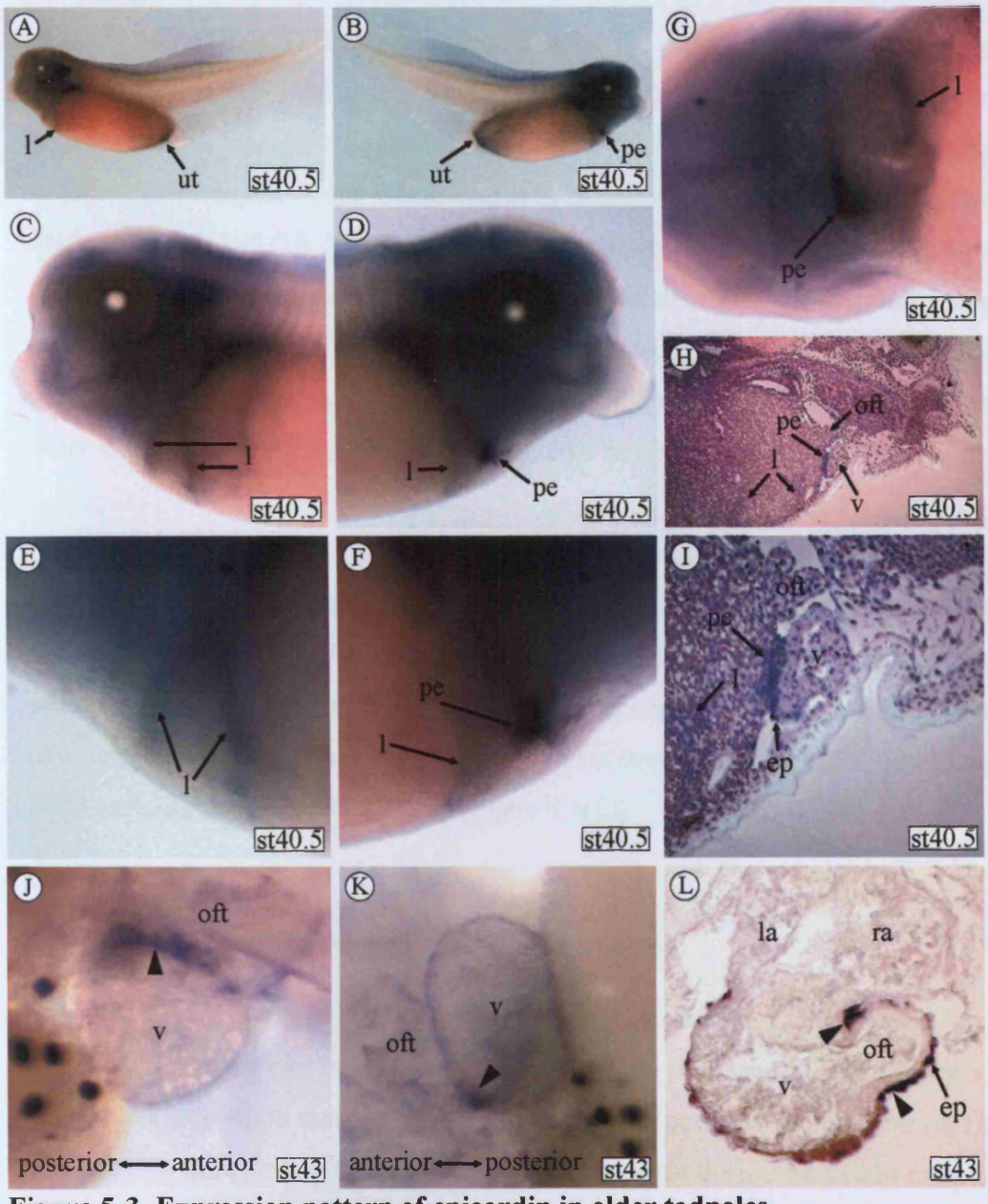

Figure 5-3. Expression pattern of epicardin in older tadpoles.

(A) to (F)- left and right lateral views of a stage 40.5 tadpole. Expression can be seen in the urinary tract (ut), liver (l), and proepicardium (pe). Expression in the proepicardium is present on the right side of the tadpole but absent from the left (G). (H) and (I)- transverse sections through a stage 40.5 tadpole. Expression can be seen in the proepicardiumn and epicardial cells migrating over the ventricle (v). Very weak expression can be seen around the liver. (J) and (K)- right lateral and ventral view of a stage 43 heart respectively. Strong expression can be seen in the junction between the ventricle and the outflow tract (oft) (arrowheads). (L)- transverse section through a stage 43 heart. Expression can be seen in the epicardium (ep) around the heart but is strongest on the right side (arrowheads).

(figures 5-3(A) to (G)). This region is present on the right side of the tadpole (figures 5-3 (B), (D), and (F)) but absent from the left (figures 5-3 (A), (C), and (E)). Sagittal, plastic sections through a stage 40.5 tadpole shows this epicardin-expressing tissue is adjacent to the septum transversum and is in contact with the ventricular myocardium (figures 5-3(H) and (I)). The location of this tissue is consistent with it being the proepicardium as was seen earlier in histological sections through a similarly staged tadpole (figures 3-7(A) to (C)). Positive cells can also be seen migrating over from the proepicardium and migrating over the surface of the ventricle (figures 5-3(H) and (I)). Very weak expression around the liver can also be observed in these sections.

Figures 5-3(J) and (K) show the exposed heart region of a stage 43 tadpole that had been prepared as described in section 4.2.1. Epicardin expression is strongest around the junction between the OFT and ventricle (figures 5-3(J) and (K)). A transverse wax section through the heart at this stage shows the epicardin-positive cells have spread over the surface of the ventricle but expression is strongest on the right side of the heart around the AV and CV canals (figure 4.3(L)).

5.2.3 Expression Pattern Of Tbx18 In Xenopus laevis

Since the *Xenopus laevis* Tbx18 orthologue has not been cloned, an *in situ* hybridisation probe was made by genomic PCR using primers designed against a Riken EST (accession number BJ048587) that corresponded to *Xenopus* laevis Tbx18. This clone was identified using a BLAST search against the mouse Tbx18 orthologue (Kraus et al., 2001) (accession number NM023814).

Expression is first observed at stage 23 in a diffuse pattern in an anterior/ventral domain posterior to the cement gland (figure 5-4(A)). Again this area corresponds to the region where the cardiac precursors are located at this stage. By stage 32, expression has become restricted to two distinct patches in the head (figure 5-4(B)), and the somites (figures 5-4(B) and (C)). The areas of expression in the head correspond to the mandibular and hyoid arches. Staining can also be seen around the eye region (figure 5-4(D)). Somitic expression is strongest in the less mature, posterior somites (figure 5-4(C)). A cranial view of a stage 33/34 embryo shows very

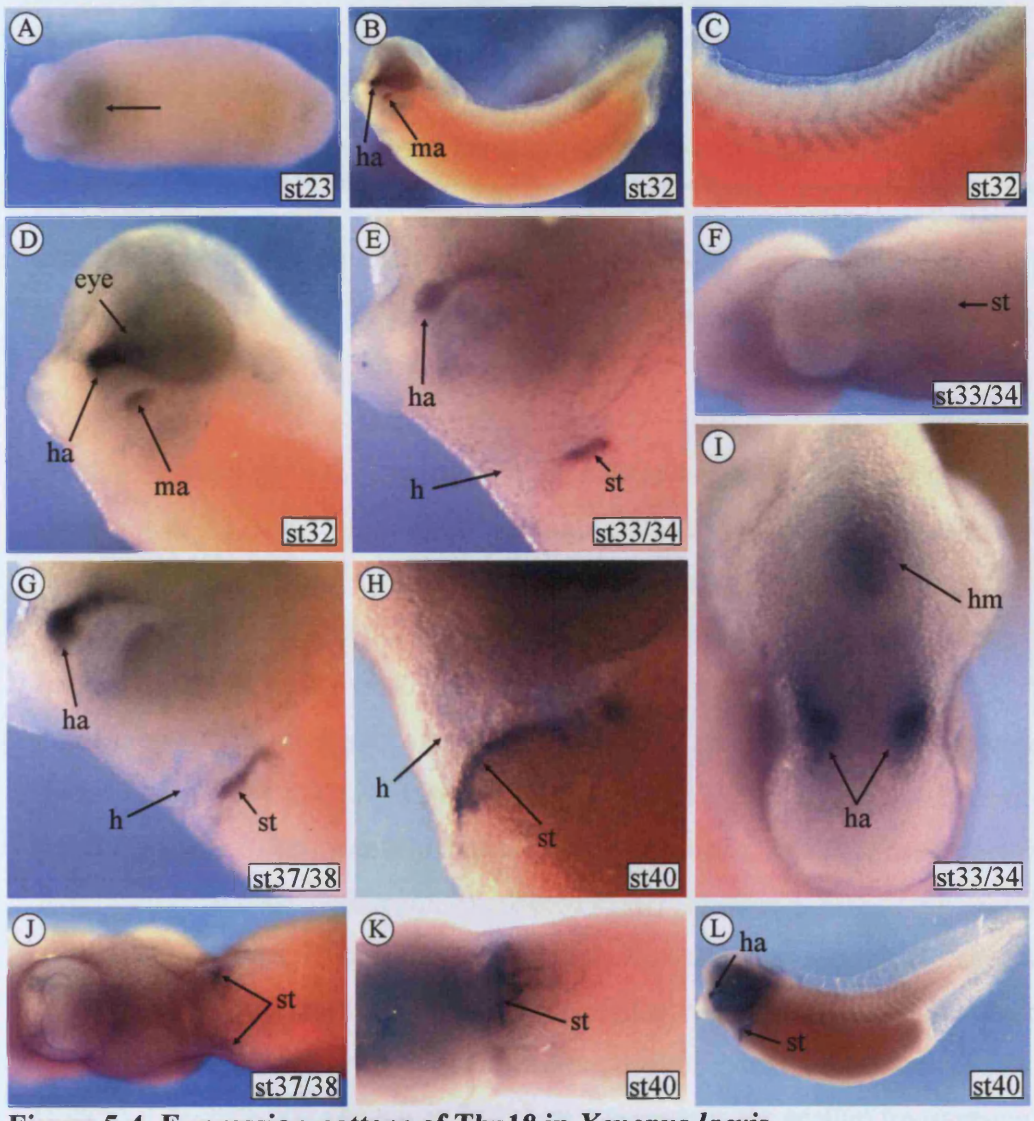

Figure 5-4. Expression pattern of Tbx18 in *Xenopus laevis*.

(A)- ventral view of stage 23 embryo. Expression is first seen in a ventral/anterior domain (arrow). (B)- by stage 32 specific expression can be seen in the mandibular (ma) and hyoid (ha) arches (close up in (D)), and the somites. (C)- expression in the somites is strongest in the more posterior, immature somites. (E)- by stage 33/34 expression is no longer seen in the mandibular arch but remains in the hyoid arch. Expression can be seen in two bilaterally symmetric patches posterior to the heart (h). This marks the beginning of septum transversum (st) development. (F)- at stage 33/34, expression cannot be seen on the ventral surface of the embryo suggesting the septum transversum has not yet begun to fuse. (G) and (J)- as development progresses the wings of septum transversum expression grow towards the ventral midline, and can now be seen on the ventral surface (J). (I)- a cranial view of the head shows expression in the hyoid arches and head mesen-

Figure 5-4. Expression pattern of Tbx18 in *Xenopus laevis* continued – chyme (hm). (H), (K) and (L)- by stage 40 the septum transversum appears to be complete. Expression remains in the hyoid arch but is no longer seen in the somites.

distinct expression in the hyoid arches and also paraxial mesenchyme of the head (figure 5-4(I)). By stage 33/34 expression can also be seen in two bilateral patches immediately posterior to the heart (figure 5-4(E)).

Initially, expression in the heart region is restricted to two distinct wings, bilateral and posterior to, the developing heart. The wings gradually extend ventrally over the next 24 hours (figures 5-4(E), (G), (H)). Ventral expression is not visible at stage 33/34 (figure 5-4(F)), but is visible by stage 37/38 (figure 5-4(J)), and by stage 40 the wings have fused at the ventral midline (figure 5-4(K)). This pattern of expression is consistent with development of the septum transversum. The septum transversum is a splanchnic mesoderm derived structure that separates the pericardial cavity from the general coelom. Later in development the septum transversum will contribute to the liver stroma, and the diaphragm. Expression in this structure is particularly significant as this is the location of the proepicardium in other vertebrate species. By stage 40 the septum transversum has fused at the ventral midline and strong gene expression can be seen (figure 5-4(H)). However, as has been seen from earlier histological data (figures 3-7(D) to (F)), there is in fact at least one gap in the septum transversum at stage 42. No distinct proepicardium-like structure can be seen at this stage, suggesting epicardium formation is taking place after stage 40.

By stage 44 an area of expression can be seen on the surface of the heart, which is more intense at the caudal limit of the heart and septum transversum (figures 5-5(A) to (D)). When comparing the left and right sides of the heart (figure 5-5(A) with (B)) it is clear that expression is most intense on the right side of the heart suggesting the proepicardium is located right of the sagittal plane, an asymmetric location similar to that found in avian embryos. Expression is also more intense in the area between the ventricle and OFT, suggesting this is the area to be first covered by the epicardium. However, this could also be an artefact caused by the cylindricality of the heart, which may result in edges appearing darker, due to the presence of more cell layers.

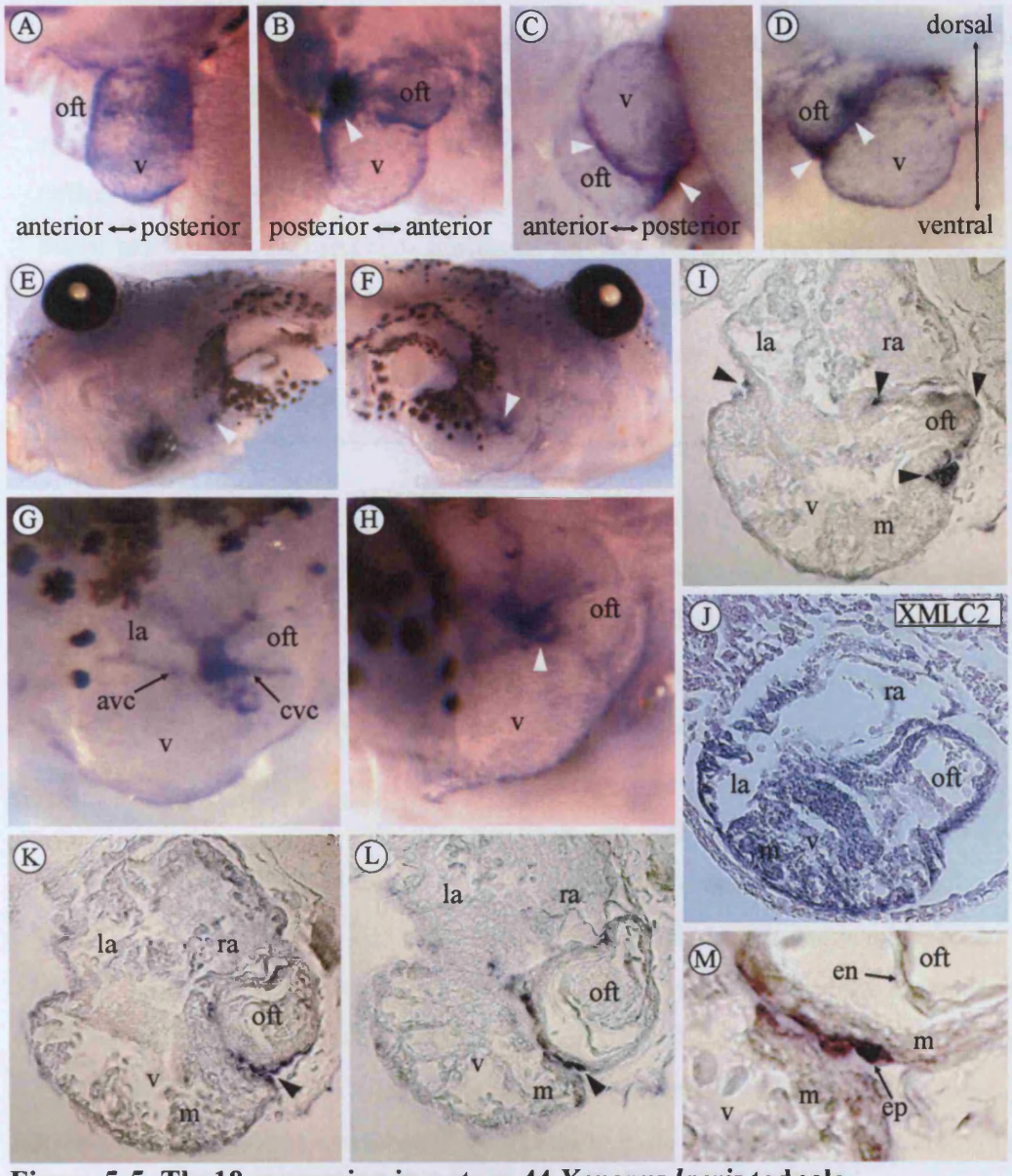

Figure 5-5. Tbx18 expression in a stage 44 *Xenopus laevis* tadpole.

(A) to (D)- left lateral, right lateral, ventral, and anterior views of a tadpole heart respectively. By this stage the heart is covered by the Tbx18-positive epicardium. The patch of intense staining on the right side (arrowhead in (B)) is absent from the left side (A). (C) and (D)- Tbx18 staining is strongest around the conoventricular canal (arrowheads). (E) to (H)- a stage 44 tadpole with the gut removed. The Tbx18 positive patch, which represents the area of attachment of the proepicardium, is clearly located to the right of the sagittal plane. (G)- posterior view of the heart. The epicardium appears to spread along the atrioventricular (avc) and conoventricular (cvc) canals. (I) to (M)- transverse sections through stage 44 hearts. (I)- Confirmation that the Tbx18-positive epicardium first spreads along the atrioventricular and conoventricular canals (arrowheads). (J)- a transverse sec-

Figure 5-5. Tbx18 expression in a stage 44 *Xenopus laevis* tadpole continued- tion through a stage 44 tadpole heart that has been stained for the myocardium-specific XMLC2. Positive staining can be seen throughout the myocardium of the entire heart. This shows the surface Tbx18 staining is unlikely to be the result of poor probe penetration. (K) and (L)- additional sections showing Tbx18 expression in the epicardium around the conoventricular canal. (M)- close up of the conoventricular region. Here the Tbx18-positive epicardium can clearly be distinguished from the myocardium (m) and the endocardium (en).

In order to observe the posterior of the heart, and hence the prospective area of proepicardium attachment, the gut was removed (figures 5-5(E) to (H)). An area of intense staining can be seen to the right of the sagittal plane at the junction between the ventricle and the OFT. No such area of staining can be observed to the left of the sagittal plane. The epicardium appears to spread preferentially along the AV and CV canals (figure 5-5(G)).

Wax transverse sections through the heart region were made in order to see the epicardial layer (figure 5-5(I) and 5-5(K) to (M)). These sections have not been counterstained. No expression was observed in the myocardium of the heart. Staining was restricted to individual epicardial cells on the surface of the heart. The staining was most intense at the AV and CV canals at the right side of the heart. Figure 5-5(J) shows a transverse section through a stage 44 tadpole heart that has been stained by wholemount *in situ* hybridisation for the myocardial specific gene XMLC2. The entire myocardium of the heart is positive. This indicates that the surface Tbx18 staining is unlikely to be due to poor probe penetration. Figure 5-5(M) shows a high magnification image of the heart wall. The Tbx18 positive epicardium can clearly be distinguished from the negative endocardium and myocardium.

5.3 Discussion

Studies in other vertebrate species have identified expression of WT1, epicardin and Tbx18 in the epicardium and proepicardium of the embryonic heart. From my studies

it is evident that epicardin Tbx18, and WT1 are expressed in the epicardium and/or proepicardium of *Xenopus laevis.*

5.3.1 WT1, Tbx18 And Epicardin Are Expressed In The Epicardium And/Or Proepicardium Of Xenopus laevis

Both Tbx18 and epicardin show a similar expression pattern on the actual surface of the heart, however their expression patterns in the general heart region are slightly different. First expression of Tbx18 around the heart region is observed in bilaterally symmetric patches posterior to the heart. These patches eventually fuse at the ventral midline. This pattern of expression is consistent with Tbx18 staining the septum transversum. Unlike Tbx18, epicardin is not seen in the developing septum transversum. The first expression of epicardin around the heart region is observed in an asymmetric region located to the right and posterior to the heart. This expression pattern is consistent with epicardin being expressed in the proepicardium. Because Tbx18 is expressed in the septum transversum, it is difficult to distinguish from wholemount *in situ* analysis if Tbx18 is also expressed in the proepicardium. WT1 on the other hand is expressed only in the proepicardium and was never observed in the epicardial layer.

Earlier histological investigations revealed a cone shaped protrusion from the septum transversum was visible at stage 42. It can be seen in sections through a similarly staged tadpole that has been stained for epicardin that this protrusion stains positively for this gene. Also epicardin positive cells can be seen migrating over from this protrusion and attaching to the surface of the ventricular myocardium. A similar section series through the heart region of a stage 42 tadpole that has been stained for Tbx18 would determine if Tbx18 is also expressed in the proepicardium as well as the septum transversum and epicardium.

Asymmetric WT1 and epicardin staining posterior and to the right of the heart, is consistent with what is known about the location of the proepicardium in avian species. An asymmetric, right-sided proepicardium also concurs with the

morphological data presented in chapter 3 and the lineage analysis presented in chapter 4.

During later stages of development, both Tbx18 and epicardin-positive cells can be seen on the surface of the heart. This staining appears to be localised to the AV and CV canals as seen in stage 43 or 44 wholemount embryos and subsequent sections through the heart regions of these embryos. These expression patterns concur with previous SEM and histological data presented in chapter 3. Here cells could be seen migrating over to the heart from an extracardiac source and attaching to the ventricular myocardium at the CV canal.

The expression data presented here, coupled with published work in other species, and the morphological data presented in chapter 3, are all consistent with WT1, epicardin and Tbx18 being expressed in the proepicardium and/or the epicardium of *Xenopus laevis*. These data also show the proepicardium of *Xenopus* is asymmetrically located to the right of the sagittal plane, and that epicardial cells spread preferentially over the AV and CV canals. The complete pattern of epicardial spreading over the heart has not been determined here. The fact that the developing epicardium is only one cell thick makes this very difficult with the level of resolution achievable with wholemount *in situ* hybridisation. However, this would be possible using the markers described here and taking high-resolution plastic sections through wholemount embryos that have been very carefully staged from stage 40 onwards.

Unfortunately none of the markers shown here are specific to the epicardium. All are expressed in other tissues, specifically the developing kidney in the case of WT1 and epicardin. A marker specific to the epicardium would allow the developmental progression of the epicardium to be analysed definitively without interference from nearby tissues such as the liver, septum transversum and the pronephros. This is also an important consideration for performing functional studies using these genes, since interrupting gene function is likely to have an effect on other tissues as well as the epicardium.

5.3.2 Existence Of Alternative Alleles

The probe used for the expression study of WT1 was made from an EST with 100% sequence identity to a published WT1 cDNA (Carroll and Vize, 1996) (accession number XLU42011). In the literature however, there exists another WT1 cDNA sequence (Semba et al., 1996) (accession number D82051). These studies describe WT1 being expressed in the pronephros from stage 23 until at least stage 30 (Semba et al., 1996) or to stage 38/39 (Carroll and Vize, 1996) at which point expression was observed in the 'heart region' (Carroll and Vize, 1996). These published sequences share only 93% sequence identity at the nucleotide level and 93% similarity at the amino acid level. Due to the high degree of similarity between the two sequences it is unlikely that the probe used in this thesis is specific to the sequence against which it was designed. In order for specific probes against each individual allele to be designed, more sequence information will be required that includes the 3'UTR. The two versions could simply be redundant alleles and have the same expression pattern and function. Alternatively they could have paralogous expression patterns and functions, whereby one paralogue is involved in kidney formation whilst the other is involved in epicardium formation. These would be important considerations for conducting functional studies. The Tbx18 *in situ* hybridisation probe was designed against the 3'UTR so is likely to be specific to that single allele. No alternative versions of epicardin exist in the literature.

All of the epicardial markers used here are tissue specific transcription factors and so it is probable that they are functionally important for epicardial formation. However, as was discussed in section 1.12, whilst numerous studies have shown all of these genes to be expressed in the epicardium of mouse and chick, and one study has suggested Tbx18 is involved in formation of the venus pole of the heart (Christoffels et al., 2006), there is as yet no definitive evidence to suggest either Tbx18 or epicardin are important for development of the epicardium. WT1 on the other hand has been demonstrated to play a number of roles in formation of the epicardium (see section 1.12.3).

5.3.3 Future Work

WT1, epicardin and Tbx18 have been shown to be expressed in the proepicardium and/or the epicardium of *Xenopus laevis*. It would be interesting to identify the regulatory regions that direct expression in these tissues. A promoter or enhancer that directs specific gene expression to the proepicardium and/or the epicardium would be a very powerful tool for further investigating epicardium development in *Xenopus*. If this regulatory element could drive GFP expression in the developing epicardium, it would be possible to observe the development of the epicardium in real time in living tadpoles.

6 Results: Morpholino Knockdown Of Candidate Genes.

6.1 Introduction

6.1.1 Perturbations Of The Epicardium

Almost all perturbations of epicardium development have been carried out in the chick. The relatively large size of chick embryos and the ease of gaining access to the embryos through the eggshell make the chick an excellent system for perturbations of the epicardium. Often these perturbations involve the insertion of a piece of eggshell membrane to block proepicardial outgrowth (Eralp et al., 2005; Gittenberger-de Groot et al., 2000; Perez-Pomares et al., 2002b; Poelmann et al., 2002). Certain aspects of epicardium development have been inhibited genetically such as the retroviral expression of Ets1/2 to block epicardium EMT (Eralp et al., 2006). More recently a photoablation technique has been employed to completely eliminate the proepicardium in the chick (Manner et al., 2005). Whilst the chick is ideally suited for these kinds of experimental manipulations later in development, *Xenopus* has been traditionally used to study much earlier developmental events. However, the recent use of MOs (Heasman, 2002) have made the study of later developmental events in *Xenopus* more accessible.

6.1.2 Antisense Morpholino Oligonucleotide Knockdown Strategy

MOs are short sections (18-22 mer) of DNA that have morpholine moieties instead of ribose moieties, and phosphodiamidate linkages instead of phosphodiester linkages (Summerton and Weller, 1997). There are two strategies for using MOs to knockdown the expression of a target gene. Translation blocking MOs are designed to be complementary to the 5' leader sequence or the sequence immediately downstream (about 25 bases) of the AUG translational start site. In this case MOs sterically block translation by preventing binding of the ribosomal translation initiation complex. Splice blocking MOs are designed to span the intron/exon boundary of pre-mRNA. In this case MOs sterically block pre-mRNA processing steps by preventing splice-directing small nuclear ribonucleoproteins (snRNP) complexes from binding to their targets at the intron/exon boundary (Draper et al., 2001). All MOs used in this study

are translation inhibition. This is because the sequence information necessary to design splice-blocking MOs is not readily available for *Xenopus*.

There are a number of different strategies that could be used to validate if the MO knockdown strategy is working. Because the MOs used here are translation inhibition, the levels of mRNA would not be expected to be altered and so RT-PCR is not a viable validation strategy. An antibody against the protein of interest could be used in a Western blot assay or immunohistochemistry in order to observe the effect of the MO on protein level. A successful MO knockdown would be expected to inhibit, or greatly reduce, protein levels. In the absence of a suitable antibody against any of the genes of interest in this study, an alternative approach was used to assess the efficacy of the MOs to recognise their target sequence and knockdown the expression of GFP (see section 6.2.1).

The above assays would show if the MO was acting on the gene of interest. However, they would not show if the MOs were acting on other genes. In order to analyse if MOs are acting specifically on their target gene a rescue experiment should be performed. If coinjection of the MO with mRNA of the target gene, with an altered 5' region to avoid being knocked down by the MO, is able to rescue all observable phenotypes then it is likely that the MO is acting specifically on its target gene.

There are three caveats that must be considered when designing a MO experiment: firstly can the MO be targeted to the tissue of interest; secondly is the longevity of the effect of the MO sufficient to affect the tissue or developmental event of interest; and finally is the MO specific to the gene of interest.

6.1.3 Is Xenopus Epicardium Development Accessible To Study Using Antisense Morpholino Oligonucleotides?

It is possible to target the area of action of a MO in *Xenopus* by injecting it into specific blastomeres. Injecting the MO at the 1-cell stage would result in ubiquitous, even distribution of the MO throughout the developing embryo. Injecting the MO at the 1-cell stage will result in the gene of interest being knocked down in every cell of

the embryo. This can have both negative and positive consequences. If the gene of interest is important in an unrelated developmental event then it is possible that a phenotype will be observable in this tissue. If this is a severe phenotype then it could mask any subtle phenotypes in the tissue of interest. However, if the phenotype is not severe it could be useful in determining if the gene of interest is actually being knocked down.

Lineage analysis has shown that blastomere dorsal (D) 2.1 of the 16-cell *Xenopus laevis* embryo makes the most significant cellular contribution to the heart (Moody, 1987). However blastomeres D1.1 and D2.2 were also shown to make less significant contributions to the heart, and blastomeres D1.2, ventral (V) 1.2 and V1.1 to make minor contributions to the heart. It can be seen that targeting a MO to the heart is not straightforward due to the complexity of cellular contributions from the early embryo. As was discussed in section 1.2 there are also a number of extracardiac contributions to the heart such as from the cardiac neural crest and the anterior heart field which complicate targeting the MO to the heart even further. The epicardium however, was shown in chapter 4 to be derived from the right side of the embryo, with little or no contribution from the left. It may be possible to use this information to target MOs to the epicardium without causing too many non-specific effects.

Because it has been shown that epicardium development in *Xenopus laevis* begins at around stage 42, it was a concern that the effect of the MO could be diminished by this time due to dilution or degradation. However, there is some evidence that MO knockdown may be a viable technique to investigate epicardium development in *Xenopus*. The longevity of the MO knockdown effect has been investigated using a GFP specific MO on transgenic lines of *Xenopus laevis* and *tropicalis* (Nutt et al., 2001). The transgenic lines have the lens-specific γcrystallin promoter driving GFP. It was shown that the MO knocked down GFP expression in the lens until at least stage 43. This suggests that at least the initial events of epicardium development should be accessible to study with MOs.

The use of the diploid species *Xenopus tropicalis* has introduced the possibility of genetic studies of organogenesis in *Xenopus* (Hirsch et al., 2002). The advantages of *Xenopus tropicalis* also extend to the use of MOs. Due to a genome duplication event,

Xenopus laevis has a pseudotetraploid genome (Bisbee et al., 1977) which has led to genetic redundancy. In order to perform a MO knockdown in *Xenopus laevis*, both paralogues of the gene of interest would have to be knocked down, which may require the use of two MOs due to divergence at the nucleotide level. The diploid species, *Xenopus tropicalis*, would be expected to have only one copy of the gene of interest. This coupled with sequence information available from the Joint Genome Initiative *Xenopus tropicalis* genome-sequencing project, make *Xenopus tropicalis* the more useful of the *Xenopus* species for conducting MO knockdowns.

6.1.4 Expected Phenotypes

In terms of phenotypes that might be expected in the heart after MO knockdown of Tbx18 or epicardin, little can be inferred from studies in other species. In mouse knockouts of both Tbx18 (Airik et al., 2006; Bussen et al., 2004) and epicardin (Cui et al., 2004; Lu et al., 2000; Quaggin et al., 1999) no cardiovascular phenotypes have been reported. However, Tbx18 has recently been implicated in the formation of the venus pole of the heart (Christoffels et al., 2006). WT1 on the other hand has been positively linked with several aspects of cardiovascular development such as correct formation of the epicardium (Moore et al., 1999) and normal development of the coronary vasculature (Wagner et al., 2005).

Despite the lack of evidence for a role of the T-box transcription factor Tbx18 and the bHLH transcription factor epicardin in epicardium development, they are tissue specific transcription factors and are known to be important for the development of other tissues in other species. A detailed description of functional studies of all candidate genes in other species is provided in section 1.12. The candidate genes have been shown to be important in a number of non heart-related developmental events. WT1 has been shown to be important for kidney and gonad development (Kreidberg et al., 1993), and the MET necessary for formation of the nephrons (Davies et al., 2004). Epicardin, like WT1, has been shown to be important for kidney as well as lung organogenesis (Quaggin et al., 1999). Epicardin has also been shown to be important for gonad development and sex differentiation (Cui et al., 2004), and spleen development (Lu et al., 2000). Finally Tbx18 has been shown to be important for

somite formation (Bussen et al., 2004; Tanaka and Tickle, 2004) and development of the urogenital system (Airik et al., 2006). Although these developmental events are not of primary importance to this study, the observation of associated phenotypes will help demonstrate the MO knockdown strategy is working.

Tbx18, epicardin and WT1 have been shown to be expressed in the proepicardium and/or the epicardium of *Xenopus laevis* and other species. They are tissue specific transcription factors that are known to be important for other tissues in which they are expressed. It is therefore reasonable to assume that they are involved in epicardium development, and therefore performing a MO experiment to knockdown their expression in *Xenopus* is a valid experiment to perform.

6.1.5 Aims Of This Chapter

This chapter will describe MO studies to impair Tbx18, epicardin and WT1 expression in the developing epicardium. Control experiments to determine if the MOs act on their target sequence will be described along with rescue experiments to determine if the MOs act specifically on their target sequence. The phenotypes of morphant embryos will be described with particular attention to the heart and epicardium. The targeting of the MOs to the developing epicardium using selective blastomere injections will be described. Finally the effect of loss of the genes on downstream targets will be described.

6.2 Results

6.2.1 Morpholino Target Specificity

In order to test the sequence specificity of the MOs, control constructs were made. These consisted of a short sequence of DNA that corresponded to the recognition sequence of each MO inserted immediately upstream of the translation start site of EGFP in the pCS2 expression vector (Turner and Weintraub, 1994). These constructs were named pCS2Tbx18·EGFP, pCS2epicardin·EGFP, and pCS2WT1·EGFP. These were linearised at their 3' ends and RNA was synthesised. A second set of constructs

were made that were identical to those above except for the addition of 5 point mutations in the MO recognition sequences. These constructs were named pCS2Tbx18ΔEGFP, pCS2epicardinΔEGFP, and pCS2WT1ΔEGFP. Again these were linearised and RNA synthesised.

100pg of RNA (in 2nl) was injected into the right cell of a two-cell stage *Xenopus laevis* embryo. Once the embryos reached the 4 cell stage 16ng of MO (in 2nl and supplemented with 1ng/nl rhodamine-dextran) was injected into one of the two cells on the right side of half of the embryos. The embryos were allowed to develop overnight. The results for the Tbx18, epicardin, and WT1 MOs are shown in figures 6-1, 6-2, and 6-3 respectively. When the wild type control construct was injected alone, EGFP fluorescence could be observed (first row of figures 6-1 to 6-3). When the wild type control construct was followed by injection of the MO (as seen by the red fluorescence of the rhodamine dextran), EGFP expression was no longer seen (second row of figures 6-1 to 6-3). When the mutated control construct was injected alone, EGFP fluorescence could again be observed (third row of figures 6-1 to 6-3). However, when the mutated control construct was followed by injection of the MO, EGFP expression could still be observed (fourth row of figures 6-1 to 6-3).

All injections were done in *Xenopus laevis* as the embryos are larger and more robust. Because the aim of the experiment was to test the ability of each MO to knock down the expression of EGFP by binding to its specific recognition sequence on the injected DNA construct, it did not matter against which species the MO had been designed.

6.2.2 Morpholino Dilution Series

The concentration at which MOs have an effect can vary greatly depending on the target gene, and higher concentrations are known to induce developmental defects due to non-specific toxicity. For both of these reasons it is important to titrate the amount of each MO used. In order to establish between what ranges of concentrations the MOs used in this study gave specific phenotypes without non-specific toxicity, a dilution series was made. Between 0.5ng and 16ng of WT1 and epicardin MO (in 2nl)

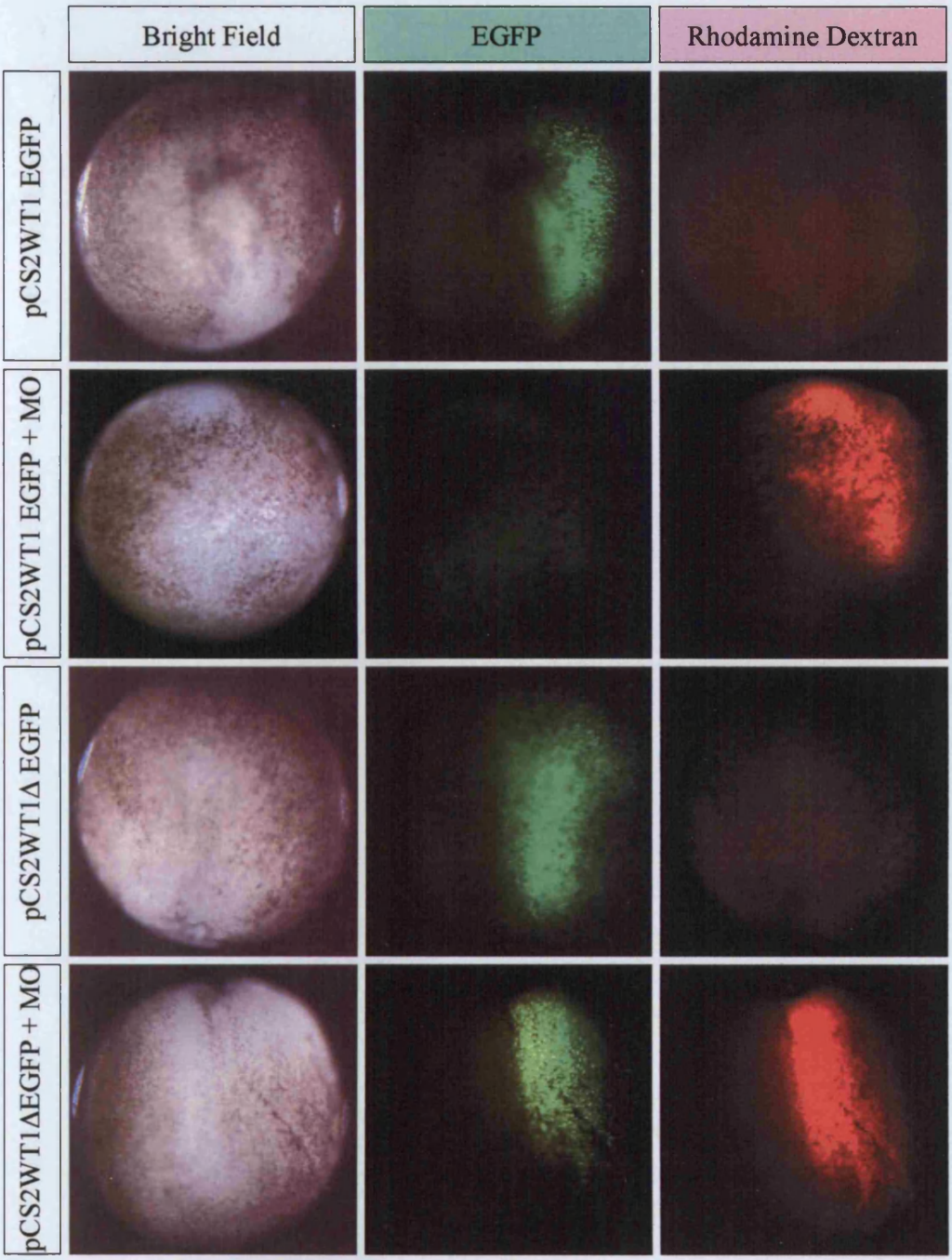

Figure 6-1. WT1 morpholino target specificity.

Injection of pCS2WT1 EGFP alone (first row) shows the EGFP is expressing correctly. Injection of pCS2WT1 EGFP together with the WT1 MO (second row) shows the MO acts on its target sequence. Injection of pCS2WT1Δ EGFP alone (third row) shows the EGFP is expressing correctly. Injection of pCS2WT1Δ EGFP together with the WT1 MO (fourth row) shows the MO does not act on target sequences similar, but not identical, to its own.

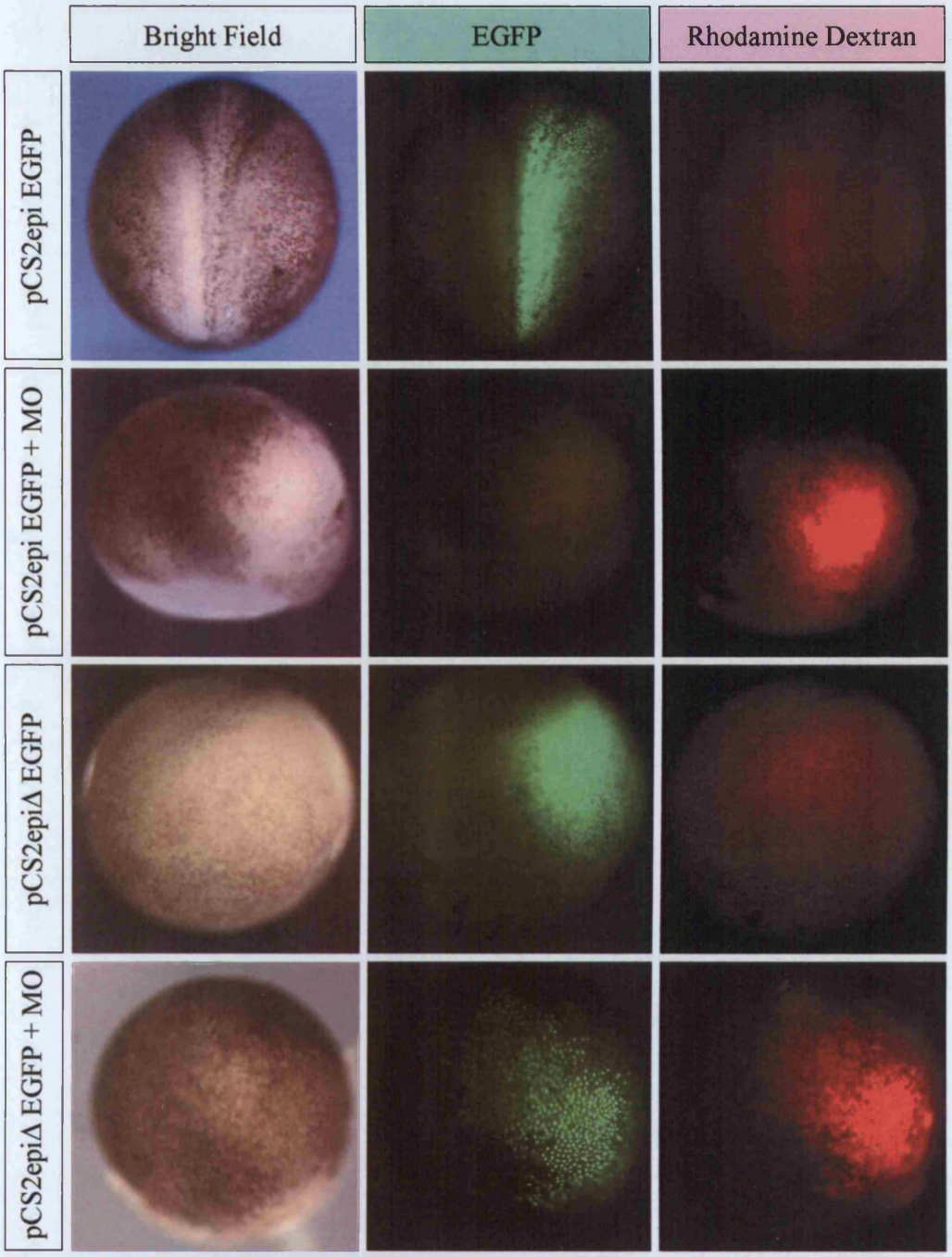

Figure 6-2. Epicardin morpholino target specificity.

Injection of pCS2epi EGFP alone (first row) shows the EGFP is expressing correctly. Injection of pCS2epi EGFP together with the epicardin MO (second row) shows the MO acts on its target sequence. Injection of pCS2epiΔ EGFP alone (third row) shows the EGFP is expressing correctly. Injection of pCS2epiΔ EGFP together with the epicardin MO (fourth row) shows the MO does not act on target sequences similar, but not identical, to its own.

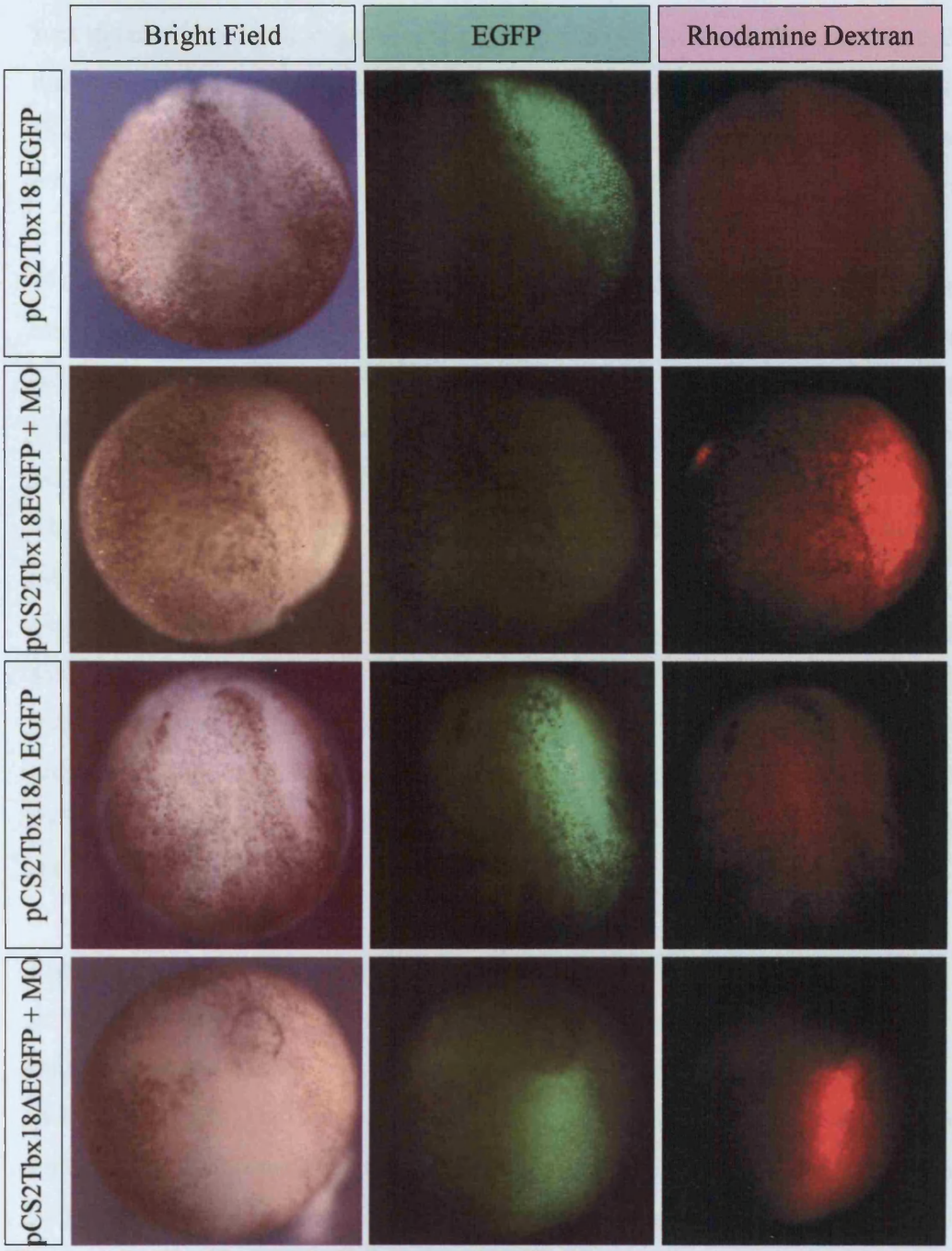

Figure 6-3. Tbx18 morpholino target specificity.

Injection of pCS2Tbx18 EGFP alone (first row) shows the EGFP is expressing correctly. Injection of pCS2Tbx18 EGFP together with the Tbx18 MO (second row) shows the MO acts on its target sequence. Injection of pCS2Tbx18Δ EGFP alone (third row) shows the EGFP is expressing correctly. Injection of pCS2Tbx18Δ EGFP together with the Tbx18 MO (fourth row) shows the MO does not act on target sequences similar, but not identical, to its own.

was injected into 1-cell stage *Xenopus laevis* embryos. Because *Xenopus tropicalis* embryos are much smaller than *Xenopus laevis* embryos, a dilution series increasing from 0.05ng of Tbx18 MO was injected into 1-cell stage *Xenopus tropicalis* embryos. MOs were supplemented with rhodamine dextran to a final concentration of 1ng/nl.

Figure 6-4 shows the dilution series for the WT1 MO. At concentrations of 1ng or 2ng the MO had no effect on the gross morphology of embryos through to feeding tadpoles. At 4ng and above the MO causes a phenotype characterised by abnormally large pronephroi and oedema. This oedema took the form of an excess of fluid in the pericardial and coelomic body cavities surrounding the heart and gut respectively. The embryos appeared normal until around stage 41 when the oedema began to form. At this concentration 13% (see figure 6-12(E) for a summary of all WT1 MO experiments) of tadpoles at stage 42 were normal, 67% showed a mild oedema such as that shown in figure 6-4(Q) and (R), whilst 20% showed a severe oedema such as that shown in figure 6-5(W) and (X). At 8ng the tadpoles again appeared normal until around stage 41 at which point the oedema began to form. At this concentration 5% of the tadpoles appeared normal at stage 42, 21% showed a mild oedema, whilst 74% showed a severe oedema.

Figure 6-5 shows the dilution series for the epicardin MO. At concentrations of 0.5ng or 1ng the MO had no effect on the gross morphology of embryos through to feeding tadpoles. At 2ng the MO was beginning to cause a phenotype very similar to that seen in WT1 embryos. The embryos appeared normal until around stage 41 at which time the pronephroi appeared enlarged and an oedema was beginning to form (figure 6-5(Q)). By stage 44 the oedema had become more severe (figure 6-5(R)). At this concentration 21% (see figure 6-13(E) for a summary of all epicardin MO experiments) of tadpoles at stage 42 were normal, 70% showed a mild oedema such as that shown in figure 6-5(Q) and (R), and 9% showed a severe oedema such as that shown in figure 6-5(W) and (X). At 4ng the tadpoles again appeared normal until around stage 41 at which point the oedema began to form. At this concentration 10% of the tadpoles appeared normal at stage 42, 32% showed a mild oedema, whilst 58% showed a severe oedema.

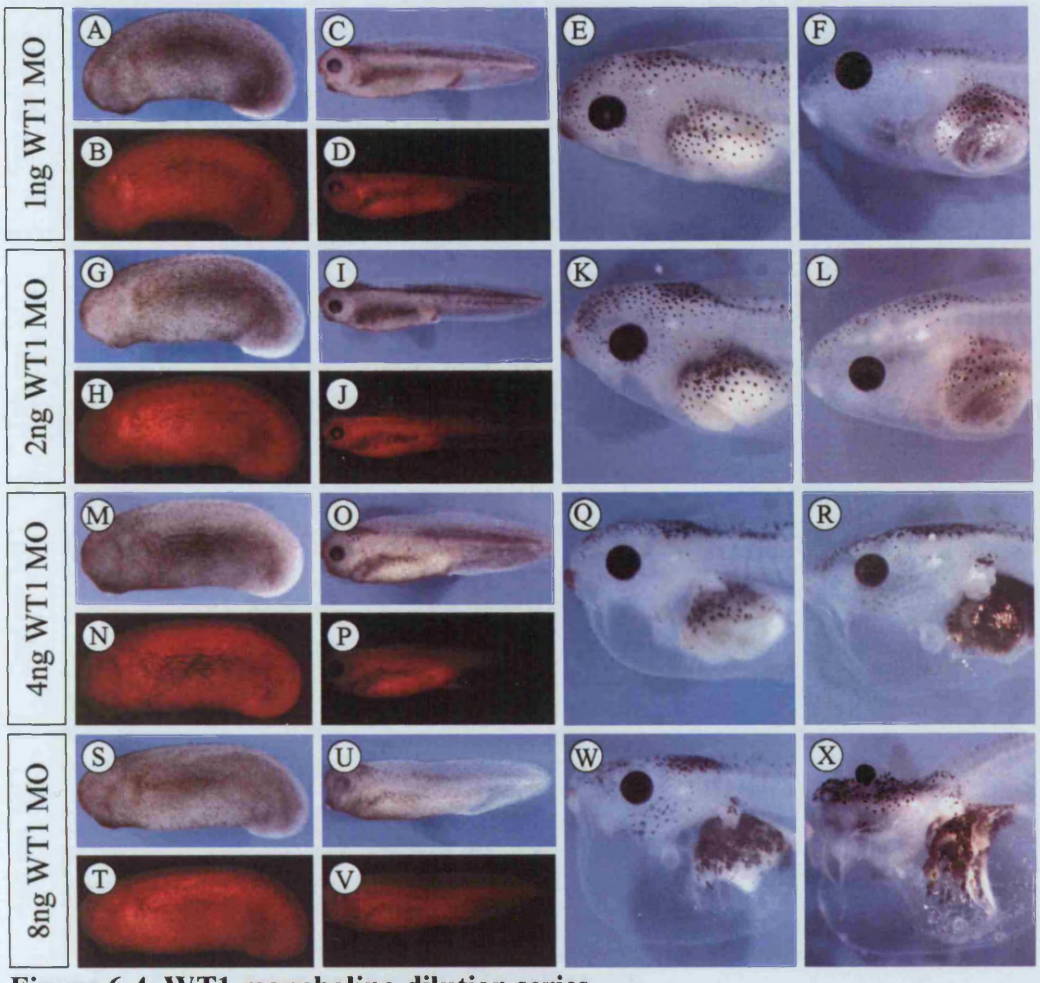

Figure 6-4. WT1 morpholino dilution series.

A serial dilution series was carried out in order to establish at what concentration the WT1 MO was having an effect. The first and second rows show injecting 1ng or 2ng has no obvious effect. At concentrations of 4ng (third row) and 8ng (fourth row) the tadpoles are characterised by oedema, with the most severe oedema being seen with the highest concentration.

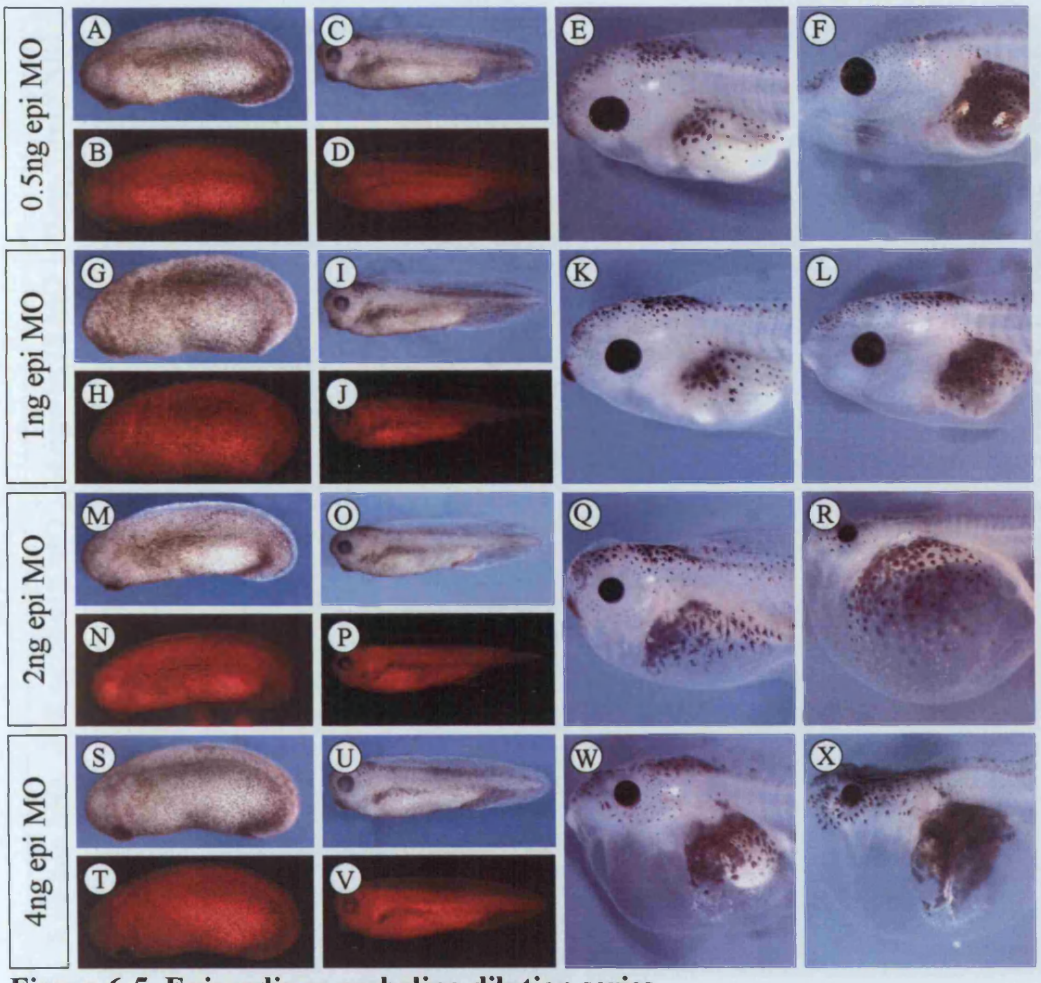

Figure 6-5. Epicardin morpholino dilution series.

A serial dilution series was carried out in order to establish at what concentration the Epicardin MO was having an effect. The first and second rows show injecting 0.5ng or 1ng has no obvious effect. At concentrations of 2ng (third row) and 4ng (fourth row) the tadpoles are characterised by oedema, with the most severe oedema being seen with the highest concentration.

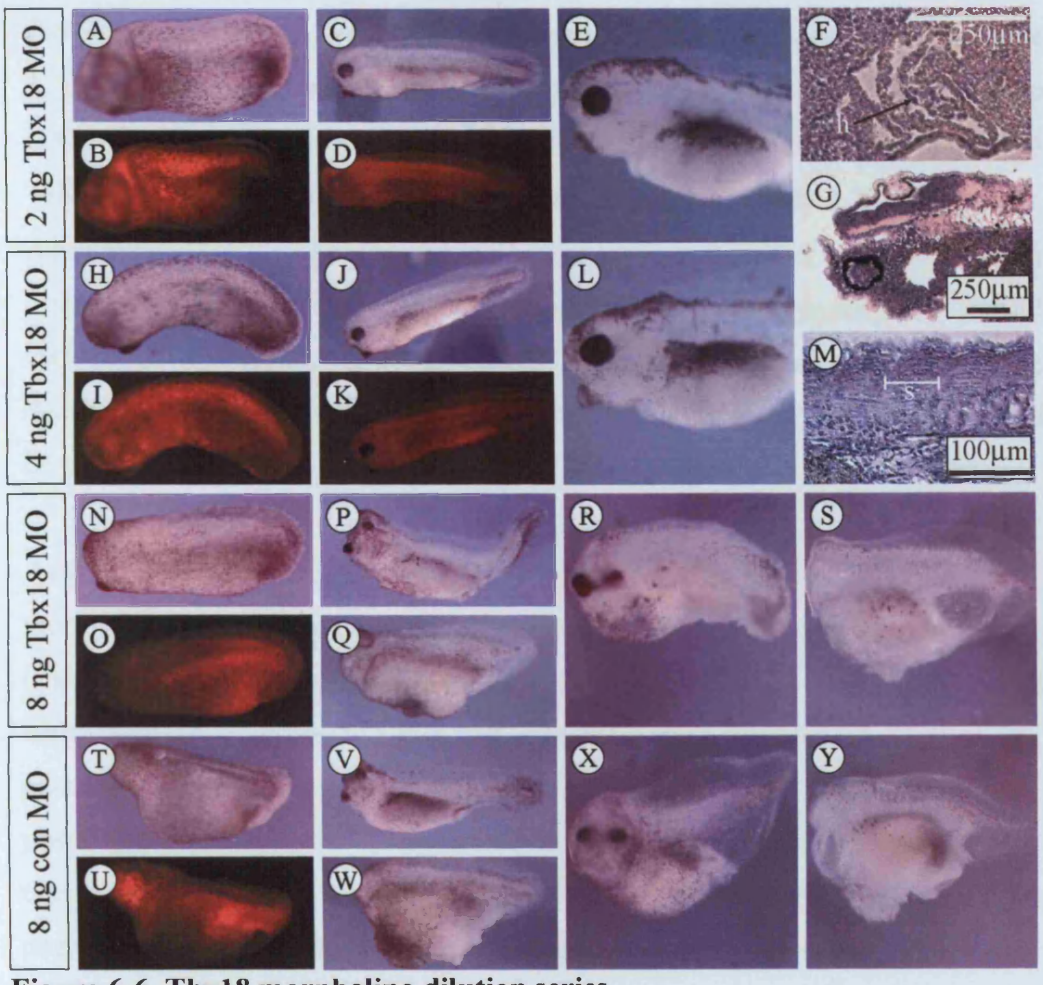

Figure 6-6. Tbx18 morpholino dilution series.

A serial dilution series was carried out in order to establish at what concentration the Tbx18 MO was having an effect. The first and second rows show injecting 2ng or 4ng has no obvious effect. (F), (G) and (M)- sagittal sections through an embryo injected with 4ng MO showing the heart (h), head musculature (figure(G)), and somites (s) appear normal. At concentrations of 8ng (third row) the embryos show a similar phenotype to embryos injected with 8ng of control morpholino (fourth row).

Because the necessary *Xenopus laevis* sequence information was not available, the Tbx18 MO was designed against the *Xenopus tropicalis* Tbx18 sequence. *Xenopus laevis* eggs have a volume of approximately 0.905µl (based on a diameter of 1.2mm) whilst *Xenopus tropicalis* eggs have a volume of approximately 0.268µl (based on a diameter of 0.6mm). *Xenopus tropicalis* eggs are therefore 3.38 times smaller than *Xenopus laevis* eggs. Empirical evidence however suggests approximately 10-fold less MO is required in *Xenopus tropicalis* to elicit a similar response to that seen in *Xenopus laevis* (Nutt et al., 2001). It was therefore anticipated that a phenotype would be observable at concentrations of around 0.4ng – 4ng.

As can be seen from figures 6-6(A) to (M) however, the embryos appeared morphologically normal up to feeding tadpole stage even when injected with concentrations of MO as high as 4ng. A change in morphology was only noticeable when embryos were injected with 8ng of MO (figures 6-6(N) to (S)). These phenotypes, which were characterised by a shortened body axis and anterior or posterior truncations however, appeared very similar to embryos injected with an equal amount of control MO (figures 6-6(T) to (Y)). In order to establish if a subtle phenotype was present that could not be detected in whole tadpoles, 7µm plastic sections were taken and stained with haematoxylin and eosin. No morphological defects were observed in regions where Tbx18 is expressed including the heart, head muscle and arches, somites and urogenital system (figure 6-6(F), (G) and (M)) and data not shown). Defects in the arches (Ataliotis et al., 2005) and somites (Rangarajan et al., 2006) of *Xenopus* have been shown to be easy to diagnose via histological sections. No such defects were observed here (figures 6-6(G) and (M)) It was concluded that the Tbx18 MO was having no specific effect, and any morphological changes observed were a result of non-specific toxicity of the MO.

6.2.3 Analysis Of Wilms tumour 1 Morphant Embryos

4ng of MO, supplemented with rhodamine dextran, was injected into 1-cell stage *Xenopus laevis* embryos. Embryos appeared morphologically normal until around stage 41 (figures 6-7(A) to (H)), when an oedema began to form around the heart and gut region (figures 6-7(D) and (H)). The oedema gradually worsened through

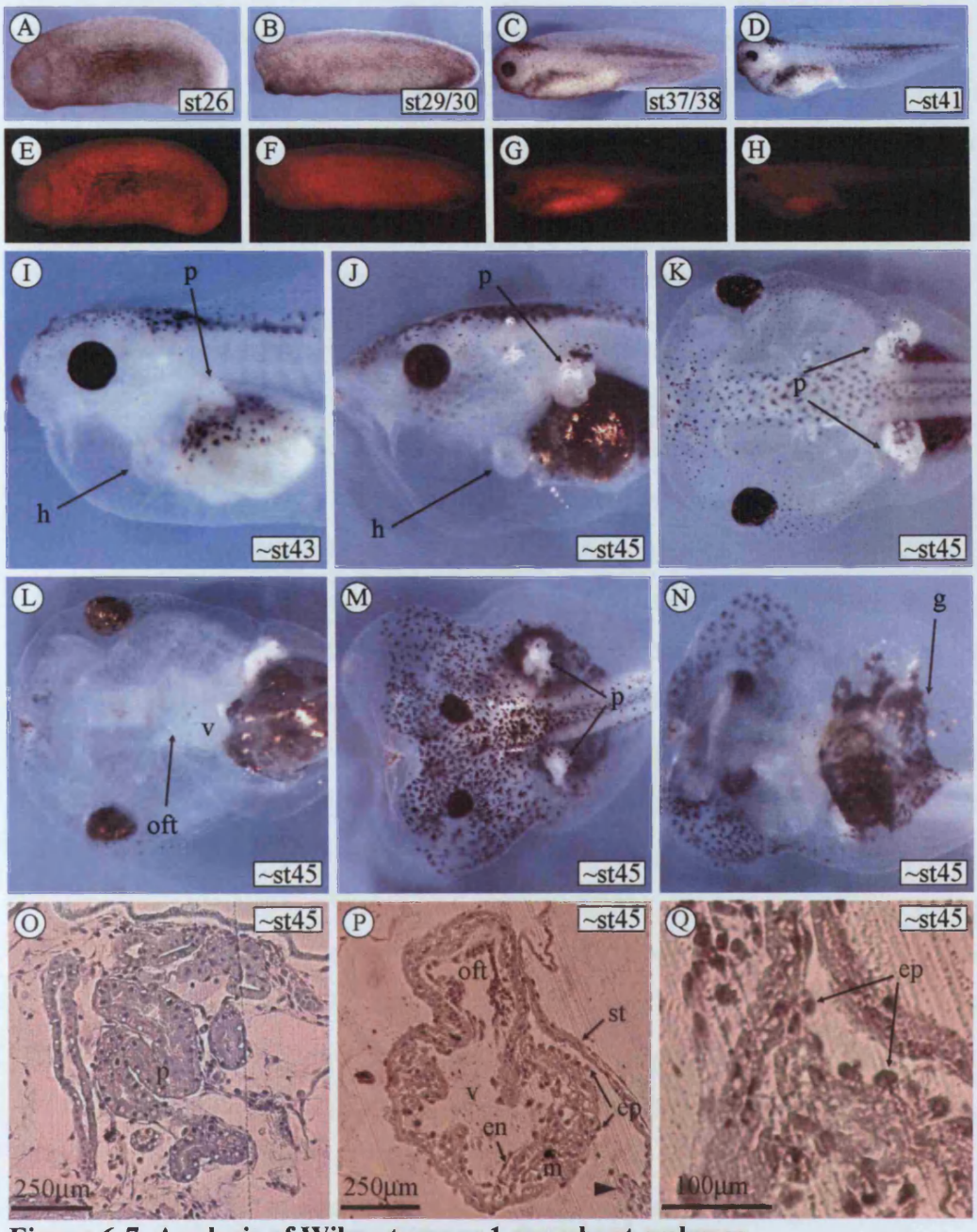

Figure 6-7. Analysis of Wilms tumour 1 morphant embryos.

All embryos injected with 4ng of MO, supplemented with rhodamine dextran, at the 1 cell stage. Embryos appear normal at stage 26 ((A) and (E)), stage 29/30 ((B) and (F)), and stage 37/38 ((C) and (G)). By stage 41 ((D) and (H)) the tadpoles begin to develop oedema around the gut and heart region. (I)- by stage 43 the oedema has become more severe and the pronephros (p) can be seen to be abnormally large. (J) (lateral), (K) (dorsal), and (L) (ventral)- by stage 45 the pronephroi have become much larger than wild type equivalent. The heart appears normal with the ventricle (v) and outflow tract (oft) clearly distinguishable (L). (M) (dorsal) and (N) (ventral)- in some instances the oedema is particularly

Figure 6-7. Analysis of Wilms tumour 1 morphant embryos continued - malformed. (O) to (Q)- sagittal sections through the pronephros and heart. (O)- the pronephros is much larger and more convoluted than in wild type tadpoles. (P) and (Q)- the heart is slightly malformed. A proepicardium-like structure (arrowhead) can be seen as well as epicardial cells (ep) on the surface of the heart.

development until approximately stage 47 when the tadpoles died possibly due to not being able to feed due to the oedema leading to deformation of the gut. The oedema is likely to be caused by disruption to pronephros development caused by the loss of WT1. The pronephroi of 87% of tadpoles appeared malformed with the remainder appearing morphologically normal. Of the tadpoles with malformed pronephroi, approximately 78% developed a mild oedema such as shown in figures 6-7(I) to (L), whilst the remainder developed a severe oedema such as that shown in figures 6-7(M) and (N). The physical appearance of the heart depended on the severity of the oedema. In tadpoles with only a mild oedema the heart appeared morphologically normal. In cases of severe oedema the heart often appeared stretched as a result of the oedema. All tadpoles with oedema died at around stage 47.

7μm sagittal plastic sections were taken and stained with haematoxylin and eosin. Sections through a stage 45 embryo with mild oedema reveal the pronephros to be much larger than in equivalently staged wild type tadpoles (figure 6-7(O)). The hearts of these tadpoles were slightly malformed and smaller than wild type equivalents, perhaps from the severity of the oedema. Also by this stage in development the myocardium of the heart should be trabeculated such as seen in figure 3-8, whereas in the morphant embryo trabeculation appeared to be reduced (figure 6-7(P)). Evidence of epicardium development could be seen. A structure that resembles the proepicardium can be seen in figure 6-7(P) (arrowhead). The location of this structure however is not where it would be expected in wild type tadpoles. The severe oedema has possibly caused the septum transversum to be displaced and therefore the proepicardium is also displaced. Despite this however, epicardial cells can be seen around the surface of the heart (figures 6-7(P) and (O)). By this stage however the epicardial cells should have formed a simple squamous epithelial layer such as seen in

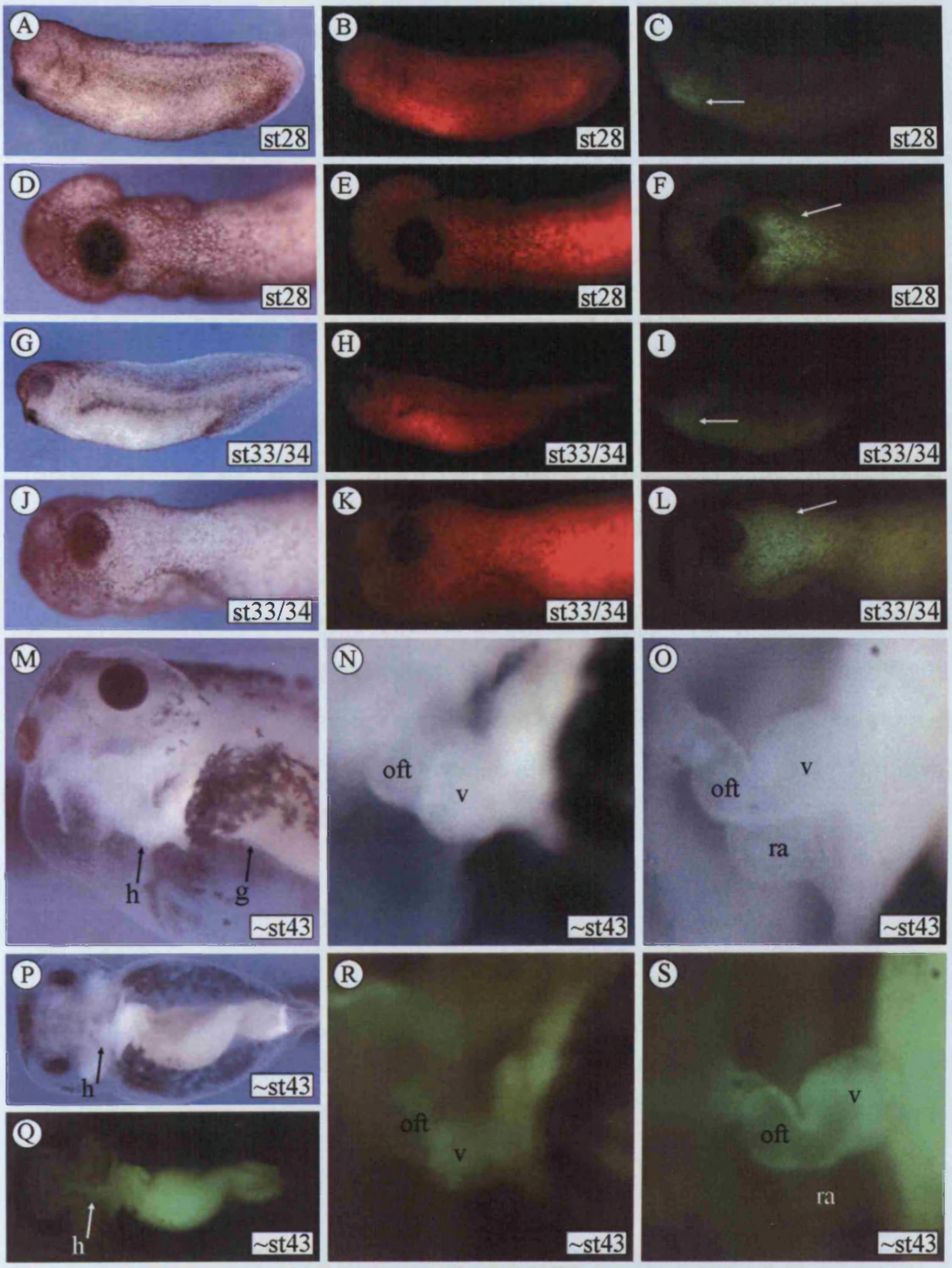

Figure 6-8. WT1 morpholino in an Nkx2.5 GFP transgenic background.

4ng MO, supplemented with rhodamine dextran, was injected into embryos obtained from a female frog carrying an Nkx2.5GFP transgene. (A) to (C) lateral, (D) to (F) ventral- the bilateral fields of cardiac mesoderm have already fused on the ventral midline by stage 28 as seen by GFP expression (white arrows). (G) to (I) lateral, (J) to (L) ventral- GFP expression can still be observed in the heart region at stage 33/34 . (M) lateral, (P) and (Q) ventral- by stage 43 the tadpole shows severe oedema around the heart (h) and gut (g) region. (N) and (R) lateral, (O) and (P) ventral- the structure of the heart appears normal. It has looped fully

Figure 6-8. Wilms tumour 1 morpholino in an Nkx2.5 GFP transgenic background continued -
and the ventricle (v), outflow tract (oft) and right atrium (ra) can clearly be distinguished. Also Nkx2.5 is driving GFP expression throughout the heart.

figure 3-8(F). In the morphant tadpoles the epicardial cells appear as individual cells and not as part of a cohesive layer (figures 6-7(P) and (Q)).

In order to better observe the hearts of morphant tadpoles, the experiment described above was repeated in Nkx2.5GFP transgenic embryos. Nkx2.5 is a cardiac specific homeobox-containing transcription factor that is expressed in cardiac precursor cells and throughout the developing heart (Tonissen et al., 1994). Eggs were obtained from a female *Xenopus laevis* that was heterozygous for the Nkx2.5GFP transgene, and were fertilised with testis from a wild type male. 4ng of MO, supplemented with rhodamine dextran, was injected into 1-cell stage embryos. Embryos were sorted for GFP expression (approximate Mendelian ratios were observed – data not shown) and for the presence rhodamine dextran

At stages 28 (figures 6-8(A) to (F)) and 33/34 (figures 6-8(G) to (L)) the embryos appeared morphologically normal and GFP was being correctly expressed in the heart primordium as would be expected in wild type embryos (Sparrow et al., 2000). By stage 43 an oedema had formed (figure 6-8(M)). Analysis of the heart region showed the heart appeared morphologically normal with GFP being correctly expressed in the clearly defined ventricle, right atrium and OFT (figures 6-8(N) to (S)).

In summary, loss of WT1 in *Xenopus* laevis causes malformation of the pronephroi that leads to oedema around the heart and gut region. The hearts of morphant tadpoles appear slightly malformed, probably due to the severity of the oedema. Epicardial cells can be seen around the heart but they appear not to have flattened into a cohesive simple squamous epithelial layer. The level of trabeculation in the heart of stage 45 tadpoles appears reduced compared to wild type equivalents.

6.2.4 Analysis Of Epicardin Morphant Embryos

2ng of MO, supplemented with rhodamine dextran, was injected into 1-cell stage *Xenopus laevis* embryos. Embryos appeared morphologically normal until around stage 41 (figures 6-9(A) to (H)), when an oedema began to form around the heart and gut region (figures 6-9(D) and (H)). Like WT1 morphants the oedema gradually worsened through development until approximately stage 47 when the tadpoles died. Again the oedema is likely to be caused by disruption to pronephros development caused by the loss of epicardin. The pronephroi of 79% of tadpoles appeared malformed with the remainder appearing morphologically normal. Of the tadpoles with malformed pronephroi, approximately 88% developed a mild oedema such as shown in figures 6-9(M) and (N), whilst the remainder developed a severe oedema such as that shown in figures 6-9(I) to (K). Again like WT1 morphant embryos the heart appeared morphologically normal in tadpoles with a mild oedema and was stretched in the case of severe oedema. All tadpoles with oedema died at around stage 47.

7μm sagittal plastic sections were taken and stained with haematoxylin and eosin. Sections through a stage 44 embryo with mild oedema reveal the severity of the pronephros malformation (figure 6-9(O)), with the pronephros appearing much larger and more convoluted than in wild type equivalents. Again the hearts of these tadpoles appeared slightly malformed, probably due to the oedema, but again there was evidence of epicardium development. Epicardial cells could be seen in various locations around the surface of the heart particularly around the CV canal (figures 6-9(P) and (Q)) such as would be seen in wild type tadpoles at this stage.

Due to the severity of the oedema that is likely caused by malformations of the pronephros, it is not possible to draw any conclusions from these results regarding the roles of WT1 and epicardin in epicardium development and the wider roles of the epicardium in heart development. The oedema is likely to put enormous strain on the heart that could account for any cardiac phenotypes observed.

In summary, loss of epicardin in *Xenopus* laevis causes malformation of the pronephroi that leads to oedema around the heart and gut region. The hearts of

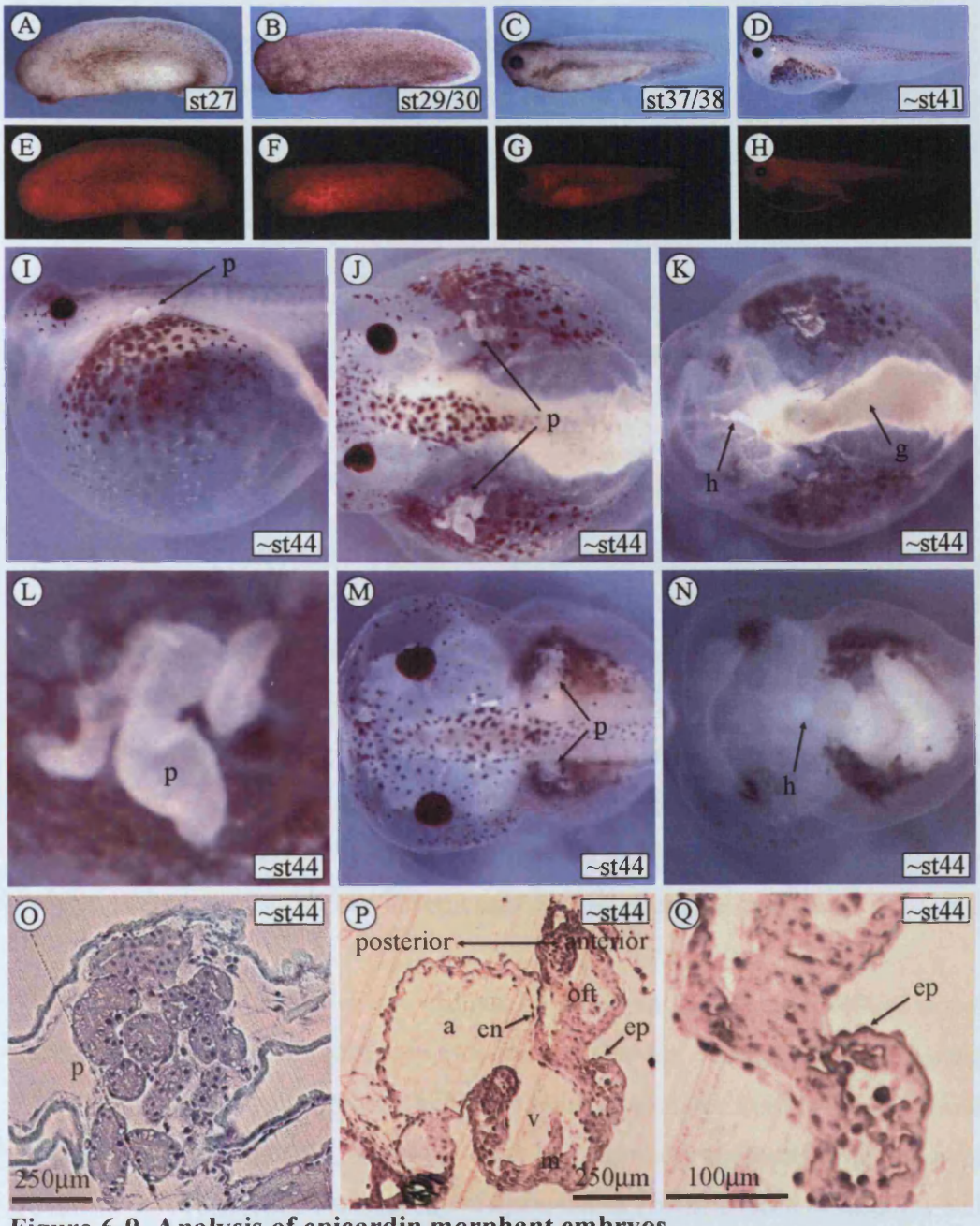

Figure 6-9. Analysis of epicardin morphant embryos.

All embryos injected with 2ng of MO, supplemented with rhodamine dextran, at the 1 cell stage. Embryos appear normal at stage 27 ((A) and (E)), stage 29/30 ((B) and (F)), and stage 37/38 ((C) and (G)). By stage 41 ((D) and (H)) the tadpoles begin to develop oedema around the gut and heart region. (I) (lateral), (J) (dorsal) and (K) ventral- by stage 44 the oedema has become severe and the pronephros (p) can be seen to be abnormally large (close up in (L)). Due to the severity of the oedema the heart (h) and gut (g) have been stretched. (M) (dorsal) and (N) (ventral)- in some instances the oedema is less severe and the heart appears grossly normal. (O) to (Q)- sagittal sections through the pronephros and

Figure 6-9. Analysis of epicardin morphant embryos continued - heart. (O)- the pronephros is much larger and more convoluted than in wild type tadpoles. (P) and (Q)- the heart is slightly malformed. Epicardial cells (ep) can be seen on the surface of the heart.

morphant tadpoles appear slightly malformed, probably due to the severity of the oedema, however epicardium cells can be seen on the surface of the heart.

6.2.5 Unilateral Morpholino Injections

It has long been known that *Xenopus* tadpoles require only one functioning pronephros to control water balance (Howland, 1916). This was demonstrated by unilateral and bilateral pronephrectomy. In the case of bilateral pronephrectomy tadpoles died from oedema, but when one pronephros was left in tact the tadpoles appeared morphologically normal. To take advantage of this fact, MOs were injected into one cell of a 2-cell stage embryo. By injecting MO into the right blastomere of the two cell embryo it was possible to target the MO to the side of the embryo from where earlier data has shown the epicardium originates (see chapter 4).

When 4ng of WT1 MO was injected into the right blastomere, only 44% of tadpoles showed oedema and of these only 14% showed a severe oedema. Of the remaining 56% of tadpoles, approximately half were indistinguishable from wild type tadpoles (figures 6-10(G) and (H)), whilst the other half showed a malformed right pronephros (figures 6-10(I) to (K)) but none of the oedematous characteristics of tadpoles with 2 malformed pronephroi. Occasionally the tail of the tadpole kinked to the right. This could be a consequence of a unilateral pronephros malformation. Strangely the right eye of many of the injected tadpoles appeared slightly less pigmented than the uninjected side (figure 6-10(E)). This difference disappeared in later development and may perhaps be a non-specific injection artefact.

7μm sagittal plastic sections were taken and stained with haematoxylin and eosin. Sections through a stage 43 tadpole with a malformed right pronephros but no

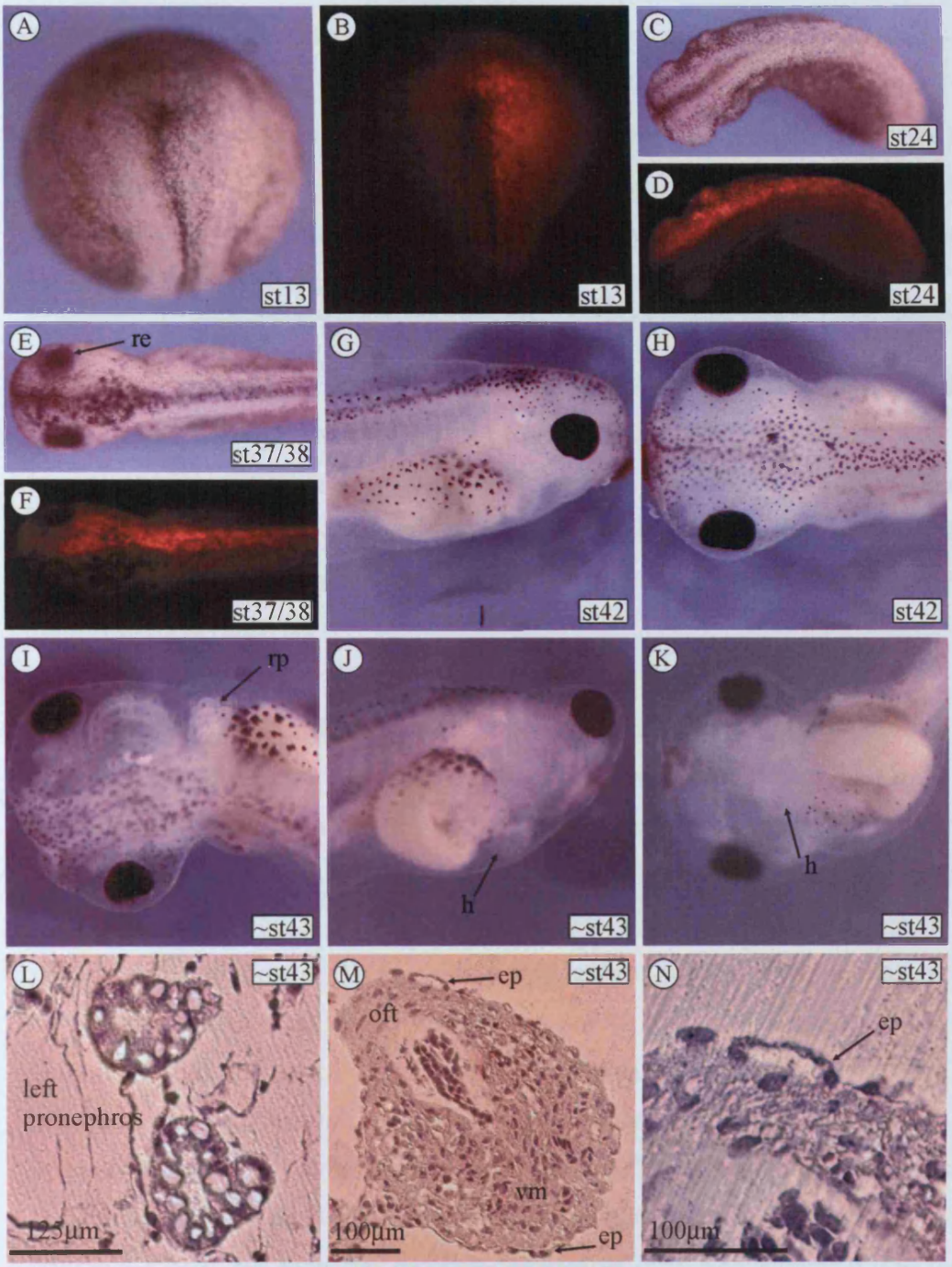

Figure 6-10. Unilateral injection of WT1 morpholino.

4ng MO, supplemented with rhodamine dextran, was injected into the right cell of a 2-cell stage embryo. Stage 13 ((A) and (B)), stage 24 ((C) and (D)), and stage 37/38 embryos ((E) and (F)) appear grossly normal except for a slight reduction in the pigment in the right eye (re) at stage 37/38 (E). (G) (lateral) and (H) (dorsal)- at stage 42 tadpoles appear normal. (I) (dorsal), (J) (lateral) and (K) (ventral)- occasionally the right pronephros (rp) appeared larger than normal but the severe oedema seen in 1-cell injections was rarely seen. The body axis of some embryos

Figure 6-10. Unilateral injection of Wilms tumour 1 morpholino continued – was curved possibly due to the asymmetric pronephric defect. (L) to (N)- sagittal sections through the pronephros and heart. (L)- the pronephros on the uninjected side appears normal. (M) and (N)- a section that has glanced through the ventricular myocardium (vm) and outflow tract (oft). The heart appears morphologically normal and epicardium cells (ep) can be seen around the ventricle.

oedema, showed that the left pronephros (figure 6-10(L)) was indistinguishable from a wild type pronephros, whilst the right pronephros was enlarged and more convoluted than wild type pronephroi such as seen in the 1-cell WT1 MO injected embryos (figure 6-7(O)). The heart appeared morphologically normal and a simple squamous epicardium could be seen, particularly around the ventricle such as seen in figures 6-10(M) and (N).

When 2ng of epicardin MO was injected into the right blastomeres, only 68% of tadpoles showed oedema and of these only 27% showed a severe oedema. Of the remaining 32% of tadpoles, approximately 40% were indistinguishable from wild type tadpoles (figures 6-11(G) and (H)), whilst the other 60% showed a malformed right pronephros (figures 6-11(I) to (K)). Of the tadpoles with a malformed right pronephros approximately half showed a mild oedema such as shown in figures 6-11(I) to (K), whilst the other half showed none of the oedematous characteristics of tadpoles with 2 malformed pronephroi. Although this reduction in the severity of the pronephric phenotype is not as marked as that seen for WT1, it still allows the epicardium to be analysed in an otherwise 'wild type' background. Like WT1 MO unilaterally injected embryos, the pigment of the right eye often appeared reduced (figure 6-11(E)), but again this problem disappeared later in development. The fact that this was seen for both WT1 and epicardin unilateral MO supports the idea that it is an injection artefact and not a specific effect of loss of gene function. There still remains the possibility that both epicardin and WT1 are involved in eye development. However this seems unlikely, as can be seen in figures 5-1 and 5-2 neither of these genes are expressed in the eye. A unilateral injection of a control MO would determine whether the effect is specific or non-specific. The rightward kinking of the

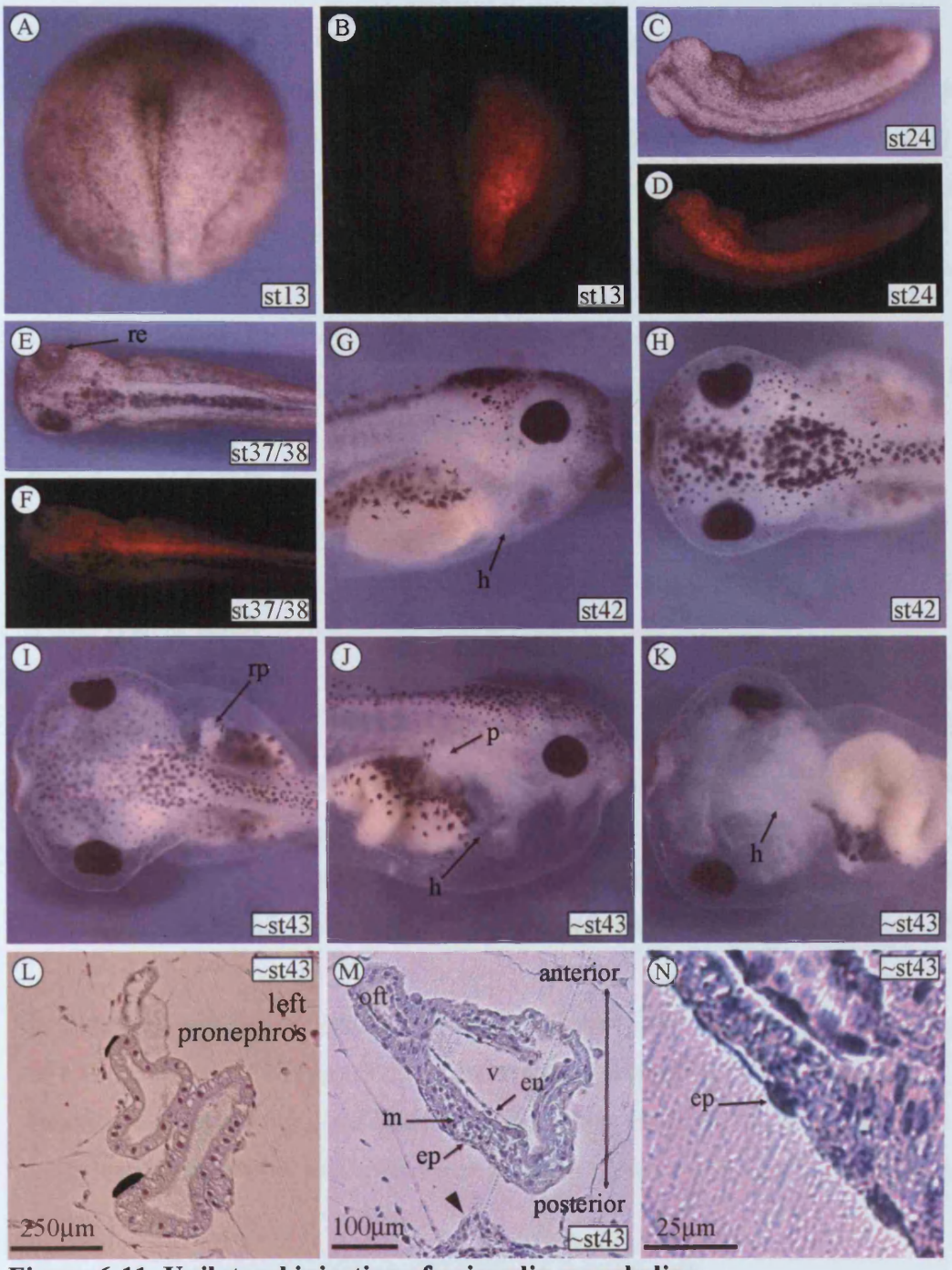

Figure 6-11. Unilateral injection of epicardin morpholino.

2ng MO, supplemented with rhodamine dextran, was injected into the right cell of a 2-cell stage embryo. Stage 13 ((A) and (B)), stage 24 ((C) and (D)), and stage 37/38 embryos ((E) and (F)) appear grossly normal except for a slight reduction in the pigment in the right eye (re) at stage 37/38 (E). (G) (lateral) and (H) (dorsal)- at stage 42 some tadpoles appear normal. (I) (dorsal), (J) (lateral) and (K) (ventral)- often the right pronephros (rp) appeared larger than normal but the severe oedema seen in 1-cell injections was observed less often. (L) to (N)-frontal sections through

Figure 6-11. Unilateral injection of epicardin morpholino continued – the pronephros and heart. (L)- the pronephros on the uninjected side appears normal. (M) and (N)- the heart appears morphologically normal and epicardium cells (ep) can be seen around the ventricle. Also a proepicardial-like structure can be seen adjacent to the septum transversum (arrowhead in (M)).

body axis that was observed in WT1 injected embryos was never observed in epicardin injected embryos.

7μm frontal plastic sections were taken and stained with haematoxylin and eosin. Sections through a stage 43 tadpole with a malformed right pronephros but no oedema, showed that the left pronephros (figure 6-11(L)) was indistinguishable from a wild type pronephros, whilst the right pronephros was enlarged and more convoluted than wild type pronephroi such as seen in the 1-cell epicardin MO injected embryos (figure 6-9(O)). The heart appeared morphologically normal and a simple squamous epicardium could be seen, particularly around the ventricle (6-11(M) and (N)). Also at this stage a proepicardium-like structure was observed adjacent to the septum transversum (figure 6-11(M) arrowhead) which closely resembles what is observable at approximately this stage in wild type tadpoles (figure 3-7(D) to (F)).

In summary, unilateral injection of WT1 or epicardin MO into the right blastomeres of a two-cell stage embryo results in grossly normal tadpoles because a single functioning pronephros is sufficient to control water balance. The hearts of these tadpoles appear normal and epicardium cells can be seen on the surface of the heart.

6.2.6 Rescue Of Wilms tumour 1 And Epicardin Morphant Phenotypes

A key test for establishing whether MOs act specifically on their target gene is to test if the phenotype can be rescued by coinjection of the MO and mRNA for the target gene. Full length cDNAs corresponding to *Xenopus laevis* WT1 and epicardin were kindly provided by Peter Vize (University of Calgary) and Andre Brandli (Swiss Federal Institute of Technology, Zurich) respectively. In order to avoid the rescue RNA also being knocked down by the MO, the MO recognition sequence on the

cDNA was altered by the addition of 5 point mutations. The WT1 and epicardin wildtype cDNAs, MOs (shown in the sense complement to aid comparison), the forward mutagenesis primers, and the resultant mutated rescue constructs are shown in table 6-1. The resultant constructs were linearised at their 3' ends and RNA was synthesised.

SEQUENCE	*ALIGNMENT*
WT1 cDNA	CTCAACTTTGGCAGATCCCAGATGGGGTCTGATGTCCGGGATATGAATCTGTTGCCTCCAGTCTC
WT1 MO	ATGGGGTCTGATGTCCGGGATATGA
Primers	CTTTGGCAGATCCCAGATGGGATCGGACGTACGTGATATGAATCTGTTGCCTCCA
Mutated cDNA	CTCAACTTTGGCAGATCCCAGATGGGATCGGACGTACGTGATATGAATCTGTTGCCTCCAGTCTC

SEQUENCE	*ALIGNMENT*
Epicardin cDNA	TCCAATGAGAAGGAGCAGCATAACAGATCATGTCCACCGGTTCTCTCAGTGAT
Epicardin MO	GCAGCATAACAGATCATGTCCACCG
Primers	TGAGAAGGAGTAGTATGACAGATCATGTCTACTGGTTCTCTCA
Mutated cDNA	TCCAATGAGAAGGAGTAGTATGACAGATCATGTCTACTGGTTCTCTCAGTGAT

Table 6-1. Alignments of Wilms tumour 1 and epicardin morpholinos, cDNAs and mutated rescue constructs.

8ng of WT1 MO was coinjected with 200pg or 400pg of RNA (figure 6-12). 8ng of WT1 MO was previously shown to cause a severe oedema in 74% of tadpoles at stage 42. When the MO was coinjected with 200pg of RNA 29% of tadpoles appeared normal, 63% showed a mild oedema, and only 8% showed the most severe oedematous phenotype. When the MO was coinjected with 400pg of RNA 65% of tadpoles appeared normal, 32% showed a mild oedema, and only 3% showed the most severe oedematous phenotype. Injecting 400pg of WT1 mRNA alone caused no noticeable phenotype.

4ng of epicardin MO was coinjected with 100pg or 200pg of RNA (figure 6-13). 4ng of epicardin MO was previously shown to cause a severe oedema in 58% of tadpoles at stage 42. When the MO was coinjected with 100pg of RNA 20% of tadpoles appeared normal, 65% showed a mild oedema, and only 15% showed the most severe oedematous phenotype. When the MO was coinjected with 200pg of RNA 59% of

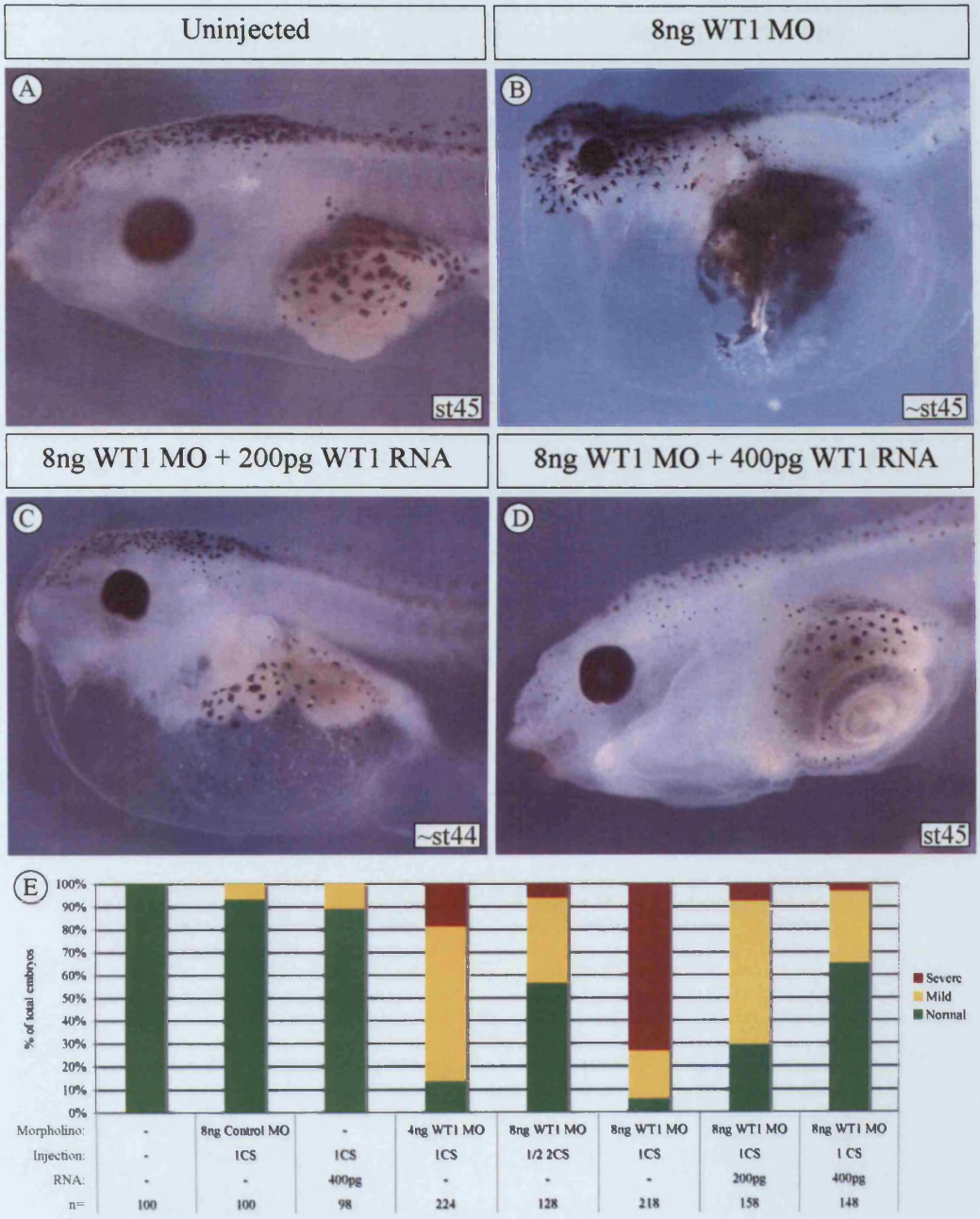

Figure 6-12. Rescue of WT1 morpholino phenotype.

8ng MO was coinjected with 200pg or 400pg of WT1 mRNA with a mutated MO recognition sequence at the 1-cell stage. (A)- wild type embryo. (B)- morphant embryo injected with 8ng MO only at 1-cell stage. (C)- embryo injected with MO and 200pg mRNA. The oedema is much less severe than seen in (B). (D)- embryo injected with MO and 400pg mRNA. The embryo appears grossly normal. (E)- summary of all WT1 MO experiments. (1CS = 1-cell stage, 1/2 2CS = 1 cell of a two cell-stage embryo)

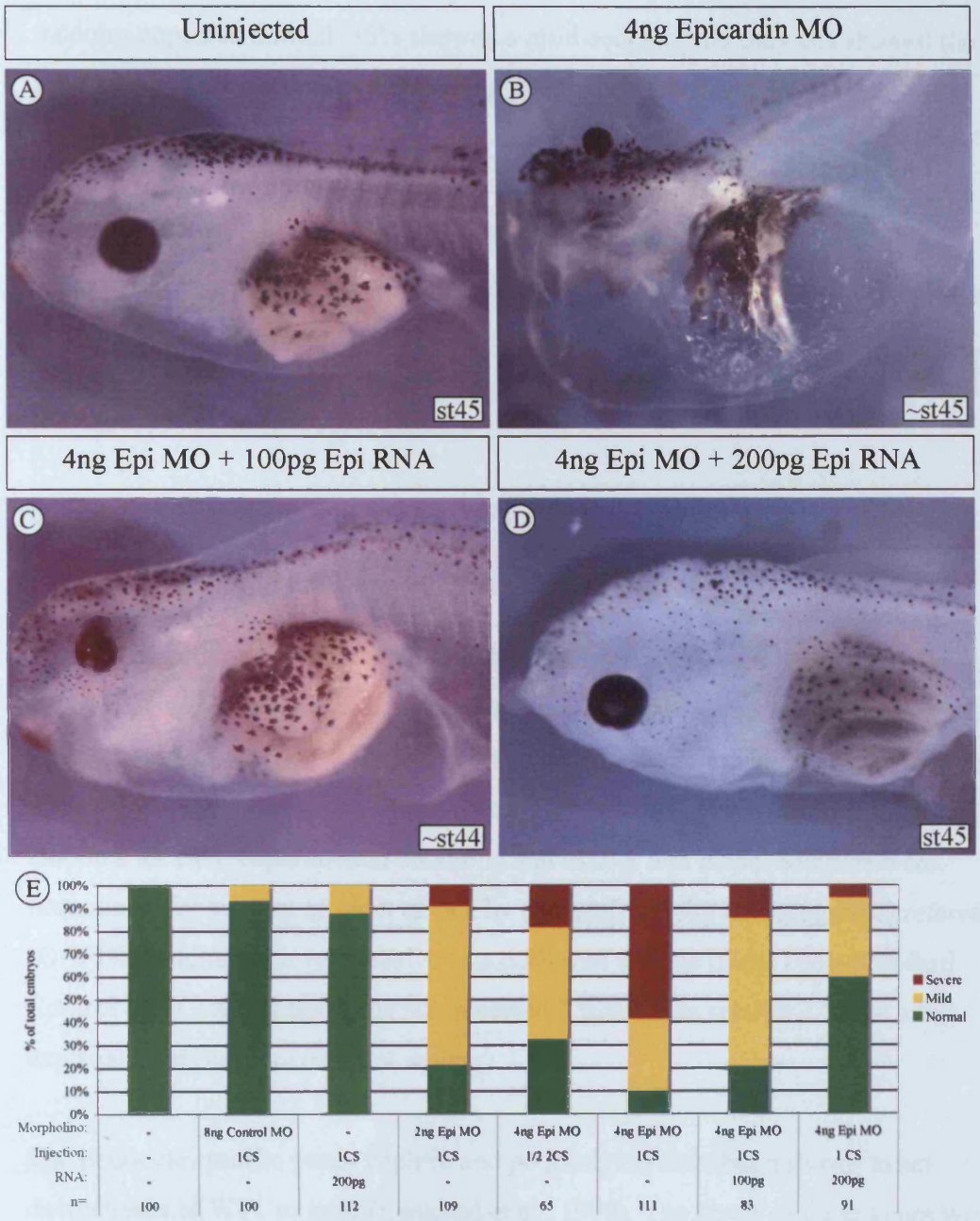

Figure 6-13. Rescue of epicardin morpholino phenotype.

4ng MO was coinjected with 100pg or 200pg of epicardin mRNA with a mutated MO recognition sequence at the 1-cell stage. (A)- wild type embryo. (B)- morphant embryo injected with 4ng MO only at 1-cell stage. (C)- embryo injected with MO and 200pg mRNA. The oedema is greatly reduced compared to (B). (D)- embryo injected with MO and 400pg mRNA. Embryos appear grossly normal. (E)- summary of all epicardin MO experiments. (1CS = 1-cell stage, 1/2 2CS = 1 cell of a two cell-stage embryo)

tadpoles appeared normal, 35% showed a mild oedema, and only 6% showed the most severe oedematous phenotype. Injecting 200pg of epicardin mRNA alone caused no noticeable phenotype.

In summary, coinjection of MO and mRNA is able to rescue both the WT1 and epicardin morphant phenotypes demonstrating that both the WT1 and epicardin MOs are acting specifically on their target genes, and the phenotypes observed were entirely caused by the specific knockdown effect of the MO.

6.2.7 Effect Of Loss Of Wilms tumour 1 And Epicardin On Downstream Target Genes And Other Markers Of The Epicardium

The rescue experiments show that the WT1 and epicardin MOs act specifically on their target sequence. Another method of determining if the gene of interest is being knocked down is to look at the effect on known downstream target genes. This was done using a quantitative RT-PCR strategy. RNA was extracted from 5 stage 42 tadpoles for each experimental condition and cDNA was made. Samples were normalised for amount of input cDNA by comparison with an endogenous reference (GAPDH) and target levels relative to a calibrator sample (GeneTools Standard Control MO). Each experiment was repeated 3 times. See section 2.14 for a full explanation of the experimental strategy.

The podocyte specific genes nephrin and podocalyxin have been shown to act downstream of WT1 in mice (Lenkkeri et al., 1999). The levels of these genes were analysed in WT1 morphant *Xenopus laevis* tadpoles. In embryos injected with 4ng of WT1 MO at the 1-cell stage, nephrin levels were 43.5% compared to embryos injected with an equivalent amount of control MO which represented 100% nephrin levels (figure 6-14(A)). When 4ng of MO was injected unilaterally to the right cell of a 2-cell embryo nephrin levels were 67% of normal (figure 6-14(A)). Podocalyxin showed a similar response with levels at 57.6% of normal when the MO was injected at the 1-cell stage and 72.9% when it was injected into the right cell of a 2-cell stage embryo (figure 6-14(B)). Levels of Tbx18 (figure 6-14(C)) and epicardin (figure 6-14(D)) were largely unaffected.

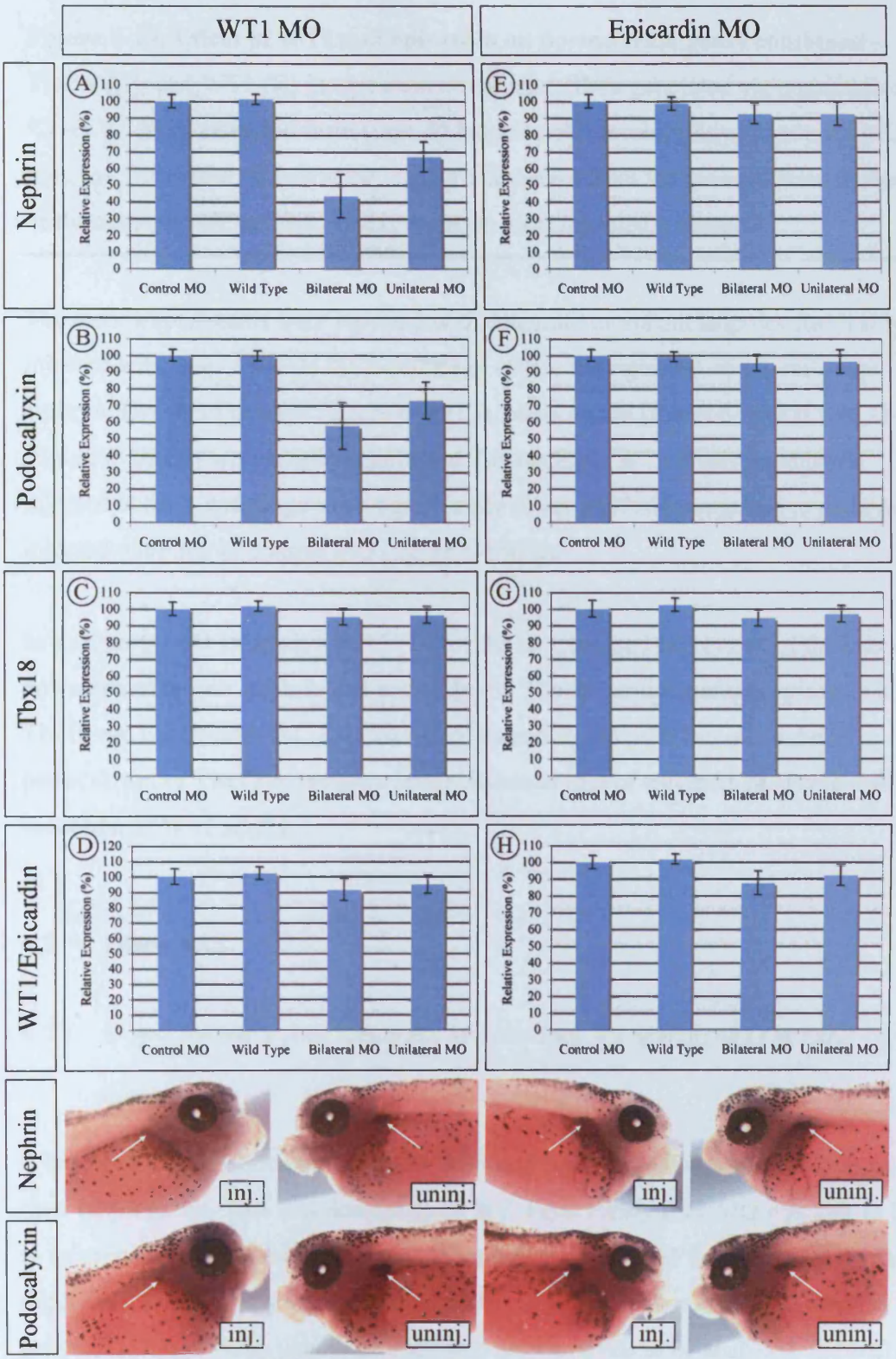

Figure 6-14. Effect of WT1 and epicardin on downstream genes.

Relative expression levels of known WT1 downstream genes and other epicardial markers in WT1 and epicardin morphants. First column- relative expression levels of nephrin (A), podocalyxin (B), Tbx18 (C), and epicardin (D) in WT1 morphants. Second column- relative expression levels of nephrin (E), podocalyxin (F),

Figure 6-14. Effect of WT1 and epicardin on downstream genes continued - Tbx18 (G), and WT1 (H) in epicardin morphants. (Data generated via quantitative RT-PCR. RNA extracted from stage 40 tadpoles. All levels relative to control MO injected. Error bars represent the standard deviation from the mean of three analyses of the same cDNA sample. All experiments were repeated 3 times.)

The same experiments were repeated with epicardin morphant tadpoles that had been injected with 2ng of MO at the 1-cell stage or into the right cell of a 2-cell stage embryo. Levels of nephrin (figure 6-14(E)), podocalyxin (figure 6-14(F)), and Tbx18 (figure 6-14(G)) were largely unaffected. Interestingly WT1 levels in embryos injected at the 1-cell stage were significantly lower at 87.6% compared to embryos injected with 2ng of control MO (figure 6-14(H)).

In summary, MO knockdown of WT1 results in decreased expression of the known downstream targets nephrin and podocalyxin. The epicardial markers epicardin and Tbx18 are unaffected. MO knockdown of epicardin has no effect on nephrin, podocalyxin or Tbx18 expression levels. Bilateral loss of epicardin results in a slight reduction in WT1 levels.

6.3 Discussion

6.3.1 Wilms tumour 1 And Epicardin Morpholinos Act Specifically On Their Target Gene

It has been demonstrated that both the WT1 and epicardin MOs act specifically on their target genes. This was demonstrated in 3 ways. Firstly each MO was able to bind to its recognition sequence and knockdown translation of GFP in the control construct experiments. This assay was designed due to the absence of antibodies against the genes of interest which would have allowed protein levels to be analysed. Secondly, in the case of WT1, the MO was seen to have an effect on the levels of the known downstream targets nephrin and podocalyxin. Finally, and most importantly, coinjection of rescue mRNA with the MO, was able to rescue the phenotype. It is perhaps surprising that the rescue experiment was so successful. The major phenotype

of the tadpoles was oedema caused by disrupted pronephros development. Tissue specific delivery of rescue RNA might be expected to rescue the phenotype, however the rescue RNA was delivered at the 1-cell stage so is ubiquitously expressed and is not specific to the pronephros. The method of delivery might be expected to result in an overexpression phenotype. However, in control injections the delivery of rescue-quantities of mRNA alone gave no over expression phenotype. Also in the case of WT1 an over expression phenotype has been reported when mRNA is injected at concentrations of 1000pg (Carroll and Vize, 1996) – over twice the maximum amount delivered in the WT1 rescue experiment.

One interesting result from the epicardin MO knockdown showed that when 2ng of MO was injected at the 1-cell stage, WT1 was expressed at only 87.6% of normal levels. It is however, unlikely that WT1 is a downstream target of epicardin, and this result is probably due to the severe malformation of the pronephros affecting other gene pathways.

6.3.2 Tbx18 Appears Not To Act On Its Target Sequence

Despite apparently binding to its recognition sequence and knocking down translation of GFP in the control construct experiment, the Tbx18 MO appeared to have no effect on its target gene. Only when injected in excessive concentrations did the MO have any effect, however the phenotypes observed were identical to embryos that had been injected with an equal amount of GeneTools standard control MO. These defects were characterised by a shortened body axis and anterior and posterior truncations. It has recently been shown that MOs can induce non-specific effects in zebrafish by induction of a p53-dependent cell death pathway (Robu et al., 2007). Here the non-specific 'morpholino phenotype' was described as having a smaller head, shortened body axis, loss of specific elements of craniofacial cartilage, and degeneration of specific nerves. This is very similar to the phenotypes observed with excessive concentrations of Tbx18 MO. Embryos injected with lower concentrations of Tbx18 MO were analysed histologically for any subtle phenotype that might not be detectable in whole tadpoles. All organ systems in which Tbx18 has been shown to be

important, including the heart, somites, musculature of the head and urogenital system appeared normal.

There are a number of possible explanations as to why the Tbx18 morphants presented no specific phenotypes. Firstly, and most likely, the MO was not knocking down its target gene. The control experiments described in section 5.2.1 involved the MO knocking down GFP by binding to its target sequence. This experiment however, was artificial in that the control constructs were designed to be identical to the MO. If the original sequence against which the MO and the control constructs were designed was incorrect then it is quite possible for the MO to knockdown expression of the control construct but have no effect on endogenous Tbx18 expression.

In order to clarify this, an antibody against Tbx18 that cross reacts with *Xenopus* would be required to detect if Tbx18 protein levels are effected in morphant embryos. Performing RNA *in situ* hybridisation or RT-PCR would be ineffectual because translation blocking MOs have no effect on transcript levels. A splice blocking MO could be designed as intron/exon boundary information is now available for *Xenopus tropicalis* via Ensembel (http://www.ensembl.org/Xenopus_tropicalis/index.html.) The efficacy of the MO could then be analysed via RT-PCR to assay for spliced versus unspliced mRNA transcripts. Alternatively observing the effect of the MO on downstream target genes, of which none are currently known, would show if Tbx18 levels are affected. However, this would not be unequivocal due to redundancy within the T-box family. Tbx18 is most closely related to Tbx15 with 92.8% similarity at the amino acid level within the T-box (Kraus et al., 2001). It is possible that these genes are sufficiently similar in sequence and structure that they act redundantly and therefore endogenous Tbx15 could 'rescue' loss of Tbx18. Indeed amphioxus is know to posses only a single Tbx18/15 homologue (Ruvinsky et al., 2000). In order to demonstrate that this is the case a double MO experiment targeting both genes would be necessary.

Redundancy within the T-box gene family is known to occur. For example a conditional mouse knockout of Tbx5 in the forelimb results in mice with no forelimbs (Rallis et al., 2003). This phenotype can be rescued by mis-expression of the hindlimb-specific Tbx4 in the forelimb (Minguillon et al., 2005). Redundancy

between Tbx18 and Tbx15 has also been suggested to account for the relatively mild limb phenotype observed in Tbx15 knockout mice (Singh et al., 2005b).

6.3.3 Xenopus Epicardium Development Is Not Accessible To Study Using Antisense Morpholino Oligonucleotides

MOs against both WT1 and epicardin have been shown to have a phenotype that is characterised by malformation of the pronephros. This phenotype would be expected from the expression patterns of these genes and from what has been observed in mouse knockout experiments. However, there is no evidence of a heart phenotype as judged by gross morphology and histological sections. It could be stated that in WT1 morphants, the epicardium does not form a coherent simple squamous epithelial layer by stage 45 which would be expected in wild type embryos. Also the hearts of these tadpoles show a reduction in trabeculation implicating the epicardium or EPDCs in myocardium development modulation. However, even these phenotypes were rescued by unilateral delivery of the MO into the right blastomere to target the epicardium but avoid the oedema caused by bilateral disruption to pronephroi morphogenesis. It is unlikely that the oedema was caused by disrupted cardiac function. Observing living morphant tadpoles under a microscope showed the heart was beating quite normally, with non-beating or slower beating hearts being the usual cause of cardiac related oedemas.

The simplest explanation of these results is that epicardium formation is happening too late in development to be accessible to disruption by MOs. It has previously been shown that injecting different concentrations of MO alters the longevity of the knockdown (Nutt et al., 2001). Here a GFP MO was used to knockdown GFP expression under the control of the lens specific γcrystallin promoter. At doses greater than 4ng, GFP expression was knocked down until at least stage 43. 1ng of MO on the other hand resulted in knockdown of GFP expression up to stage 30, at which point the protein began to be translated with normal levels being reached by stage 43. A tradeoff therefore exists between delivering sufficient MO for the knockdown to be long-lived enough to effect protein levels when epicardium formation begins, and limiting the effect of nonspecific toxicity and more importantly the effect on other

organ systems such as seen here in the case of WT1 and epicardin in the pronephros. Pronephros development, although a relatively late event itself, occurs much earlier than epicardium development and so was easily disrupted by the MOs.

In conclusion, MOs are not a viable tool for investigating development of the epicardium in *Xenopus*. In order to investigate epicardium development an alternative knockdown or interference strategy is required. Some possible alternatives to MOs will be discussed in chapter 7.

7 Summary And Future Directions

7.1 Summary Of Results

7.1.1 Development And Structure Of Xenopus Epicardium

A number of novel results have been described in this thesis regarding the development and structure of *Xenopus laevis* epicardium. Firstly the myocardium of the adult frog heart was shown to be extensively trabeculated and have a very thin compact layer, both of which negate the necessity for coronary vasculature. Nevertheless, despite these differences it has also been established that adult *Xenopus laevis* does have an epicardium. The epicardium is a single-celled simple squamous epithelial layer that is often in close association with the underlying myocardium whilst at other locations a sub-epicardial space is present.

The proepicardium, the origin of the epicardium, begins to project from the septum transversum between stages 40 and 42. The septum transversum was shown to be incomplete at the time of proepicardial outgrowth. The proepicardium, which at stage 42 is a cone shaped protrusion with dimensions of approximately 161μm wide by 133μm high, is located to the right of the sagittal plane. Cells appear to migrate over from the proepicardium both as free floating cell aggregates and via a bridge formed by the physical attachment of the proepicardium to the myocardium. Both the size and location of the proepicardium, and the method of proepicardial outgrowth and attachment, are similar to what is known in chick embryos (Ho and Shimada, 1978; Manner, 1992; Nahirney et al., 2003). Cells from the proepicardium attach at the point where the AV and CV canals converge, then continue to spread preferentially along the AV and CV canals and over the surface of the heart. The heart appears to be completely covered by the epicardium by stage 45.

7.1.2 The Early Embryonic Origins Of Xenopus Epicardium

Lineage analysis experiments demonstrated that the epicardium primarily originates from the right dorsal blastomere of the 4-cell embryo. If any contribution from the left dorsal blastomere is made it is very minor or else it occurs after stage 47. It was not

possible to analyse tadpoles beyond stage 47 due to the thickening epidermis preventing penetration of the X-gal substrate.

7.1.3 Transcription Factors Expressed In The Epicardium And/Or Proepicardium Of Xenopus

The transcription factors, WT1, epicardin and Tbx18, have been definitively shown to be expressed in the proepicardium and/or the epicardium of *Xenopus laevis*. WT1 was shown to be expressed in the proepicardium but was not seen in the developing epicardium itself or the septum transversum. Epicardin was shown to be expressed in both the proepicardium and the developing epicardium, but not the septum transversum. Finally Tbx18 was shown to be expressed in the developing epicardium and the septum transversum. Expression of epicardin in the proepicardium allowed the precise time of proepicardial outgrowth to be determined. The first expression of epicardin in the proepicardium was seen at stage 40.5. Expression of Tbx18 and epicardin confirmed that the proepicardium attaches at the convergence of the AV and CV canals, and also allowed visualisation of the epicardium as it migrated and covered the surface of the heart.

7.1.4 The Role Of The Epicardium In Xenopus Heart Development

MOs against WT1 and epicardin were shown to act specifically on their target genes. These MOs caused a phenotype in morphant tadpoles associated with malformations of the pronephros, a structure in which both of these genes are expressed. However, epicardium development was apparently unaffected in morphant tadpoles and no heart phenotypes were observed. It was concluded that epicardium formation is occurring too late in development to be accessible to study via MOs, and an alternative strategy should be sought.

7.2 Future Directions

7.2.1 Alternative Strategies For Perturbing Epicardium Development In Xenopus Species

A suitable alternative to MOs is transgenesis, a technique that is relatively easy to perform in *Xenopus*. Three genes have been shown to be expressed in the proepicardium and/or epicardium of *Xenopus laevis*. A regulatory element from WT1, epicardin or Tbx18 that drives tissue specific expression in the proepicardium and/or epicardium would be a powerful tool for functional studies of epicardium development. The regulatory element could be used to direct tissue specific perturbations of the epicardium and proepicardium. For example tBID, a member of the Bcl2 family of death agonist and antagonist proteins, has recently been used to induce tissue-specific cell death in *Xenopus laevis* (Du Pasquier et al., 2007). When transgenic tadpoles were generated that had tBID under the control of the promoter of the lens specific gene γcrystallin (Offield et al., 2000), complete absence of the lens was observed. No other tissues were affected. This technique could be used to induce tissue specific cell death of the epicardium or proepicardium which would allow thorough investigation of the role of the epicardium in development of the heart in *Xenopus laevis*.

Generating transgenic *Xenopus* embryos is a fairly simple procedure (Smith et al., 2006). Linear DNA containing the transgene is incubated with sperm nuclei that have had their membranes disrupted with detergent treatment. This results in random incorporation of the transgene into the male genome. The sperm nuclei are then injected into unfertilised eggs. The proportion of embryos that receive the transgene ranges from 10 to 40% of the total number of surviving embryos. These percentages are fairly small but many hundreds of eggs can be injected in a single morning so sufficient transgenic embryos can be generated.

One of the main problems with generating transgenic embryos in this manner is the random integration of the transgene into the male genome. This often results in multiple copy number integrations and every embryo having a unique site of integration, both of which can lead to variable transgene expression levels and

inconsistent phenotypes. A binary transgenic system can be used to avoid these problems. Here stable transgenic lines can be generated in which gene regulatory elements are separated from biological effectors in different frog lines using the binary Gal4-UAS system from yeast. The activator line carries the Gal4 transcription factor under the control of a tissue specific promoter. The effector line carries DNA-binding motifs for Gal4 (UAS) linked to the gene of interest. Crossing these lines results in the effector gene being transcribed in the spatiotemporal manner of the activator promoter. For example crossing a line that has the ubiquitous CMV promoter driving Gal4 with a line that has GFP downstream of UAS results in embryos that express GFP in every cell (Hartley et al., 2002). An activator line that has a proepicardium and/or epicardium specific promoter driving Gal4 could be crossed with a variety of effector lines carrying a variety of constructs such as GFP, dominant negative constructs, and the cell-death protein tBID.

Some preliminary experiments have been carried out to identify a proepicardium and/or epicardium specific promoter. *Xenopus tropicalis* Tbx18 and epicardin were identified on the JGI *Xenopus tropicalis* genome sequence. Various lengths of DNA upstream from the transcriptional start sight of Tbx18 and epicardin were PCR amplified from *Xenopus tropicalis* genomic DNA and cloned in front of GFP. Transgenic *Xenopus laevis* embryos were produced via sperm nuclear injection and analysed for promoter activity as seen by GFP fluorescence. However, 3.5Kb of sequence upstream of either Tbx18 or epicardin was insufficient to drive GFP expression in transgenic tadpoles. Longer upstream sequences of Tbx18 and epicardin could be tried together with WT1 promoter regions. A region of the mouse Serum Response Factor (SRF) gene between bases –322 and –1500 upstream of the translational start site has been shown to drive specific expression in the proepicardium but not the epicardium (Nelson et al., 2004). This region could also be tested in *Xenopus*.

Dominant negative and dominant active constructs could be used to analyse the function of candidate genes. Tbx18 would be a good candidate here because such constructs have previously been made for another T-box gene - Tbx5 (Rallis et al., 2003). Here 2 dominant-negative constructs of Tbx5 were made. The first was a truncated construct that contained only the N-terminus and T-domain. The second

was a construct that contained the N-terminus and T-domain fused to the transcriptional repressor domain of the *Drosophila* Engrailed protein, a region known to act as an active repressor (Jaynes and O'Farrell, 1991). *Drosophila* Engrailed fusion proteins have previously been shown to act as dominant-negative constructs in a range of tissues and organisms (Markel et al., 2002; Yu et al., 2001). Both of these dominant-negative constructs would be expected to compete with endogenous Tbx5 protein for DNA-binding sites upstream of Tbx5 target genes. The truncated construct would fail to activate expression of target genes, whilst the Engrailed-fusion protein would directly repress gene expression. Both dominant negative constructs showed equal efficacy at blocking endogenous Tbx5 gene function.

As a complementary strategy to dominant-negative forms of Tbx18, dominant-active constructs could also be made. Again this strategy has previously been employed in the case of Tbx5 (Rallis et al., 2003). Here the N-terminal region of Tbx5, including the DNA-binding T-domain, was fused to the transcriptional activation domain of the herpes simplex virus trans-inducing factor VP16 (Ohashi et al., 1994). This fusion construct would be expected to bind to the endogenous DNA-binding sites upstream of Tbx5 target genes and to activate their expression. The construct was found to effectively activate targets of Tbx5.

7.2.2 Alternative Methods Of Analysis

All morphant phenotypes in this thesis were analysed primarily in whole tadpoles and then in histological sections. Perhaps other methods of analysis would allow greater sensitivity in detecting subtle phenotypes. Confocal microscopy has successfully been used to construct extremely detailed images of *Xenopus* tadpole hearts up to and beyond stage 45 (Kolker et al., 2000). The benefits of this method of analysis were recently highlighted in the case of the cardiac specific homeobox-containing transcription factor Nkx2.10. In an early experiment it was concluded that over expression of Nkx2.10 in *Xenopus* does not result in an enlarged heart (Newman et al., 2000) such as is seen following over expression of the closely related genes Nkx2.3 and Nkx2.5 (Chen and Schwartz, 1996; Cleaver et al., 1996). In a recent study, over expression of Nkx2.10 again had no effect on the size of the heart,

however reduction of Nkx2.10 levels following injection of a MO resulted in a reduction of heart size (Allen et al., 2006). Using a confocal microscope and imaging software, the exact volumes of morphant and control hearts could be measured and any subtle differences analysed. As well as a reduction in heart size, several other defects were observed. A decrease in trabeculation, a failure of the atria to move to a more anterior position and rightward misplacement of the atrial septum were also observed in morphant embryos. Many of these phenotypes are sufficiently subtle to be overlooked in non-confocal microscopy based analyses.

The confocal analyses described above were carried out by incubating fixed tadpoles with a fluorescein isothiocyanate (FITC) conjugated pholloidin antibody and illuminating them on a confocal microscope with a FITC-GFP filter with an emission filter limit of 535 nm (Allen et al., 2006). Pholloidin is one of a group of toxins from the death cap fungus (*Amanita phalloides*). It binds to actin filaments and so stains all muscle fibres including the heart. This causes all muscle fibres to fluoresce and so can result in images with a lot of background. A more specific way to perform the analyses would be to use a transgenic line. For example the experiment could be performed in a tadpole that has GFP under the control of a proepicardium and/or epicardium specific regulatory element. Tadpoles could then be fixed and stained with an anti-GFP antibody conjugated to a suitable fluorophor and analysed with confocal microscopy. Only cells within the proepicardium and/or the epicardium would fluoresce and so there would be no background fluorescence.

8 References

Airik, R., Bussen, M., Singh, M. K., Petry, M., and Kispert, A. (2006). Tbx18 regulates the development of the ureteral mesenchyme. J Clin Invest *116*, 663-674.

Allen, B. G., Allen-Brady, K., and Weeks, D. L. (2006). Reduction of XNkx2-10 expression leads to anterior defects and malformation of the embryonic heart. Mech Dev *123*, 719-729.

Altschul, S. F., Gish, W., Miller, W., Myers, E. W., and Lipman, D. J. (1990). Basic local alignment search tool. J Mol Biol *215*, 403-410.

Ataliotis, P., Ivins, S., Mohun, T. J., and Scambler, P. J. (2005). XTbx1 is a transcriptional activator involved in head and pharyngeal arch development in Xenopus laevis. Dev Dyn *232*, 979-991.

Barbaux, S., Niaudet, P., Gubler, M. C., Grunfeld, J. P., Jaubert, F., Kuttenn, F., Fekete, C. N., Souleyreau-Therville, N., Thibaud, E., Fellous, M., and McElreavey, K. (1997). Donor splice-site mutations in WT1 are responsible for Frasier syndrome. Nat Genet *17*, 467-470.

Basson, C. T., Bachinsky, D. R., Lin, R. C., Levi, T., Elkins, J. A., Soults, J., Grayzel, D., Kroumpouzou, E., Traill, T. A., Leblanc-Straceski, J., *et al.* (1997). Mutations in human TBX5 [corrected] cause limb and cardiac malformation in Holt-Oram syndrome. Nat Genet *15*, 30-35.

Batlle, E., Sancho, E., Franci, C., Dominguez, D., Monfar, M., Baulida, J., and Garcia De Herreros, A. (2000). The transcription factor snail is a repressor of E-cadherin gene expression in epithelial tumour cells. Nat Cell Biol *2*, 84-89.

Begemann, G., Gibert, Y., Meyer, A., and Ingham, P. W. (2002). Cloning of zebrafish T-box genes tbx15 and tbx18 and their expression during embryonic development. Mech Dev *114*, 137-141.

Benjamin, L. E., Hemo, I., and Keshet, E. (1998). A plasticity window for blood vessel remodelling is defined by pericyte coverage of the preformed endothelial network and is regulated by PDGF-B and VEGF. Development *125*, 1591-1598.

Bisbee, C. A., Baker, M. A., Wilson, A. C., Haji-Azimi, I., and Fischberg, M. (1977). Albumin phylogeny for clawed frogs (Xenopus). Science *195*, 785-787.

Bogers, A. J., Gittenberger-de Groot, A. C., Poelmann, R. E., Peault, B. M., and Huysmans, H. A. (1989). Development of the origin of the coronary arteries, a matter of ingrowth or outgrowth? Anat Embryol (Berl) *180*, 437-441.

Bordzilovskaya, N. P., Detlaff, T. A., Duhon, S. T., and Malacinski, G. M. (1989). Developmental stage series of axolotl embryos. In: Armstrong JB, Malacinski GM (eds) Developmental biology of the axolotl. Oxford University Press, New York.

Brennan, J., Karl, J., and Capel, B. (2002). Divergent vascular mechanisms downstream of Sry establish the arterial system in the XY gonad. Dev Biol *244*, 418-428.

Breslow, N. E., and Beckwith, J. B. (1982). Epidemiological features of Wilms' tumor: results of the National Wilms' Tumor Study. J Natl Cancer Inst *68*, 429-436.

Bruick, R. K. (2000). Expression of the gene encoding the proapoptotic Nip3 protein is induced by hypoxia. Proc Natl Acad Sci U S A *97*, 9082-9087.

Bruneau, B. G., Logan, M., Davis, N., Levi, T., Tabin, C. J., Seidman, J. G., and Seidman, C. E. (1999). Chamber-specific cardiac expression of Tbx5 and heart defects in Holt-Oram syndrome. Dev Biol *211*, 100-108.

Bruneau, B. G., Nemer, G., Schmitt, J. P., Charron, F., Robitaille, L., Caron, S., Conner, D. A., Gessler, M., Nemer, M., Seidman, C. E., and Seidman, J. G. (2001). A murine model of Holt-Oram syndrome defines roles of the T-box transcription factor Tbx5 in cardiogenesis and disease. Cell *106*, 709-721.

Buckler, A. J., Pelletier, J., Haber, D. A., Glaser, T., and Housman, D. E. (1991). Isolation, characterization, and expression of the murine Wilms' tumor gene (WT1) during kidney development. Mol Cell Biol *11*, 1707-1712.

Bussen, M., Petry, M., Schuster-Gossler, K., Leitges, M., Gossler, A., and Kispert, A. (2004). The T-box transcription factor Tbx18 maintains the separation of anterior and posterior somite compartments. Genes Dev *18*, 1209-1221.

Cai, C. L., Zhou, W., Yang, L., Bu, L., Qyang, Y., Zhang, X., Li, X., Rosenfeld, M. G., Chen, J., and Evans, S. (2005). T-box genes coordinate regional rates of proliferation and regional specification during cardiogenesis. Development *132*, 2475-2487.

Cano, A., Perez-Moreno, M. A., Rodrigo, I., Locascio, A., Blanco, M. J., del Barrio, M. G., Portillo, F., and Nieto, M. A. (2000). The transcription factor snail controls epithelial-mesenchymal transitions by repressing E-cadherin expression. Nat Cell Biol *2*, 76-83.

Carmona, R., Gonzalez-Iriarte, M., Macias, D., Perez-Pomares, J. M., Garcia-Garrido, L., and Munoz-Chapuli, R. (2000). Immunolocalization of the transcription factor Slug in the developing avian heart. Anat Embryol (Berl) *201*, 103-109.

Carmona, R., Gonzalez-Iriarte, M., Perez-Pomares, J. M., and Munoz-Chapuli, R. (2001). Localization of the Wilm's tumour protein WT1 in avian embryos. Cell Tissue Res *303*, 173-186.

Carroll, T. J., and Vize, P. D. (1996). Wilms' tumor suppressor gene is involved in the development of disparate kidney forms: evidence from expression in the Xenopus pronephros. Dev Dyn *206*, 131-138.

Chambers, A. E., Logan, M., Kotecha, S., Towers, N., Sparrow, D., and Mohun, T. J. (1994). The RSRF/MEF2 protein SL1 regulates cardiac muscle-specific transcription of a myosin light-chain gene in Xenopus embryos. Genes Dev *8*, 1324-1334.

Chen, C. Y., and Schwartz, R. J. (1996). Recruitment of the tinman homolog Nkx-2.5 by serum response factor activates cardiac alpha-actin gene transcription. Mol Cell Biol *16*, 6372-6384.

Chen, J., Kubalak, S. W., and Chien, K. R. (1998). Ventricular muscle-restricted targeting of the RXRalpha gene reveals a non-cell-autonomous requirement in cardiac chamber morphogenesis. Development *125*, 1943-1949.

Cheng, G., Wessels, A., Gourdie, R. G., and Thompson, R. P. (2002). Spatiotemporal and tissue specific distribution of apoptosis in the developing chick heart. Dev Dyn *223*, 119-133.

Choi, Y. S., and Gumbiner, B. (1989). Expression of cell adhesion molecule E-cadherin in Xenopus embryos begins at gastrulation and predominates in the ectoderm. J Cell Biol *108*, 2449-2458.

Christoffels, V. M., Mommersteeg, M. T., Trowe, M. O., Prall, O. W., de Gier-de Vries, C., Soufan, A. T., Bussen, M., Schuster-Gossler, K., Harvey, R. P., Moorman, A. F., and Kispert, A. (2006). Formation of the venous pole of the heart from an Nkx2-5-negative precursor population requires Tbx18. Circ Res *98*, 1555-1563.

Cleaver, O. B., Patterson, K. D., and Krieg, P. A. (1996). Overexpression of the tinman-related genes XNkx-2.5 and XNkx-2.3 in Xenopus embryos results in myocardial hyperplasia. Development *122*, 3549-3556.

Colvin, J. S., White, A. C., Pratt, S. J., and Ornitz, D. M. (2001). Lung hypoplasia and neonatal death in Fgf9-null mice identify this gene as an essential regulator of lung mesenchyme. Development *128*, 2095-2106.

Compton, L. A., Potash, D. A., Mundell, N. A., and Barnett, J. V. (2006). Transforming growth factor-beta induces loss of epithelial character and smooth muscle cell differentiation in epicardial cells. Dev Dyn *235*, 82-93.

Cremer, H., Chazal, G., Goridis, C., and Represa, A. (1997). NCAM is essential for axonal growth and fasciculation in the hippocampus. Mol Cell Neurosci *8*, 323-335.

Cui, S., Ross, A., Stallings, N., Parker, K. L., Capel, B., and Quaggin, S. E. (2004). Disrupted gonadogenesis and male-to-female sex reversal in Pod1 knockout mice. Development *131*, 4095-4105.

Davies, J. A., Ladomery, M., Hohenstein, P., Michael, L., Shafe, A., Spraggon, L., and Hastie, N. (2004). Development of an siRNA-based method for repressing specific genes in renal organ culture and its use to show that the Wt1 tumour suppressor is required for nephron differentiation. Hum Mol Genet *13*, 235-246.

De Haan, R. L. (1965). Morphogenesis of the vertebrate heart. In: Organogenesis, eds R.L.De Haan and H. Ursprung. New York: Holt Rinehart and Winston. .

de Lange, F. J., Moorman, A. F., Anderson, R. H., Manner, J., Soufan, A. T., de Gier-de Vries, C., Schneider, M. D., Webb, S., van den Hoff, M. J., and Christoffels, V. M. (2004). Lineage and morphogenetic analysis of the cardiac valves. Circ Res *95*, 645-654.

Delong, K. T. (1962). Quantitative analysis of blood circulation through the frog heart. Science *138*, 693-694.

DeRuiter, M. C., Poelmann, R. E., VanderPlas-de Vries, I., Mentink, M. M., and Gittenberger-de Groot, A. C. (1992). The development of the myocardium and endocardium in mouse embryos. Fusion of two heart tubes? Anat Embryol (Berl) *185*, 461-473.

Dettman, R. W., Denetclaw, W., Jr., Ordahl, C. P., and Bristow, J. (1998). Common epicardial origin of coronary vascular smooth muscle, perivascular fibroblasts, and intermyocardial fibroblasts in the avian heart. Dev Biol *193*, 169-181.

Draper, B. W., Morcos, P. A., and Kimmel, C. B. (2001). Inhibition of zebrafish fgf8 pre-mRNA splicing with morpholino oligos: a quantifiable method for gene knockdown. Genesis *30*, 154-156.

Dressler, G. R., and Douglass, E. C. (1992). Pax-2 is a DNA-binding protein expressed in embryonic kidney and Wilms tumor. Proc Natl Acad Sci U S A *89*, 1179-1183.

Du Pasquier, D., Chesneau, A., Ymlahi-Ouazzani, Q., Boistel, R., Pollet, N., Ballagny, C., Sachs, L. M., Demeneix, B., and Mazabraud, A. (2007). tBid mediated activation of the mitochondrial death pathway leads to genetic ablation of the lens in Xenopus laevis. Genesis *45*, 1-10.

Eid, H., Larson, D. M., Springhorn, J. P., Attawia, M. A., Nayak, R. C., Smith, T. W., and Kelly, R. A. (1992). Role of epicardial mesothelial cells in the modification of phenotype and function of adult rat ventricular myocytes in primary coculture. Circ Res *71*, 40-50.

Eralp, I., Lie-Venema, H., Bax, N. A., Wijffels, M. C., Van Der Laarse, A., Deruiter, M. C., Bogers, A. J., Van Den Akker, N. M., Gourdie, R. G., Schalij, M. J., *et al.* (2006). Epicardium-derived cells are important for correct development of the Purkinje fibers in the avian heart. Anat Rec A Discov Mol Cell Evol Biol *288*, 1272-1280.

Eralp, I., Lie-Venema, H., DeRuiter, M. C., van den Akker, N. M., Bogers, A. J., Mentink, M. M., Poelmann, R. E., and Gittenberger-de Groot, A. C. (2005). Coronary artery and orifice development is associated with proper timing of epicardial outgrowth and correlated Fas-ligand-associated apoptosis patterns. Circ Res *96*, 526-534.

Folkman, J., and D'Amore, P. A. (1996). Blood vessel formation: what is its molecular basis? Cell *87*, 1153-1155.

Forsythe, J. A., Jiang, B. H., Iyer, N. V., Agani, F., Leung, S. W., Koos, R. D., and Semenza, G. L. (1996). Activation of vascular endothelial growth factor gene transcription by hypoxia-inducible factor 1. Mol Cell Biol *16*, 4604-4613.

Fransen, M. E., and Lemanski, L. F. (1989). Studies of heart development in normal and cardiac lethal mutant axolotls: a review. Scanning Microsc *3*, 1101-1115; discussion 1115-1106.

Fransen, M. E., and Lemanski, L. F. (1990). Epicardial development in the axolotl, Ambystoma mexicanum. Anat Rec *226*, 228-236.

Fransen, M. E., and Lemanski, L. F. (1991). Extracellular matrix of the developing heart in normal and cardiac lethal mutant axolotls, Ambystoma mexicanum. Anat Rec *230*, 387-405.

George, E. L., Georges-Labouesse, E. N., Patel-King, R. S., Rayburn, H., and Hynes, R. O. (1993). Defects in mesoderm, neural tube and vascular development in mouse embryos lacking fibronectin. Development *119*, 1079-1091.

Gerth, V. E., Zhou, X., and Vize, P. D. (2005). Nephrin expression and three-dimensional morphogenesis of the Xenopus pronephric glomus. Dev Dyn *233*, 1131-1139.

Gittenberger-de Groot, A. C., Blom, N. M., Aoyama, N., Sucov, H., Wenink, A. C., and Poelmann, R. E. (2003). The role of neural crest and epicardium-derived cells in conduction system formation. Novartis Found Symp *250*, 125-134; discussion 134-141, 276-129.

Gittenberger-de Groot, A. C., Vrancken Peeters, M. P., Bergwerff, M., Mentink, M. M., and Poelmann, R. E. (2000). Epicardial outgrowth inhibition leads to compensatory mesothelial outflow tract collar and abnormal cardiac septation and coronary formation. Circ Res *87*, 969-971.

Gittenberger-de Groot, A. C., Vrancken Peeters, M. P., Mentink, M. M., Gourdie, R. G., and Poelmann, R. E. (1998). Epicardium-derived cells contribute a novel population to the myocardial wall and the atrioventricular cushions. Circ Res *82*, 1043-1052.

Gonzalez-Sanchez, A., and Bader, D. (1990). In vitro analysis of cardiac progenitor cell differentiation. Dev Biol *139*, 197-209.

Gormley, J. P., and Nascone-Yoder, N. M. (2003). Left and right contributions to the Xenopus heart: implications for asymmetric morphogenesis. Dev Genes Evol *213*, 390-398.

Gourdie, R. G., Harris, B. S., Bond, J., Justus, C., Hewett, K. W., O'Brien, T. X., Thompson, R. P., and Sedmera, D. (2003). Development of the cardiac pacemaking and conduction system. Birth Defects Res C Embryo Today *69*, 46-57.

Gourdie, R. G., Mima, T., Thompson, R. P., and Mikawa, T. (1995). Terminal diversification of the myocyte lineage generates Purkinje fibers of the cardiac conduction system. Development *121*, 1423-1431.

Grau, Y., Carteret, C., and Simpson, P. (1984). Mutations and Chromosomal Rearrangements Affecting the Expression of Snail, a Gene Involved in Embryonic Patterning in DROSOPHILA MELANOGASTER. Genetics *108*, 347-360.

Guo, J. K., Menke, A. L., Gubler, M. C., Clarke, A. R., Harrison, D., Hammes, A., Hastie, N. D., and Schedl, A. (2002). WT1 is a key regulator of podocyte function: reduced expression levels cause crescentic glomerulonephritis and mesangial sclerosis. Hum Mol Genet *11*, 651-659.

Haberich, F. J. (1965). The functional separation of venous and arterial blood in the univentricular frog heart. Ann N Y Acad Sci *127*, 459-476.

Haenig, B., and Kispert, A. (2004). Analysis of TBX18 expression in chick embryos. Dev Genes Evol *214*, 407-411.

Hall, C. E., Hurtado, R., Hewett, K. W., Shulimovich, M., Poma, C. P., Reckova, M., Justus, C., Pennisi, D. J., Tobita, K., Sedmera, D., *et al.* (2004). Hemodynamic-dependent patterning of endothelin converting enzyme 1 expression and differentiation of impulse-conducting Purkinje fibers in the embryonic heart. Development *131*, 581-592.

Hamburger, V., and Hamilton, H. L. (1992). A series of normal stages in the development of the chick embryo. 1951. Dev Dyn *195*, 231-272.

Harrelson, Z., Kelly, R. G., Goldin, S. N., Gibson-Brown, J. J., Bollag, R. J., Silver, L. M., and Papaioannou, V. E. (2004). Tbx2 is essential for patterning the atrioventricular canal and for morphogenesis of the outflow tract during heart development. Development *131*, 5041-5052.

Hartley, K. O., Nutt, S. L., and Amaya, E. (2002). Targeted gene expression in transgenic Xenopus using the binary Gal4-UAS system. Proc Natl Acad Sci U S A *99*, 1377-1382.

Hastie, N. D. (1992). Dominant negative mutations in the Wilms tumour (WT1) gene cause Denys-Drash syndrome--proof that a tumour-suppressor gene plays a crucial role in normal genitourinary development. Hum Mol Genet *1*, 293-295.

Hatcher, C. J., Goldstein, M. M., Mah, C. S., Delia, C. S., and Basson, C. T. (2000). Identification and localization of TBX5 transcription factor during human cardiac morphogenesis. Dev Dyn *219*, 90-95.

Hay, E. D. (1995). An overview of epithelio-mesenchymal transformation. Acta Anat (Basel) *154*, 8-20.

Heasman, J. (2002). Morpholino oligos: making sense of antisense? Dev Biol *243*, 209-214.

Hidai, H., Bardales, R., Goodwin, R., Quertermous, T., and Quertermous, E. E. (1998). Cloning of capsulin, a basic helix-loop-helix factor expressed in progenitor cells of the pericardium and the coronary arteries. Mech Dev *73*, 33-43.

Hirsch, N., Zimmerman, L. B., and Grainger, R. M. (2002). Xenopus, the next generation: X. tropicalis genetics and genomics. Dev Dyn *225*, 422-433.

Hiruma, T., and Hirakow, R. (1989). Epicardial formation in embryonic chick heart: computer-aided reconstruction, scanning, and transmission electron microscopic studies. Am J Anat *184*, 129-138.

Ho, E., and Shimada, Y. (1978). Formation of the epicardium studied with the scanning electron microscope. Dev Biol *66*, 579-585.

Horb, M. E., and Thomsen, G. H. (1999). Tbx5 is essential for heart development. Development *126*, 1739-1751.

Howland, R. B. (1916). On the Effect of Removal of the Pronephros of the Amphibian Embryo. Proc Natl Acad Sci U S A *2*, 231-234.

Hu, N., Connuck, D. M., Keller, B. B., and Clark, E. B. (1991). Diastolic filling characteristics in the stage 12 to 27 chick embryo ventricle. Pediatr Res *29*, 334-337.

Hu, N., Sedmera, D., Yost, H. J., and Clark, E. B. (2000). Structure and function of the developing zebrafish heart. Anat Rec *260*, 148-157.

Hu, N., Yost, H. J., and Clark, E. B. (2001). Cardiac morphology and blood pressure in the adult zebrafish. Anat Rec *264*, 1-12.

Huang, A., Campbell, C. E., Bonetta, L., McAndrews-Hill, M. S., Chilton-MacNeill, S., Coppes, M. J., Law, D. J., Feinberg, A. P., Yeger, H., and Williams, B. R. (1990). Tissue, developmental, and tumor-specific expression of divergent transcripts in Wilms tumor. Science *250*, 991-994.

Hyer, J., Johansen, M., Prasad, A., Wessels, A., Kirby, M. L., Gourdie, R. G., and Mikawa, T. (1999). Induction of Purkinje fiber differentiation by coronary arterialization. Proc Natl Acad Sci U S A *96*, 13214-13218.

Jan, Y. N., and Jan, L. Y. (1993). HLH proteins, fly neurogenesis, and vertebrate myogenesis. Cell *75*, 827-830.

Jaynes, J. B., and O'Farrell, P. H. (1991). Active repression of transcription by the engrailed homeodomain protein. Embo J *10*, 1427-1433.

Jerome, L. A., and Papaioannou, V. E. (2001). DiGeorge syndrome phenotype in mice mutant for the T-box gene, Tbx1. Nat Genet *27*, 286-291.

Johansen, K. (1965). Cardiovascular dynamics in fishes, amphibians, and reptiles. Ann N Y Acad Sci *127*, 414-442.

Kadesch, T. (1993). Consequences of heteromeric interactions among helix-loop-helix proteins. Cell Growth Differ *4*, 49-55.

Kalman, F., Viragh, S., and Modis, L. (1995). Cell surface glycoconjugates and the extracellular matrix of the developing mouse embryo epicardium. Anat Embryol (Berl) *191*, 451-464.

Kastner, P., Grondona, J. M., Mark, M., Gansmuller, A., LeMeur, M., Decimo, D., Vonesch, J. L., Dolle, P., and Chambon, P. (1994). Genetic analysis of RXR alpha developmental function: convergence of RXR and RAR signaling pathways in heart and eye morphogenesis. Cell *78*, 987-1003.

Kaufman, M. H., and Navaratnam, V. (1981). Early differentiation of the heart in mouse embryos. J Anat *133*, 235-246.

Kelly, R. G., Brown, N. A., and Buckingham, M. E. (2001). The arterial pole of the mouse heart forms from Fgf10-expressing cells in pharyngeal mesoderm. Dev Cell *1*, 435-440.

Kirby, M. L., Gale, T. F., and Stewart, D. E. (1983). Neural crest cells contribute to normal aorticopulmonary septation. Science *220*, 1059-1061.

Kirby, M. L., and Waldo, K. L. (1990). Role of neural crest in congenital heart disease. Circulation *82*, 332-340.

Kirby, M. L., and Waldo, K. L. (1995). Neural crest and cardiovascular patterning. Circ Res *77*, 211-215.

Kirschner, K. M., Wagner, N., Wagner, K. D., Wellmann, S., and Scholz, H. (2006). The Wilms tumor suppressor Wt1 promotes cell adhesion through transcriptional activation of the alpha4integrin gene. J Biol Chem *281*, 31930-31939.

Kispert, A., and Hermann, B. G. (1993). The Brachyury gene encodes a novel DNA binding protein. Embo J *12*, 4898-4899.

Kispert, A., Koschorz, B., and Herrmann, B. G. (1995). The T protein encoded by Brachyury is a tissue-specific transcription factor. Embo J *14*, 4763-4772.

Klein, S. L., Strausberg, R. L., Wagner, L., Pontius, J., Clifton, S. W., and Richardson, P. (2002). Genetic and genomic tools for Xenopus research: The NIH Xenopus initiative. Dev Dyn *225*, 384-391.

Klymkowsky, M. W., Maynell, L. A., and Polson, A. G. (1987). Polar asymmetry in the organization of the cortical cytokeratin system of Xenopus laevis oocytes and embryos. Development *100*, 543-557.

Kolker, S. J., Tajchman, U., and Weeks, D. L. (2000). Confocal imaging of early heart development in Xenopus laevis. Dev Biol *218*, 64-73.

Komiyama, M., Ito, K., and Shimada, Y. (1987). Origin and development of the epicardium in the mouse embryo. Anat Embryol (Berl) *176*, 183-189.

Kraus, F., Haenig, B., and Kispert, A. (2001). Cloning and expression analysis of the mouse T-box gene Tbx18. Mech Dev *100*, 83-86.

Kreidberg, J. A., Sariola, H., Loring, J. M., Maeda, M., Pelletier, J., Housman, D., and Jaenisch, R. (1993). WT-1 is required for early kidney development. Cell *74*, 679-691.

Kroll, K. L., and Amaya, E. (1996). Transgenic Xenopus embryos from sperm nuclear transplantations reveal FGF signaling requirements during gastrulation. Development *122*, 3173-3183.

Kwee, L., Baldwin, H. S., Shen, H. M., Stewart, C. L., Buck, C., Buck, C. A., and Labow, M. A. (1995). Defective development of the embryonic and extraembryonic circulatory systems in vascular cell adhesion molecule (VCAM-1) deficient mice. Development *121*, 489-503.

Lackie, P. M., Zuber, C., and Roth, J. (1991). Expression of polysialylated N-CAM during rat heart development. Differentiation *47*, 85-98.

Lagercrantz, J., Farnebo, F., Larsson, C., Tvrdik, T., Weber, G., and Piehl, F. (1998). A comparative study of the expression patterns for vegf, vegf-b/vrf and vegf-c in the developing and adult mouse. Biochim Biophys Acta *1398*, 157-163.

Lane, M. C., and Sheets, M. D. (2006). Heading in a new direction: implications of the revised fate map for understanding Xenopus laevis development. Dev Biol *296*, 12-28.

Lavine, K. J., Yu, K., White, A. C., Zhang, X., Smith, C., Partanen, J., and Ornitz, D. M. (2005). Endocardial and epicardial derived FGF signals regulate myocardial proliferation and differentiation in vivo. Dev Cell *8*, 85-95.

Lee, J. M., Dedhar, S., Kalluri, R., and Thompson, E. W. (2006). The epithelial-mesenchymal transition: new insights in signaling, development, and disease. J Cell Biol *172*, 973-981.

Lenkkeri, U., Mannikko, M., McCready, P., Lamerdin, J., Gribouval, O., Niaudet, P. M., Antignac, C. K., Kashtan, C. E., Homberg, C., Olsen, A., *et al.* (1999). Structure of the gene for congenital nephrotic syndrome of the finnish type (NPHS1) and characterization of mutations. Am J Hum Genet *64*, 51-61.

Lepilina, A., Coon, A. N., Kikuchi, K., Holdway, J. E., Roberts, R. W., Burns, C. G., and Poss, K. D. (2006). A dynamic epicardial injury response supports progenitor cell activity during zebrafish heart regeneration. Cell *127*, 607-619.

Li, Q. Y., Newbury-Ecob, R. A., Terrett, J. A., Wilson, D. I., Curtis, A. R., Yi, C. H., Gebuhr, T., Bullen, P. J., Robson, S. C., Strachan, T., *et al.* (1997). Holt-Oram syndrome is caused by mutations in TBX5, a member of the Brachyury (T) gene family. Nat Genet *15*, 21-29.

Lie-Venema, H., Gittenberger-de Groot, A. C., van Empel, L. J., Boot, M. J., Kerkdijk, H., de Kant, E., and DeRuiter, M. C. (2003). Ets-1 and Ets-2 transcription factors are essential for normal coronary and myocardial development in chicken embryos. Circ Res *92*, 749-756.

Lobb, R. R., Antognetti, G., Pepinsky, R. B., Burkly, L. C., Leone, D. R., and Whitty, A. (1995). A direct binding assay for the vascular cell adhesion molecule-1 (VCAM1) interaction with alpha 4 integrins. Cell Adhes Commun *3*, 385-397.

Lu, J., Chang, P., Richardson, J. A., Gan, L., Weiler, H., and Olson, E. N. (2000). The basic helix-loop-helix transcription factor capsulin controls spleen organogenesis. Proc Natl Acad Sci U S A *97*, 9525-9530.

Lu, J., Richardson, J. A., and Olson, E. N. (1998). Capsulin: a novel bHLH transcription factor expressed in epicardial progenitors and mesenchyme of visceral organs. Mech Dev *73*, 23-32.

Lu, J. R., McKinsey, T. A., Xu, H., Wang, D. Z., Richardson, J. A., and Olson, E. N. (1999). FOG-2, a heart- and brain-enriched cofactor for GATA transcription factors. Mol Cell Biol *19*, 4495-4502.

Macias, D., Perez-Pomares, J. M., Garcia-Garrido, L., Carmona, R., and Munoz-Chapuli, R. (1998). Immunoreactivity of the ets-1 transcription factor correlates with areas of epithelial-mesenchymal transition in the developing avian heart. Anat Embryol (Berl) *198*, 307-315.

Manner, J. (1992). The development of pericardial villi in the chick embryo. Anat Embryol (Berl) *186*, 379-385.

Manner, J. (1993). Experimental study on the formation of the epicardium in chick embryos. Anat Embryol (Berl) *187*, 281-289.

Manner, J. (1999). Does the subepicardial mesenchyme contribute myocardioblasts to the myocardium of the chick embryo heart? A quail-chick chimera study tracing the fate of the epicardial primordium. Anat Rec *255*, 212-226.

Manner, J., Schlueter, J., and Brand, T. (2005). Experimental analyses of the function of the proepicardium using a new microsurgical procedure to induce loss-of-proepicardial-function in chick embryos. Dev Dyn *233*, 1454-1463.

Markel, H., Chandler, J., and Werr, W. (2002). Translational fusions with the engrailed repressor domain efficiently convert plant transcription factors into dominant-negative functions. Nucleic Acids Res *30*, 4709-4719.

Markwald, R., Eisenberg, C., Eisenberg, L., Trusk, T., and Sugi, Y. (1996). Epithelial-mesenchymal transformations in early avian heart development. Acta Anat (Basel) *156*, 173-186.

Mic, F. A., Haselbeck, R. J., Cuenca, A. E., and Duester, G. (2002). Novel retinoic acid generating activities in the neural tube and heart identified by conditional rescue of Raldh2 null mutant mice. Development *129*, 2271-2282.

Minguillon, C., Del Buono, J., and Logan, M. P. (2005). Tbx5 and Tbx4 are not sufficient to determine limb-specific morphologies but have common roles in initiating limb outgrowth. Dev Cell *8*, 75-84.

Mjaatvedt, C. H., Nakaoka, T., Moreno-Rodriguez, R., Norris, R. A., Kern, M. J., Eisenberg, C. A., Turner, D., and Markwald, R. R. (2001). The outflow tract of the heart is recruited from a novel heart-forming field. Dev Biol *238*, 97-109.

Mohun, T., and Sparrow, D. (1997). Early steps in vertebrate cardiogenesis. Curr Opin Genet Dev *7*, 628-633.

Mohun, T. J., Leong, L. M., Weninger, W. J., and Sparrow, D. B. (2000). The morphology of heart development in Xenopus laevis. Dev Biol *218*, 74-88.

Molkentin, J. D. (2000). The zinc finger-containing transcription factors GATA-4, -5, and -6. Ubiquitously expressed regulators of tissue-specific gene expression. J Biol Chem *275*, 38949-38952.

Moody, S. A. (1987). Fates of the blastomeres of the 16-cell stage Xenopus embryo. Dev Biol *119*, 560-578.

Moore, A. W., McInnes, L., Kreidberg, J., Hastie, N. D., and Schedl, A. (1999). YAC complementation shows a requirement for Wt1 in the development of epicardium, adrenal gland and throughout nephrogenesis. Development *126*, 1845-1857.

Morabito, C. J., Dettman, R. W., Kattan, J., Collier, J. M., and Bristow, J. (2001). Positive and negative regulation of epicardial-mesenchymal transformation during avian heart development. Dev Biol *234*, 204-215.

Moss, J. B., Xavier-Neto, J., Shapiro, M. D., Nayeem, S. M., McCaffery, P., Drager, U. C., and Rosenthal, N. (1998). Dynamic patterns of retinoic acid synthesis and response in the developing mammalian heart. Dev Biol *199*, 55-71.

Munoz-Chapuli, R., Gallego, A., and Perez-Pomares, J. M. (1997). A Reaction-Diffusion Model can Account for the Anatomical Pattern of the Cardiac Conal Valves in Fish. J Theor Biol *185*, 233-240.

Munoz-Chapuli, R., Macias, D., Gonzalez-Iriarte, M., Carmona, R., Atencia, G., and Perez-Pomares, J. M. (2002). [The epicardium and epicardial-derived cells: multiple functions in cardiac development.]. Rev Esp Cardiol *55*, 1070-1082.

Muñoz-Chápuli, R., Macías, D., Ramos, C., Gallego, A., and De Andrés, V. (1996). Development of the subepicardial mesenchyme and the early cardiac vessels in the dogfish (Scyliorhinus canicula).

Murre, C., McCaw, P. S., Vaessin, H., Caudy, M., Jan, L. Y., Jan, Y. N., Cabrera, C. V., Buskin, J. N., Hauschka, S. D., Lassar, A. B., and et al. (1989). Interactions between heterologous helix-loop-helix proteins generate complexes that bind specifically to a common DNA sequence. Cell *58*, 537-544.

Nahirney, P. C., Mikawa, T., and Fischman, D. A. (2003). Evidence for an extracellular matrix bridge guiding proepicardial cell migration to the myocardium of chick embryos. Dev Dyn *227*, 511-523.

Nakajima, Y., Yamagishi, T., Hokari, S., and Nakamura, H. (2000). Mechanisms involved in valvuloseptal endocardial cushion formation in early cardiogenesis: roles of transforming growth factor (TGF)-beta and bone morphogenetic protein (BMP). Anat Rec *258*, 119-127.

Nelson, T. J., Duncan, S. A., and Misra, R. P. (2004). Conserved enhancer in the serum response factor promoter controls expression during early coronary vasculogenesis. Circ Res *94*, 1059-1066.

Newman, C. S., Chia, F., and Krieg, P. A. (1997). The XHex homeobox gene is expressed during development of the vascular endothelium: overexpression leads to an increase in vascular endothelial cell number. Mech Dev *66*, 83-93.

Newman, C. S., Reecy, J., Grow, M. W., Ni, K., Boettger, T., Kessel, M., Schwartz, R. J., and Krieg, P. A. (2000). Transient cardiac expression of the tinman-family homeobox gene, XNkx2-10. Mech Dev *91*, 369-373.

Nicola, S., Risebro, C. A., Melville, A. A., Moses, K., Schwartz, R. J., Chien, K. R., and Riley, P. R. (2007). Thymosin {beta}4 is essential for coronary vessel development and promotes neovascularisation via adult epicardium. Ann N Y Acad Sci.

Nieto, M. A., Bennett, M. F., Sargent, M. G., and Wilkinson, D. G. (1992). Cloning and developmental expression of Sna, a murine homologue of the Drosophila snail gene. Development *116*, 227-237.

Nieto, M. A., Sargent, M. G., Wilkinson, D. G., and Cooke, J. (1994). Control of cell behavior during vertebrate development by Slug, a zinc finger gene. Science *264*, 835-839.

Nieuwkoop, P. D. (1996). What are the key advantages and disadvantages of urodele species compared to anurans as a model system for experimental analysis of early development? Int J Dev Biol *40*, 617-619.

Nieuwkoop, P. D., and Faber, J. (1994). Normal Table of Xenopus laevis (Daudin).

Nutt, S. L., Bronchain, O. J., Hartley, K. O., and Amaya, E. (2001). Comparison of morpholino based translational inhibition during the development of Xenopus laevis and Xenopus tropicalis. Genesis *30*, 110-113.

Offield, M. F., Hirsch, N., and Grainger, R. M. (2000). The development of Xenopus tropicalis transgenic lines and their use in studying lens developmental timing in living embryos. Development *127*, 1789-1797.

Ohashi, Y., Brickman, J. M., Furman, E., Middleton, B., and Carey, M. (1994). Modulating the potency of an activator in a yeast in vitro transcription system. Mol Cell Biol *14*, 2731-2739.

Olivey, H. E., Mundell, N. A., Austin, A. F., and Barnett, J. V. (2006). Transforming growth factor-beta stimulates epithelial-mesenchymal transformation in the proepicardium. Dev Dyn *235*, 50-59.

Ornitz, D. M., Xu, J., Colvin, J. S., McEwen, D. G., MacArthur, C. A., Coulier, F., Gao, G., and Goldfarb, M. (1996). Receptor specificity of the fibroblast growth factor family. J Biol Chem *271*, 15292-15297.

Papaioannou, V. E. (2001). T-box genes in development: from hydra to humans. Int Rev Cytol *207*, 1-70.

Pelletier, J., Bruening, W., Li, F. P., Haber, D. A., Glaser, T., and Housman, D. E. (1991). WT1 mutations contribute to abnormal genital system development and hereditary Wilms' tumour. Nature *353*, 431-434.

Perez-Pomares, J. M., Carmona, R., Gonzalez-Iriarte, M., Atencia, G., Wessels, A., and Munoz-Chapuli, R. (2002a). Origin of coronary endothelial cells from epicardial mesothelium in avian embryos. Int J Dev Biol *46*, 1005-1013.

Perez-Pomares, J. M., Macias, D., Garcia-Garrido, L., and Munoz-Chapuli, R. (1997). Contribution of the primitive epicardium to the subepicardial mesenchyme in hamster and chick embryos. Dev Dyn *210*, 96-105.

Perez-Pomares, J. M., Macias, D., Garcia-Garrido, L., and Munoz-Chapuli, R. (1998a). Immunolocalization of the vascular endothelial growth factor receptor-2 in the subepicardial mesenchyme of hamster embryos: identification of the coronary vessel precursors. Histochem J *30*, 627-634.

Perez-Pomares, J. M., Macias, D., Garcia-Garrido, L., and Munoz-Chapuli, R. (1998b). The origin of the subepicardial mesenchyme in the avian embryo: an immunohistochemical and quail-chick chimera study. Dev Biol *200*, 57-68.

Perez-Pomares, J. M., Phelps, A., Sedmerova, M., Carmona, R., Gonzalez-Iriarte, M., Munoz-Chapuli, R., and Wessels, A. (2002b). Experimental studies on the spatiotemporal expression of WT1 and RALDH2 in the embryonic avian heart: a model for the regulation of myocardial and valvuloseptal development by epicardially derived cells (EPDCs). Dev Biol *247*, 307-326.

Perez-Pomares, J. M., Phelps, A., Sedmerova, M., and Wessels, A. (2003). Epicardial-like cells on the distal arterial end of the cardiac outflow tract do not derive from the proepicardium but are derivatives of the cephalic pericardium. Dev Dyn *227*, 56-68.

Pinco, K. A., Liu, S., and Yang, J. T. (2001). alpha4 integrin is expressed in a subset of cranial neural crest cells and in epicardial progenitor cells during early mouse development. Mech Dev *100*, 99-103.

Poelmann, R. E., Gittenberger-de Groot, A. C., Mentink, M. M., Bokenkamp, R., and Hogers, B. (1993). Development of the cardiac coronary vascular endothelium, studied with antiendothelial antibodies, in chicken-quail chimeras. Circ Res *73*, 559-568.

Poelmann, R. E., Lie-Venema, H., and Gittenberger-de Groot, A. C. (2002). The role of the epicardium and neural crest as extracardiac contributors to coronary vascular development. Tex Heart Inst J *29*, 255-261.

Poss, K. D., Wilson, L. G., and Keating, M. T. (2002). Heart regeneration in zebrafish. Science *298*, 2188-2190.

Quaggin, S. E., Schwartz, L., Cui, S., Igarashi, P., Deimling, J., Post, M., and Rossant, J. (1999). The basic-helix-loop-helix protein pod1 is critically important for kidney and lung organogenesis. Development *126*, 5771-5783.

Rallis, C., Bruneau, B. G., Del Buono, J., Seidman, C. E., Seidman, J. G., Nissim, S., Tabin, C. J., and Logan, M. P. (2003). Tbx5 is required for forelimb bud formation and continued outgrowth. Development *130*, 2741-2751.

Ramsdell, A. F., Bernanke, J. M., and Trusk, T. C. (2006). Left-right lineage analysis of the embryonic Xenopus heart reveals a novel framework linking congenital cardiac defects and laterality disease. Development *133*, 1399-1410.

Rangarajan, J., Luo, T., and Sargent, T. D. (2006). PCNS: a novel protocadherin required for cranial neural crest migration and somite morphogenesis in Xenopus. Dev Biol *295*, 206-218.

Reckova, M., Rosengarten, C., deAlmeida, A., Stanley, C. P., Wessels, A., Gourdie, R. G., Thompson, R. P., and Sedmera, D. (2003). Hemodynamics is a key epigenetic factor in development of the cardiac conduction system. Circ Res *93*, 77-85.

Robu, M. E., Larson, J. D., Nasevicius, A., Beiraghi, S., Brenner, C., Farber, S. A., and Ekker, S. C. (2007). p53 activation by knockdown technologies. PLoS Genet *3*, e78.

Romano, L. A., and Runyan, R. B. (1999). Slug is a mediator of epithelial-mesenchymal cell transformation in the developing chicken heart. Dev Biol *212*, 243-254.

Romano, L. A., and Runyan, R. B. (2000). Slug is an essential target of TGFbeta2 signaling in the developing chicken heart. Dev Biol *223*, 91-102.

Rose, E. A., Glaser, T., Jones, C., Smith, C. L., Lewis, W. H., Call, K. M., Minden, M., Champagne, E., Bonetta, L., Yeger, H., and et al. (1990). Complete physical map of the WAGR region of 11p13 localizes a candidate Wilms' tumor gene. Cell *60*, 495-508.

Rothenberg, F., Hitomi, M., Fisher, S. A., and Watanabe, M. (2002). Initiation of apoptosis in the developing avian outflow tract myocardium. Dev Dyn *223*, 469-482.

Rugh, R. (1968). The Mouse. Its Reproduction and Development. Minneapolis: Burgess. .

Ruvinsky, I., Silver, L. M., and Gibson-Brown, J. J. (2000). Phylogenetic analysis of T-Box genes demonstrates the importance of amphioxus for understanding evolution of the vertebrate genome. Genetics *156*, 1249-1257.

Rychter, Z., and Ostadal, B. (1971). Mechanism of the development of coronary arteries in chick embryo. Folia Morphol (Praha) *19*, 113-124.

Santer, R. M., and Cobb, J. L. (1972). The fine structure of the heart of the teleost, Pleuronectes platessa L. Z Zellforsch Mikrosk Anat *131*, 1-14.

Sargent, M. G., and Bennett, M. F. (1990). Identification in Xenopus of a structural homologue of the Drosophila gene snail. Development *109*, 967-973.

Sater, A. K., and Jacobson, A. G. (1990). The restriction of the heart morphogenetic field in Xenopus laevis. Dev Biol *140*, 328-336.

Savagner, P., Yamada, K. M., and Thiery, J. P. (1997). The zinc-finger protein slug causes desmosome dissociation, an initial and necessary step for growth factor-induced epithelial-mesenchymal transition. J Cell Biol *137*, 1403-1419.

Schaefer, K. S., Doughman, Y. Q., Fisher, S. A., and Watanabe, M. (2004). Dynamic patterns of apoptosis in the developing chicken heart. Dev Dyn *229*, 489-499.

Schreckenberg, G. M., and Jacobson, A. G. (1975). Normal stages of development of the axolotl. Ambystoma mexicanum. Dev Biol *42*, 391-400.

Schulte, I., Schlueter, J., Abu-Issa, R., Brand, T., and Manner, J. (2007). Morphological and molecular left-right asymmetries in the development of the proepicardium: a comparative analysis on mouse and chick embryos. Dev Dyn *236*, 684-695.

Schumacher, V., Schneider, S., Figge, A., Wildhardt, G., Harms, D., Schmidt, D., Weirich, A., Ludwig, R., and Royer-Pokora, B. (1997). Correlation of germ-line mutations and two-hit inactivation of the WT1 gene with Wilms tumors of stromal-predominant histology. Proc Natl Acad Sci U S A *94*, 3972-3977.

Sejima, H., Isokawa, K., Shimizu, O., Morikawa, T., Ootsu, H., Numata, K., Fukai, M., Kubota, S., and Toda, Y. (2001). Possible participation of isolated epicardial cell clusters in the formation of chick embryonic epicardium. J Oral Sci *43*, 109-116.

Semba, K., Saito-Ueno, R., Takayama, G., and Kondo, M. (1996). cDNA cloning and its pronephros-specific expression of the Wilms' tumor suppressor gene, WT1, from Xenopus laevis. Gene *175*, 167-172.

Shepard, J. L., and Zon, L. I. (2000). Developmental derivation of embryonic and adult macrophages. Curr Opin Hematol *7*, 3-8.

Shinbrot, E., Peters, K. G., and Williams, L. T. (1994). Expression of the platelet-derived growth factor beta receptor during organogenesis and tissue differentiation in the mouse embryo. Dev Dyn *199*, 169-175.

Simrick, S., Masse, K., and Jones, E. A. (2005). Developmental expression of Pod 1 in Xenopus laevis. Int J Dev Biol *49*, 59-63.

Singh, M. K., Christoffels, V. M., Dias, J. M., Trowe, M. O., Petry, M., Schuster-Gossler, K., Burger, A., Ericson, J., and Kispert, A. (2005a). Tbx20 is essential for cardiac chamber differentiation and repression of Tbx2. Development *132*, 2697-2707.

Singh, M. K., Petry, M., Haenig, B., Lescher, B., Leitges, M., and Kispert, A. (2005b). The T-box transcription factor Tbx15 is required for skeletal development. Mech Dev *122*, 131-144.

Sive, H. L., Grainger, R. M., and Harland, R. M. (2000). Early development of Xenopus laevis. A laboratory manual (New York: Cold Spring Harbor Laboratory Press).

Slack, J. M., and Forman, D. (1980). An interaction between dorsal and ventral regions of the marginal zone in early amphibian embryos. J Embryol Exp Morphol *56*, 283-299.

Smart, N., Risebro, C. A., Melville, A. A., Moses, K., Schwartz, R. J., Chien, K. R., and Riley, P. R. (2007). Thymosin beta4 induces adult epicardial progenitor mobilization and neovascularization. Nature *445*, 177-182.

Smith, D. E., Franco del Amo, F., and Gridley, T. (1992). Isolation of Sna, a mouse gene homologous to the Drosophila genes snail and escargot: its expression pattern suggests multiple roles during postimplantation development. Development *116*, 1033-1039.

Smith, J. (1999). T-box genes: what they do and how they do it. Trends Genet *15*, 154-158.

Smith, S. J., Fairclough, L., Latinkic, B. V., Sparrow, D. B., and Mohun, T. J. (2006). Xenopus laevis transgenesis by sperm nuclear injection. Nat Protoc *1*, 2195-2203.

Sparrow, D. B., Cai, C., Kotecha, S., Latinkic, B., Cooper, B., Towers, N., Evans, S. M., and Mohun, T. J. (2000). Regulation of the tinman homologues in Xenopus embryos. Dev Biol *227*, 65-79.

Stennard, F. A., Costa, M. W., Lai, D., Biben, C., Furtado, M. B., Solloway, M. J., McCulley, D. J., Leimena, C., Preis, J. I., Dunwoodie, S. L., *et al.* (2005). Murine T-box transcription factor Tbx20 acts as a repressor during heart development, and is essential for adult heart integrity, function and adaptation. Development *132*, 2451-2462.

Stuckmann, I., Evans, S., and Lassar, A. B. (2003). Erythropoietin and retinoic acid, secreted from the epicardium, are required for cardiac myocyte proliferation. Dev Biol *255*, 334-349.

Sucov, H. M., Dyson, E., Gumeringer, C. L., Price, J., Chien, K. R., and Evans, R. M. (1994). RXR alpha mutant mice establish a genetic basis for vitamin A signaling in heart morphogenesis. Genes Dev *8*, 1007-1018.

Sugishita, Y., Leifer, D. W., Agani, F., Watanabe, M., and Fisher, S. A. (2004). Hypoxia-responsive signaling regulates the apoptosis-dependent remodeling of the embryonic avian cardiac outflow tract. Dev Biol *273*, 285-296.

Summerton, J., and Weller, D. (1997). Morpholino antisense oligomers: design, preparation, and properties. Antisense Nucleic Acid Drug Dev *7*, 187-195.

Svensson, E. C., Tufts, R. L., Polk, C. E., and Leiden, J. M. (1999). Molecular cloning of FOG-2: a modulator of transcription factor GATA-4 in cardiomyocytes. Proc Natl Acad Sci U S A *96*, 956-961.

Taber, L. A., Keller, B. B., and Clark, E. B. (1992). Cardiac mechanics in the stage-16 chick embryo. J Biomech Eng *114*, 427-434.

Takebayashi-Suzuki, K., Yanagisawa, M., Gourdie, R. G., Kanzawa, N., and Mikawa, T. (2000). In vivo induction of cardiac Purkinje fiber differentiation by coexpression of preproendothelin-1 and endothelin converting enzyme-1. Development *127*, 3523-3532.

Takeuchi, J. K., Mileikovskaia, M., Koshiba-Takeuchi, K., Heidt, A. B., Mori, A. D., Arruda, E. P., Gertsenstein, M., Georges, R., Davidson, L., Mo, R., *et al.* (2005). Tbx20 dose-dependently regulates transcription factor networks required for mouse heart and motoneuron development. Development *132*, 2463-2474.

Tanaka, M., and Tickle, C. (2004). Tbx18 and boundary formation in chick somite and wing development. Dev Biol *268*, 470-480.

Tevosian, S. G., Deconinck, A. E., Cantor, A. B., Rieff, H. I., Fujiwara, Y., Corfas, G., and Orkin, S. H. (1999). FOG-2: A novel GATA-family cofactor related to multitype zinc-finger proteins Friend of GATA-1 and U-shaped. Proc Natl Acad Sci U S A *96*, 950-955.

Tevosian, S. G., Deconinck, A. E., Tanaka, M., Schinke, M., Litovsky, S. H., Izumo, S., Fujiwara, Y., and Orkin, S. H. (2000). FOG-2, a cofactor for GATA transcription factors, is essential for heart morphogenesis and development of coronary vessels from epicardium. Cell *101*, 729-739.

Tidball, J. G. (1992). Distribution of collagens and fibronectin in the subepicardium during avian cardiac development. Anat Embryol (Berl) *185*, 155-162.

Tomanek, R. J., Ratajska, A., Kitten, G. T., Yue, X., and Sandra, A. (1999). Vascular endothelial growth factor expression coincides with coronary vasculogenesis and angiogenesis. Dev Dyn *215*, 54-61.

Tonissen, K. F., Drysdale, T. A., Lints, T. J., Harvey, R. P., and Krieg, P. A. (1994). XNkx-2.5, a Xenopus gene related to Nkx-2.5 and tinman: evidence for a conserved role in cardiac development. Dev Biol *162*, 325-328.

Tran, C. M., and Sucov, H. M. (1998). The RXRalpha gene functions in a non-cell-autonomous manner during mouse cardiac morphogenesis. Development *125*, 1951-1956.

Turner, D. L., and Weintraub, H. (1994). Expression of achaete-scute homolog 3 in Xenopus embryos converts ectodermal cells to a neural fate. Genes Dev *8*, 1434-1447.

Ubbels, G. A., Hara, K., Koster, C. H., and Kirschner, M. W. (1983). Evidence for a functional role of the cytoskeleton in determination of the dorsoventral axis in Xenopus laevis eggs. J Embryol Exp Morphol *77*, 15-37.

Viragh, S., and Challice, C. E. (1981). The origin of the epicardium and the embryonic myocardial circulation in the mouse. Anat Rec *201*, 157-168.

Viragh, S., Szabo, E., and Challice, C. E. (1989). Formation of the primitive myo- and endocardial tubes in the chicken embryo. J Mol Cell Cardiol *21*, 123-137.

Vize, P. D., Jones, E. A., and Pfister, R. (1995). Development of the Xenopus pronephric system. Dev Biol *171*, 531-540.

von Scheven, G., Bothe, I., Ahmed, M. U., Alvares, L. E., and Dietrich, S. (2006). Protein and genomic organisation of vertebrate MyoR and Capsulin genes and their expression during avian development. Gene Expr Patterns *6*, 383-393.

Vrancken Peeters, M. P., Gittenberger-de Groot, A. C., Mentink, M. M., and Poelmann, R. E. (1999). Smooth muscle cells and fibroblasts of the coronary arteries derive from epithelial-mesenchymal transformation of the epicardium. Anat Embryol (Berl) *199*, 367-378.

Vrancken Peeters, M. P., Mentink, M. M., Poelmann, R. E., and Gittenberger-de Groot, A. C. (1995). Cytokeratins as a marker for epicardial formation in the quail embryo. Anat Embryol (Berl) *191*, 503-508.

Wagner, N., Wagner, K. D., Theres, H., Englert, C., Schedl, A., and Scholz, H. (2005). Coronary vessel development requires activation of the TrkB neurotrophin receptor by the Wilms' tumor transcription factor Wt1. Genes Dev *19*, 2631-2642.

Waldo, K. L., Kumiski, D. H., Wallis, K. T., Stadt, H. A., Hutson, M. R., Platt, D. H., and Kirby, M. L. (2001). Conotruncal myocardium arises from a secondary heart field. Development *128*, 3179-3188.

Waldo, K. L., Willner, W., and Kirby, M. L. (1990). Origin of the proximal coronary artery stems and a review of ventricular vascularization in the chick embryo. Am J Anat *188*, 109-120.

Wallingford, J. B., Carroll, T. J., and Vize, P. D. (1998). Precocious expression of the Wilms' tumor gene xWT1 inhibits embryonic kidney development in Xenopus laevis. Dev Biol *202*, 103-112.

Wasylyk, B., Hahn, S. L., and Giovane, A. (1993). The Ets family of transcription factors. Eur J Biochem *211*, 7-18.

Watanabe, M., Choudhry, A., Berlan, M., Singal, A., Siwik, E., Mohr, S., and Fisher, S. A. (1998). Developmental remodeling and shortening of the cardiac outflow tract involves myocyte programmed cell death. Development *125*, 3809-3820.

Watanabe, M., Jafri, A., and Fisher, S. A. (2001). Apoptosis is required for the proper formation of the ventriculo-arterial connections. Dev Biol *240*, 274-288.

Watanabe, M., Timm, M., and Fallah-Najmabadi, H. (1992). Cardiac expression of polysialylated NCAM in the chicken embryo: correlation with the ventricular conduction system. Dev Dyn *194*, 128-141.

Wehrle-Haller, B., and Imhof, B. (2002). The inner lives of focal adhesions. Trends Cell Biol *12*, 382-389.

Weninger, W. J., Geyer, S. H., Mohun, T. J., Rasskin-Gutman, D., Matsui, T., Ribeiro, I., Costa Lda, F., Izpisua-Belmonte, J. C., and Muller, G. B. (2006). High-

resolution episcopic microscopy: a rapid technique for high detailed 3D analysis of gene activity in the context of tissue architecture and morphology. Anat Embryol (Berl) *211*, 213-221.

Weninger, W. J., and Mohun, T. (2002). Phenotyping transgenic embryos: a rapid 3-D screening method based on episcopic fluorescence image capturing. Nat Genet *30*, 59-65.

Wu, H., Lee, S. H., Gao, J., Liu, X., and Iruela-Arispe, M. L. (1999). Inactivation of erythropoietin leads to defects in cardiac morphogenesis. Development *126*, 3597-3605.

Xavier-Neto, J., Shapiro, M. D., Houghton, L., and Rosenthal, N. (2000). Sequential programs of retinoic acid synthesis in the myocardial and epicardial layers of the developing avian heart. Dev Biol *219*, 129-141.

Ya, J., van den Hoff, M. J., de Boer, P. A., Tesink-Taekema, S., Franco, D., Moorman, A. F., and Lamers, W. H. (1998). Normal development of the outflow tract in the rat. Circ Res *82*, 464-472.

Yamashita, J., Itoh, H., Hirashima, M., Ogawa, M., Nishikawa, S., Yurugi, T., Naito, M., Nakao, K., and Nishikawa, S. (2000). Flk1-positive cells derived from embryonic stem cells serve as vascular progenitors. Nature *408*, 92-96.

Yang, J. T., Rayburn, H., and Hynes, R. O. (1995). Cell adhesion events mediated by alpha 4 integrins are essential in placental and cardiac development. Development *121*, 549-560.

Yu, X., St Amand, T. R., Wang, S., Li, G., Zhang, Y., Hu, Y. P., Nguyen, L., Qiu, M. S., and Chen, Y. P. (2001). Differential expression and functional analysis of Pitx2 isoforms in regulation of heart looping in the chick. Development *128*, 1005-1013.